

AD-A257 343



2

NAVAL POSTGRADUATE SCHOOL Monterey, California



DTIC
ELECTE
NOV 24 1992
S C D

THESIS

QUANTITATIVE FORCE MEASUREMENTS
OF PNEUMATIC CONTROL
ON A WING/STRAKE MODEL

by

James Griffin Willson

September, 1992

Thesis Advisor:

Richard M. Howard

Approved for public release; distribution is unlimited.

92-30067



9 2

REPORT DOCUMENTATION PAGE				
1a. REPORT SECURITY CLASSIFICATION UNCLASSIFIED			1b. RESTRICTIVE MARKINGS	
2a. SECURITY CLASSIFICATION AUTHORITY			3. DISTRIBUTION/AVAILABILITY OF REPORT Approved for public release; distribution is unlimited.	
2b. DECLASSIFICATION/DOWNGRADING SCHEDULE				
4. PERFORMING ORGANIZATION REPORT NUMBER(S)			5. MONITORING ORGANIZATION REPORT NUMBER(S)	
6a. NAME OF PERFORMING ORGANIZATION Naval Postgraduate School	6b. OFFICE SYMBOL (If applicable) 31	7a. NAME OF MONITORING ORGANIZATION Naval Postgraduate School		
6c. ADDRESS (City, State, and ZIP Code) Monterey, CA 93943-5000		7b. ADDRESS (City, State, and ZIP Code) Monterey, CA 93943-5000		
8a. NAME OF FUNDING/SPONSORING ORGANIZATION	8b. OFFICE SYMBOL (If applicable)	9. PROCUREMENT INSTRUMENT IDENTIFICATION NUMBER		
8c. ADDRESS (City, State, and ZIP Code)		10. SOURCE OF FUNDING NUMBERS		
		Program Element No.	Project No.	Task No.
				Work Unit Accession Number
11. TITLE (Include Security Classification) QUANTITATIVE FORCE MEASUREMENTS OF PNEUMATIC CONTROL ON A WING/STRAKE MODEL				
12. PERSONAL AUTHOR(S) Willson, James G.				
13a. TYPE OF REPORT Master's Thesis	13b. TIME COVERED From To	14. DATE OF REPORT (year, month, day) September 1992	15. PAGE COUNT 119	
16. SUPPLEMENTARY NOTATION The views expressed in this thesis are those of the author and do not reflect the official policy or position of the Department of Defense or the U.S. Government.				
17. COSATI CODES			18. SUBJECT TERMS (continue on reverse if necessary and identify by block number)	
FIELD	GROUP	SUBGROUP		
			Strake, Vortex Control, Blowing, Vortex Interaction, Enhanced Lift	
19. ABSTRACT (continue on reverse if necessary and identify by block number) A low-speed wind-tunnel study to quantitatively measure the lift and drag effects of pneumatically controlling a leading edge vortex generated by a half-span, generic-fighter-wing model was conducted. The study measured the added lift and drag upon the model, throughout a range of angles of attack, utilizing blowing tubes of different geometry and orientations. The effects of blowing upon the high pressure side of the strake were also investigated. Results showed that the effects of blowing were limited to changes in lift with no apparent changes in drag. Blowing appeared to reattach the flow during the initial stages of wing stall. Blowing increased lift by a maximum of 3.75% at angles of attack greater than 25 degrees. The effects of blowing appeared oscillatory with respect to angle of attack. Blowing rates were varied from $C_{mu} = 0.0$ to 0.0035 in an attempt to determine an optimum. It was found that changes in blowing rates had little effect upon delta C_L .				
20. DISTRIBUTION/AVAILABILITY OF ABSTRACT <input checked="" type="checkbox"/> UNCLASSIFIED/UNLIMITED <input type="checkbox"/> SAME AS REPORT <input type="checkbox"/> DTIC USERS			21. ABSTRACT SECURITY CLASSIFICATION	
22a. NAME OF RESPONSIBLE INDIVIDUAL Richard M. Howard			22b. TELEPHONE (Include Area code) 408-646-2870	22c. OFFICE SYMBOL AA/Ho

Approved for public release; distribution is unlimited.

QUANTITATIVE FORCE MEASUREMENTS
OF PNEUMATIC CONTROL
ON A WING/STRAKE MODEL

by

James Griffin Willson
Lieutenant, United States Navy
B.S., United States Naval Academy, 1984

Submitted in partial fulfillment
of the requirements for the degree of

MASTER OF SCIENCE IN AERONAUTICAL ENGINEERING

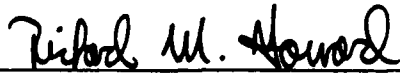
from the

NAVAL POSTGRADUATE SCHOOL
September 1992

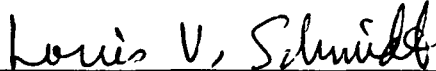
Author:


James Griffin Willson

Approved by:



Richard M. Howard, Thesis Advisor



Louis V. Schmidt, Second Reader



Daniel J. Collins, Chairman

Department of Aeronautics and Astronautics

ABSTRACT

A low-speed wind-tunnel study to quantitatively measure the lift and drag effects of pneumatically controlling a leading edge vortex generated by a half-span, generic-fighter-wing model was conducted. The study measured the added lift and drag upon the model, throughout a range of angles of attack, utilizing blowing tubes of different geometry and orientations. The effects of blowing upon the high pressure side of the strake were also investigated. Results showed that the effects of blowing were limited to changes in lift with no apparent changes in drag. Blowing appeared to reattach the flow during the initial stages of wing stall. Blowing increased lift by a maximum of 3.75% at angles of attack greater than 25° . The effects of blowing appeared oscillatory with respect to angle of attack. Blowing rates were varied from $C_\mu=0.0$ to 0.0035 in an attempt to determine an optimum. It was found that changes in blowing rates had little effect upon ΔC_L .

DTIC QUALITY INSPECTED 4

Accession For	
NTIS GRAD	<input checked="checked" type="checkbox"/>
DTIC TAB	<input type="checkbox"/>
Unannounced	<input type="checkbox"/>
Justification	
By	
Distribution/	
Availability Codes	
Dist	Avail and/or Special
A-1	

TABLE OF CONTENTS

	Page
I. INTRODUCTION.....	1
II. BACKGROUND.....	4
A. ROACH AND KUHLMAN'S WING STRAKE STUDY.....	4
B. LEMAY AND ROGERS' WATER TUNNEL STUDY.....	6
C. NAVIER-STOKES SIMULATION OF AN AIR JET IN CROSSFLOW.....	8
D. CELIK AND ROBERTS' FOREBODY AND WING BLOWING STUDY.....	9
E. GUYTON AND MAERKI X-29 STUDY.....	12
F. KERN'S WING/STRAKE JUNCTION STUDY.....	12
III. EXPERIMENT AND PROCEDURES.....	15
A. OVERVIEW.....	15
B. APPARATUS.....	15
1. Wind Tunnel.....	15
2. Wing/Strake Model.....	17
3. Blowing Apparatus and Coefficient Determination.....	18
4. Balance and Turntable.....	21
5. Data Acquisition Hardware.....	22
6. Data Acquisition Software.....	23
C. EXPERIMENTAL CONDITIONS.....	24

D. EXPERIMENTAL PROCEDURE.....	25
1. Pre-run Calibration and Test.....	25
2. Testing Procedures.....	27
3. Tests Holding C_{μ} Constant Varying AOA.....	30
4. Tests Holding AOA Constant Varying C_{μ}	33
E. EXPERIMENTAL CORRECTIONS.....	36
1. Wake and Solid Blockage Corrections.....	36
2. Tunnel Velocity Drift Corrections.....	38
3. Low Frequency Velocity Surge Correction.....	38
IV. DISCUSSION AND RESULTS.....	40
A. OVERVIEW.....	40
B. BASELINE MODEL PERFORMANCE.....	40
C. TESTS HOLDING C_{μ} CONSTANT VARYING AOA.....	42
1. Blowing Port #1, Jet $\angle=45^{\circ}$, Incl. $\angle=0^{\circ}$, $C_{\mu}=0.0035$	42
2. Blowing Port #1, Jet $\angle=45^{\circ}$, Incl. $\angle=0^{\circ}$, $C_{\mu}=0.0022$	44
3. Blowing Port #1, Jet $\angle=45^{\circ}$, Incl. $\angle=10^{\circ}$, $C_{\mu}=0.0022$	46
4. Blowing Port #3, Jet $\angle=45^{\circ}$, Incl. $\angle=-25^{\circ}$, $C_{\mu}=0.0022$	47
D. TESTS HOLDING AOA CONSTANT VARYING C_{μ}	48
1. Overview.....	48

2.	Blowing Configurations without Drift	
	Corrections.....	49
a)	Early Test Runs.....	50
3.	Blowing Configurations with Drift Checks.....	51
a)	Blowing Port #1.....	52
b)	Blowing Port #2.....	52
c)	Blowing Port #3.....	53
V.	CONCLUSIONS AND RECOMMENDATIONS.....	55
A.	CONCLUSIONS.....	55
B.	RECOMMENDATIONS.....	56
1.	Flow Visualization.....	57
2.	Provide Velocity Sampling to Reduce Error.....	57
3.	Conduct More Tests Varying C_μ at AOA's other	
	than 35°	58
4.	Conduct More Tests Varying AOA at Constant C_μ	58
	LIST OF REFERENCES.....	60
	APPENDIX A. FIGURES.....	62
	APPENDIX B. MODEL DESIGN.....	90
	APPENDIX C. HP48SX PLENUM PRESSURE PROGRAM.....	98
	APPENDIX D. MULTI3.BAS PROGRAM LISTING.....	100
	APPENDIX E. WIND-TUNNEL CHECKLIST.....	110
	INITIAL DISTRIBUTION LIST.....	112

I. INTRODUCTION

Advanced tactical fighter aircraft require an edge in maneuverability to be effective in combat. Recent efforts have been expended in the exploitation of high lift generated at high angles of attack. Aircraft such as the F/A-18 and YF-23 generate from a strake strong counter-rotating leading-edge vortices that extend over the wing. These vortices greatly enhance the lift of the aircraft, particularly at high angles of attack ($\alpha > 20^\circ$). Thus during rapid pitching maneuvers (or during slow fighting at high angles of attack), an advantage can be gained over a more conventionally-designed aircraft. From a combat survivability point of view, this advantage can reduce the aircraft susceptibility to an opposing threat of another aircraft. Also, obtaining a kill is much easier because the aircraft has a greater pointing ability.

This advantage does not come without its price. The aircraft experiences increasing loss of lateral and directional controllability as angle of attack is increased. Coupling is another effect of the vortex phenomena where the individual vortices intertwine around each other. Generally, this effect is destructive to lift generated. Additionally, the breakdown point of the leading-edge vortex can place additional stress on the structure of the aircraft

near the burst point. The F/A-18 flow fence modification is an example of an engineering modification required because of this effect.

Besides the wing and strake vortices generated by advanced fighter wings, forebody vortices are also generated by the nose of the aircraft. Much research has been recently conducted investigating methods of controlling the strengths and positions of both types of vortices. Almost all studies limited their investigation to flow visualization of the vortex burst points. The research has been concentrated in the area of pneumatic blowing either at the forebody or across the wing/strake surface. It has been shown that blowing at these positions increases the strengths of the vortices and delays their breakdown. This phenomenon resulted in an increase in lift or, if asymmetrically applied, a rolling or yawing moment. These effects were not only a result of changes in the vortex strength, but also changes in the positions of the vortices. This effect is true for both forebody blowing or strake blowing. [Ref. 1-8]

This research continued to study the effects of blowing, near the apex of a generic-fighter wing/strake, on the lift generated at high angles of attack. Particular emphasis was placed on the acquisition of quantitative lift and drag data. Blowing ports of different positions and angles about

the leading edge extension (LEX) were examined. The effects of blowing upon the high pressure side of the strake were also investigated. A half-span wooden model with a generic planform, similar in size and shape to the F/A-18 and with a strake similar to the YF-23, was used for the collection of this data.

II. BACKGROUND

The effects of vortex breakdown behavior have been studied for over a decade. However, the topic of vortex control has only just recently been stressed to a high degree of importance. The past three years have produced much in understanding methods of controlling the breakdown of the leading edge extension (LEX) vortices. Nearly all of this work has been in the discipline of flow visualization (velocity profile mapping) as discussed below. Some investigations of forebody blowing quantitatively measured the yawing moments that were the result of forebody blowing. Lift, drag, and rolling-moment, which are all effects of wing/strake blowing, were studied little in previous investigations.

A. ROACH AND KUHLMAN'S WING STRAKE STUDY

Roach and Kuhlman [Ref. 1 & 2] used laser light sheet and Laser Doppler Anemometry to map the flowfield of LEX vortices and the effects of blowing on the breakdown and coupling locations. A generic fighter wing-body model constructed with interchangeable strakes and blowing ports was used (Figure 1, [Ref. 2]). The wing and strake were flat plates with sharp beveled leading edges (45°). The model was designed to provide pneumatic blowing at four

locations on each side of the fuselage. Blowing was provided through two different types of brass blowing tubes each with an outer diameter of 0.16 cm ($\cong 1/16$ in.). The first type was oriented to blow parallel to the leading edge of the strake.

The second was a short tube angling 35° from the fuselage side (jet angle). Roach and Kuhlman used a blowing coefficient of $C_\mu = 0.016$, which was based on results of LeMay and Rogers [Ref. 3]. C_μ is defined as:

$$C_\mu = \frac{\dot{m}_j V_j}{q S} \quad (1)$$

Where:

\dot{m}_j	mass flow rate of the blowing jet
V_j	velocity of the blowing jet
q_∞	freestream dynamic pressure
S	aircraft wing reference area

Roach and Kuhlman's results showed that the best delay in vortex breakdown for the short strake was obtained by using the short tubes (jet angle = 35°) with an inclination of -10° at the forward most blowing port located near the apex of the strake. The same was true for the longer strake. Tangential blowing at the aforementioned port position was equally effective for the longer strake. However, the tangential blowing used a $+10^\circ$ inclination to the wing. Roach and Kuhlman were only able to delay the

breakdown of the strake vortex. This delay was quantitatively measured by visualizing the breakdown point in reference to the wing. They were unable to control the breakdown of the wing vortex.

B. LEMAY AND ROGERS' WATER TUNNEL STUDY

LeMay and Rogers [Ref. 3] conducted water tunnel experiments using a 4/100-scale generic fighter model. Roach and Kuhlman's model was patterned after this model. Therefore this model is nearly identical to the previous model except for the following. LeMay's model was a smaller scale than Roach's. The model was configured with removable vertical stabilizers so that their effect upon vortex breakdown could be determined. LeMay's optimum blowing coefficient (C_{μ}) varied between 0.01 and 0.03, based on vortex burst location and behavior.

Use of a water tunnel yielded better pictures of the vortex flow characteristics than did the laser sheet photography of Roach and Kuhlman. All of LeMay and Roger's photos from a side view showed that the strake vortex initially was entrained to a point high on the model until it encountered the wing vortex. At this point the vortex was pulled down to near the wing surface. Some coupling of the strake and wing vortices often occurred. Coupling of the vortices favorably delayed the vortex breakdown as angle

of attack increased to 24° . Beyond 24° the coupling effect promoted early vortex breakdown.

LeMay and Rogers' photos clearly showed that the blowing lifted the strake vortex further away from the wing surface. This response resulted in a vortex of increased strength and a delay in the burst point. LeMay and Rogers proposed that this effect resulted from the vortex moving away from the separated flow region and associated adverse pressure gradient present on the wing.

Not all blowing produced a desired result. Some blowing configurations promoted the interaction of the wing and strake vortices resulting in an earlier breakdown. These were typically from ports located on the fuselage side behind the wing-strake junction. This interaction would most likely result in a loss of lift instead of an enhancement of it.

LeMay and Rogers investigated multiple jet angles and inclination angles. They found that the most optimal blowing configuration was a location of one-third of the way down the strake with a jet angle of 35° and an inclination angle of 20° . This result was different from that of Roach and Kuhlman. Their Reynolds number was 270,000 (based on a root chord of 28.14 cm.) in air and that of LeMay and Rogers was 11,500 (reference length unspecified) in water.

This difference may account for some of the variance of optimum blowing locations.

C. NAVIER-STOKES SIMULATION OF AN AIR JET IN CROSSFLOW

Roth, Fearn, and Thakur [Ref. 4] evaluated a Navier-Stokes computer simulation of an air jet blowing perpendicular to a freestream crossflow. In their paper they explained that the characteristics of the jet (i.e., size, shape, pressure distribution) were functions of the effective velocity ratio of the two flows. The jet plume consisted of a counter-rotating vortex pair, whose generation was the result of a high adverse pressure gradient upstream of the jet and a low pressure region behind the jet (Figure 2, [Ref. 4]). The region of lowest pressure was found symmetrically 135° from the upstream centerline axis (Figure 3, [Ref. 4]). As freestream air passed from the high to low pressure regions around the jet, some of the freestream air was entrained into the vortex plume (Figure 4, [Ref. 4]). Thus the entrainment of the strake vortex by a blowing jet was a function of the effective velocity ratio of the two flows and not of the blowing coefficient.

In the blowing coefficient equation (1), all of the variables describing the freestream are in the denominator and those for the blowing jet are in the numerator. Different effective velocity ratios are possible for the

same blowing coefficient. A reduction in the radius of the blowing tube would result in a reduction in mass flow and an increase in velocity for a given plenum pressure. If the jet flow was choked, then mass flow became a linear function of plenum pressure. LeMay and Rogers, being in a water tunnel, had a small model at low freestream velocity. Roach and Kuhlman had a larger model at higher velocity. The bores of both models blowing ports were approximately the same diameter. Thus it can be assumed that their effective velocity ratios were different despite similar blowing coefficients.

LeMay and Rogers also investigated the effects of vertical stabilizers on the vortex breakdown both with and without blowing. It was found that in all cases blowing completely decoupled the wing and strake vortices at all angles of attack. Without blowing, a 30° outward canted vertical stabilizer resulted in significantly earlier vortex breakdown than for the baseline case. LeMay and Rogers in their recommendations stated that there is a need for the collection of force data for these effects.

D. CELIK AND ROBERTS' FOREBODY AND WING BLOWING STUDY

Another investigation of the effects of blowing on a wing was conducted by Celik and Roberts [Ref. 5] at Stanford University. Their model was a forebody and delta wing combination with a cylindrical ogive nose (Figure 5, [Ref.

5)). They investigated two different types of blowing, forebody and tangential blowing along the leading edge of the delta wing. All blowing was from slots instead of blowing ports. Forebody slots were mounted along the cylindrical side of the forebody and not along the ogive nose piece. The slots on the wing were mounted along the leading edge angling upward. It is important to note that the slot style of blowing is not commonly used by most engineers investigating blowing as a means of control and is not the type used in the investigation. Side forces, yawing moment, and rolling moment were measured against changes in the blowing coefficient (C_{μ}) and various orientations of the model.

Celik and Roberts' results showed that there was a reversal of forces and moments that occurred at low blowing coefficients. This response was the result of the generated vortex sheet being blown across to the other side of the model at the higher blowing coefficients. Forebody blowing appeared to be more effective than the tangential slot leading edge blowing. It is significant to note that the change in the rolling moment generated by forebody blowing was stronger for configurations where the wing had a rounded leading edge than for wings with sharp leading edges. This result was believed to be due to the difference in the location of the vortex emanating from the delta wing with

the different edges. It was also noted that forebody blowing seemed to be most efficient at the small to moderate blowing rates of $C_{\mu} = 0.001$ to 0.003 . Maximum observed rolling moment increase was $\Delta C_l \cong 0.09$.

Forebody blowing has been extensively studied in conjunction with the X-29 fighter aircraft. Cornelius, Pandit, Osborn and Guyton [Ref. 6] investigated several geometric nozzle configurations on an X-29 forebody wind tunnel model. The forebody model consisted of two pairs of nozzle blocks located at two axial positions from the nose. A strake was also mounted from the nose apex to approximately 18% of the forebody-model's length. Nozzle plugs of different shapes were then placed at these positions. The most effective configuration for a nozzle was discovered to be a converging contraction nozzle. This design was modified with an extended slotted throat region.

Results of the modified nozzle showed the exiting flow to be spread out into a two-dimensional sheet. This sheet of the blowing jet had a three-fold increase in entrainment properties over conventional axisymmetric nozzles. Cornelius' et al. investigation showed that the best orientation of the nozzle was canted in 60° from the longitudinal axis. The forward-most position for the blowing plugs was the best.

E. GUYTON AND MAERKI X-29 STUDY

The X-29 investigation continued with further isolated forebody tests and a fully configured X-29 model. The results of these tests were published in a paper by Guyton and Maerki. [Ref. 7] The investigation was expanded to include new orientations of the nozzles, Reynolds number effects, Mach number effects and dynamic response of blowing. Nozzle orientations were still shown to be optimized when aimed inward 60° . At high blowing rates ($C_\mu = 0.0120$), yawing moments generated by blowing was severely degraded by high freestream Mach numbers ($M = 0.5$). Low blowing rates ($C_\mu \cong 0.0060$) were not significantly affected by high Mach numbers but did see more effect from changes in angle of attack. The slope of yawing moment versus α increased significantly starting at $\alpha = 20^\circ$ to 30° .

F. KERN'S WING/STRAKE JUNCTION STUDY

Steven Kern, of the Naval Air Development Center, conducted a numerical investigation on the effects of geometry modifications at the junction of a wing and a strake [Ref. 8]. Kern used a wing/strake geometry that was based on modern fighter aircraft being developed and flown today (Figure 6 [Ref. 8]). His wing and strake were flat plates with 20° bevelled edges. He then developed three fillets to be placed at the junction of the wing/strake.

These fillets were described as linear, smooth parabolic and diamond shaped (Figure 7 [Ref. 8]). Kern used two types of computational methods for generating his results. The first was the Three-dimensional Euler/Navier-Stokes Aerodynamic Method (TEAM), used for inviscid rotational flow analysis. The second was the Navier-Stokes Time Dependent (NASTD) method (developed by McDonnell Aircraft Co.), used for viscous analysis. His study limited its research to angles of attack (AOA) less than 30° .

Kern first developed inviscid baseline-vortex positions, lift, and drag information. At $AOA = 10^{\circ}$, two well-defined vortices developed. As expected, one developed from the leading edge of the strake and the other from the leading edge of the wing. As AOA was increased, the two vortices became stronger and started to intertwine. As the vortices began to strengthen, the point where they began to intertwine moved further upstream. At 22.5° , after the wing had started to stall ($AOA = 19^{\circ}$), the two vortex cores merged into one.

In the viscous study, the vortex locations seemed to correspond to those of the inviscid study with one exception. Vortex tearing, a phenomenon not normally seen in numerical studies, was discovered along the wing-leading-edge vortex. It was caused by the interaction of the wing and strake vortices.

Of the three fillets used, the diamond shaped fillet had the most favorable effect with angle-of-attack increases. At 10° AOA, it increased lift by 13.6 percent. At 22.5° AOA it increased lift by 17.9 percent. The parabolic fillet at high angle of attack was found to be unfavorable. It decreased lift at 22.5° AOA by 4.0 percent.

III. EXPERIMENT AND PROCEDURES

A. OVERVIEW

A wing/strake model was designed and constructed at the Naval Postgraduate School (NPS) for low-speed wind-tunnel tests in the NPS low-speed, single-return wind tunnel. The model was mounted in a reflection plane mode with lift and drag measurements being made by a wall balance (see Ref. 9 for a discussion of the calibration). Data was acquired from the signal conditioning assembly through a multiplexer, amplifier, and analog-to-digital converter, and stored on a floppy disk. The results were reduced to lift and drag coefficients.

B. APPARATUS

The primary equipment used was the NPS low-speed wind tunnel, external strain-gage wall balance, signal conditioning assembly, balance calibration rig, wing/strake model, data acquisition system, and data reduction software.

1. Wind Tunnel

The Naval Postgraduate School wind tunnel is a low-speed, single-return, wind tunnel powered by a 100 hp electric motor. The motor is coupled to a three-blade variable-pitch fan and a four-speed truck transmission (Figure 8). The four-speed transmission provides for smooth

operation up to 200 mph. A set of stator blades immediately following the fan removes the swirl effect of the fan on the flow. A combination of turning vanes at each corner, two fine-wire-mesh screens at the entrance to the settling chamber, and a settling chamber to test-section contraction ratio of 10:1 reduce the axial-velocity turbulence level to approximately 0.2 percent [Ref. 11].

Atmospheric vents at the downstream end of the test section establish the tunnel static pressure level at approximately atmospheric pressure. The test section cross-sectional area is 8.75 square feet. Corner lighting and a reflection plane were mounted. A remote-controlled turntable mounted flush with the reflection plane allowed the angle of attack of the model to be varied from -18° to $+200^{\circ}$. The temperature of the tunnel air was measured with a dial thermometer mounted on the tunnel wall extending into the settling chamber [Ref. 11].

The test-section dynamic pressure, q , was determined by measuring the static pressure difference, Δp , between the test section and the settling chamber using a water micromanometer. The pressure difference measured by the micromanometer was converted to the test-section dynamic pressure and test-section reference velocity from a previous calibration. The resulting conversion equations (2 & 3) are shown: [Ref. 10]

$$q_{\infty} = 2.047 (1.1149 \Delta p - 0.026749) \quad (2)$$

$$V_{\infty} = \sqrt{\frac{2q_{\infty}}{\rho}} \quad (3)$$

Where:

ρ	air density (slugs/ft ³)
Δp	micromanometer reading in cm of H ₂ O
q_{∞}	test-section dynamic pressure (lbf/ft ²)
2.047	constant converting cm of H ₂ O to lbf/ft ²
1.1149	tunnel calibration factor
-0.026749	tunnel calibration intercept
V_{∞}	reference velocity (ft/sec)

The wind-tunnel calibration factor, 1.1149, and tunnel calibration intercept, -0.026749, corrected the micromanometer reading, Δp , to test-section dynamic pressure, q . The calibration factor was found by plotting the actual dynamic pressure measured by a pitot-static tube mounted in the test section versus the measured pressure difference. [Ref. 10]

2. Wing/Strake Model

The wing/strake model was designed as a half-model for compatibility with the existing reflection-plane model base and balance previously installed in the wind tunnel. The half-model was of a generic agile-fighter fuselage. The strake and wing used matched the shape described in Kern's

paper [Ref. 8]. The model and wing/strake were fabricated from mahogany by NPS personnel. There were two main sections to the model: the ogive nose, and the wing/strake. The model base and wing section were removable and the base was the same as used by Kersh and Schmidt [Ref. 9, 10]. The model mounted flush to the wind-tunnel reflection plane with only enough gap to prevent binding. Figure 9 shows a sketch of the model. See Appendix B for the model design process and the resultant geometric parameters. [Ref. 10]

3. Blowing Apparatus and Coefficient Determination

A blowing apparatus had to be constructed for the existing model base to support pneumatic control of the strake vortices. The blowing tubes, plenum and regulator were constructed by Naval Postgraduate School personnel. The plenum chamber was constructed out of steel and was rectangular in shape, measuring 4" X 2" X 2". Three brass tubes measuring 1/8" O.D. (0.086" I.D.) were manufactured for directing the blowing jet onto the strake. Tube #1 was bent 30°, tube #2 was bent 45°, and tube #3 was bent 60° (Figure 10).

Naval Postgraduate School shop air was used to supply the air required at pressures up to 75 psig. Shop air was drawn from a fitting located behind the test section of the wind tunnel. The air was passed through a high pressure hose to a regulator where the plenum pressure was

controlled (Figure 11). The regulator was connected to the plenum chamber inside the model by means of Tygon[®] tubing attached by bayonet fittings. The Tygon[®] tubing measured 3/8 inches outer diameter and 1/8 inches inner diameter and was 10 feet in length. The tubing had a Darcy friction factor of 0.04 and experienced approximately a 25 psi drop from the regulator to the plenum chamber [Ref. 12]. Another tube from the plenum chamber was connected to a pressure gage so that stagnation pressure inside the plenum chamber could be read. The plenum chamber was then connected to the brass tubes by another 13 inches of Tygon[®] tubing. These tubes, that extended through the fuselage out of the model, were used to direct the blowing onto the wing.

Appendix B describes the model and its construction. Blowing-tube holes were measured and placed according to Figures B3 and B4 in Appendix B. Blowing port #1 (towards the center of the model) is the forward-most port on the low pressure side of the strake. Port #2 is immediately aft of that. Port #3 is opposite of #1 on the high pressure side of the model.

No reference to blowing on the high pressure side of the strake has ever been made in any of the research material. This concept is believed to be new to this thesis. This author felt that blowing at this position

could lead to stronger vortices by increasing the mass flow of air rounding the edge of the strake.

Blowing coefficient (C_μ) was determined by means of Fanno flow equations [Ref. 13]. The assumption that the flow was sonic at the exit was required for this calculation. This assumption is legitimate for stagnation pressures that are two to three times the ambient air pressure. The equations were then worked backwards from the exit to determine the required pressure inside the plenum. This method, although not as accurate as using sonic chokes to measure mass flow rate, was well within the accuracy required by this experiment. The equations were first verified by hand and then programmed into an HP48SX scientific programmable calculator (Appendix C). A listing of this program is attached in Appendix C. HP48SX's equipped with the Hewlett Packard Solve Equation Library Card[®] can use a Darcy function, programmed into its Read Only Memory (ROM), to solve for the Fanning friction factor. This card eliminates the need for an interactive step where the user must look up the Fanning friction factor in a Moody diagram. [Ref. 14]

Plenum stagnation pressures were then calculated for a range of C_μ 's and regressed into equation form to be used later in data reduction (Figure 12). Figure 12 shows that the plenum pressure verses C_μ relationship was linear.

Since mass flow rate was low (≈ 0.017 lbm/s), the temperature had no effect in the calculations. A ΔT of 60°F was required to change plenum pressure 0.1 psig. This level of temperature change was far beyond any temperature fluctuation that could occur in the physical system. Thus temperature was factored out of the regression.

Assuming that the flow was sonic at the exit of the tube legitimized the equation only for pressures $\approx > 20$ psig. However, it is noted that the lines above 20 psig are linear with slopes that pass through the origin. Since zero pressure differential caused no flow to take place, the origin was considered a hard point in the regression. It was therefore assumed that the physical process was linear throughout the range of pressures. Thus this chart and the associated equation were used throughout the study and greatly reduced the required instrumentation needed for the experiment.

4. Balance and Turntable

The NPS low-speed wind tunnel's external strain-gage balance and turntable, shown in Figure 13, was originally designed and built by NPS personnel in 1974 for the measurement of normal and axial forces and pitching moment on reflection-plane mounted models. Each external strain-gage bridge had four active legs for both sensitivity and automatic temperature compensation reasons. The normal and

axial moments were measured by four orthogonal strain-gage bridges cemented on flexures that were integral to the balance column. Each orthogonal pair was separated by a vertical distance of 26.5 inches. The balance installation, which rotates with the model, allows body axis forces (normal and axial) to be determined. [Ref. 9]

A balance calibration procedure and associated calibration rig was developed by Kersh with the help of NPS personnel [Ref. 10]. The balance was calibrated by Schmidt before this thesis as part of parallel research being conducted. The calibration procedure and associated calibration rig are described in his thesis [Ref. 9].

5. Data Acquisition Hardware

Each strain-gage bridge had an independent voltage supply for its signal conditioning assembly. Zeroing and calibration was allowed through each bridge's signal conditioner assembly. The differential bridge voltage from each balance channel's signal conditioner assembly was passed through a 1000-gain low-noise amplifier, routed to a National Instruments 12-bit MC-MIO-16-9 analog to digital conversion board that was attached to an IBM P/S-2 micro computer. The A-D board was capable of a 4.88mV resolution at a gain of one. The sampling period of the A-D board could be varied. It was found that a sampling period less than 2.25 millisecond was needed to average out an

unacceptable level of noise in the voltage output. A sketch of the data acquisition system is shown in Figure 14 [Ref. 9, 10].

6. Data Acquisition Software

The data acquisition software consisted of a Quick Basic program. The program, titled MULTI3.BAS, was a modified version of MULTI2.BAS used by Schmidt [Ref. 9]. The program controls a 12-bit analog to digital conversion card and the acquisition flow structure. The voltage outputs of the four balance channels were sampled 1000 times per sample group. Each sample per group was spaced by the software at 2.25 millisecond intervals to filter out high frequency noise. The voltage readings for each channel were then averaged. Multiple sample groups were recorded for each data point and were averaged to reduce low frequency noise. In general, noise and internal error were reduced to less than 1 percent. The average channel readings were used to calculate the normal and axial force using equations found in Appendix D. The normal and axial forces at the given angle of attack were used to calculate the lift and drag forces using equations (4) and (5). [Ref. 9, 10]

$$\text{DRAG} = (\text{Axial Force}) \sin(\text{AOA}) - (\text{Normal Force}) \cos(\text{AOA}) \quad (4)$$

$$\text{LIFT} = (\text{Axial Force}) \cos(\text{AOA}) + (\text{Normal Force}) \sin(\text{AOA}) \quad (5)$$

The data from the runs were stored for later reduction. The files generated by MULTI3.BAS were later manipulated by the spread sheet and converted lift and drag forces into C_L and C_D after accounting for test conditions and making necessary corrections for tunnel blockage and balance calibration. The data acquisition program is listed in Appendix D. Graphs were produced by Axum™ Technical Graphics and Data Analysis software after importing the spread sheets. [Ref. 9, 10]

C. EXPERIMENTAL CONDITIONS

There were numerous variables that could affect flow separation and vortex formation at high angles of attack. The following parameters were kept as constant as possible:

- Reynolds number = 6.87×10^5 to 6.91×10^5 based on wing MAC = 10.63 inches
- Test section DP = 8.44 cm of H₂O
- Test section velocity = 125 ft/sec
- Test section Mach number = 0.11

Wind tunnel low-frequency fluctuations in velocity were found to be strongly effected by tunnel temperature. Excessive velocity fluctuations were avoided by keeping the tunnel operating temperature below 70 degrees. If the tunnel temperature rose above this value, the tunnel was shut down and allowed to cool.

A 1/8-inch gap existed between the base plate of the model and the reflection plane. This gap was made possible by placing 1/8" thick washers under each platter attachment bolt. No slippage occurred from using the washers. The gap was needed to prevent the model from resting on the reflection plane and thus transferring loads to the reflection plane. No correction was applied for the gap distance. The gap did not adversely affect the experimental results since the experiment was a comparative study of lift enhancement between the blowing and non-blowing conditions. [Ref. 10]

The vibration of the tunnel itself could not be controlled resulting in both high and low-frequency noise. Wind tunnel vibration was possibly transferred to the tunnel balance by way of the model even though no contact is made between the tunnel and the balance. The electrical outputs of the strain-gage bridges were averaged over time to filter out random noise. Because a small number of sample groups were taken per data point, no elimination of a sample outside the standard deviation was done. [Ref. 10]

D. EXPERIMENTAL PROCEDURE

1. Pre-run Calibration and Test

The external strain-gage balance was initially calibrated by LT. Dean Schmidt as a part of a parallel thesis being conducted at the same time. Reference 9

illustrates the procedure that was used to find the coefficients for the calibration matrices. First, the calibration rig was attached to the balance turntable plate. The calibration rig head was lined up vertically and horizontally with the stand and cable using a level. The IBM P/S-2 microcomputer was then energized and MULTI2.BAS was loaded. The Pacific Amplifier gain switch was turned to one and the gain output was adjusted by a set screw to ± 50 μ volts. Voltages for each channel were read on a digital multimeter. The gain was increased to 1000 and the gain input adjusted to ± 500 μ volts. A-D board gain was set to 1. Channels (2), (4), (6), (8) were read and recorded. [Ref. 9, 10]

Initially no weight was attached to the calibration rig assembly. MULTI2.BAS prompted the user for the angle of attack of the model. The displayed axial and normal forces found should be less than 0.05 lbf. If the resultant normal and axial forces were greater than 0.05 lbf, then the offset voltages from channels (2) through (8) were checked and reentered. [Ref. 10]

Once the balance was zeroed the turntable was rotated to 0 and 90 degrees. Suspending weights from the calibration rig with the turntable at 0 degrees imparted a pure normal moment to the balance. Rotating the turntable to 90 degrees and suspending weights induced a pure axial

moment on the balance. Successively larger weights were then hung from the balance calibration rig and the normal and axial forces calculated by the program MULTI2.BAS. After each weight was hung from the balance the zero offsets of the channels were checked to ensure that they had not drifted. Zero offsets for each channel were updated before each experimental run. [Ref. 9, 10]

2. Testing Procedures

The key to any successful experiment is standard procedures. For this purpose a standardized checklist was developed to insure that all steps were carried out and in the correct order. This checklist is attached in Appendix E. A separate checklist was always used for each wind tunnel session. Any deviations from the checklist, observations critical to data, or misentered parameters into MULTI3.BAS were annotated on the back side of the checklist to insure the information was taken into account during data reduction. For example, if the angles of attack were entered wrong into the program, the lift and drag information in the data file would be erroneous. The axial and normal forces were still accurate. Instead of reperforming the test, inserting formulas (4 & 5) into the spreadsheet corrected the error.

The initial section on the checklist described the conditions of the test. MULTI3.BAS's first question asked

for the last six letters of the output data files. The information in the first section of the checklist was used in the determination of the file name. This was so that the files could later be easily identified. The first two letters in the data files were determined by MULTI3.BAS to distinguish between blowing and non-blowing, force and voltage files. The remaining characters were the blowing tube position (Figure B4), the blowing tube number (Figure 10), and the inclination angle. Negative inclination angles were preceded by the letter 'N' since '-' was not a valid character in DOS filenames. MULTI3.BAS was capable of appending multiple data files to each other. This allowed multiple wind tunnel runs to be kept in a single data file.

The first step in each wind tunnel testing session was to zero the ambient pressure on the liquid and digital manometers. For the liquid micromanometer this was accomplished by setting the dial to 0.00 and adjusting the screw under the reservoir until the bottom of the meniscus of the fluid was in line with the crosshair. The digital manometer was adjusted by setting the read-out to zero using the "zero" knob. The liquid micromanometer was then set to the desired height of fluid (8.44 cm for this experiment) by use of the electric motor.

The model was then configured for the test. Shop air hoses were first connected to the regulator and then to

the model. The blowing tube for the test was then installed into the proper port and secured by the set screws inside the model. The model was then reassembled and vacant blowing ports were taped over. Tight tool control was required to prevent foreign object damage (FOD) to the wind-tunnel fan section. Before the first run of the day, FOD sweeps were conducted in the settling chamber, the test section and the diffuser aft of the test section.

Before each test run, a verification of the proper angle of attack (AOA) on the lower turntable section of the balance was performed. The model was constructed with the up-side towards the outside viewing window. The turntable's AOA markings were for a model constructed with the up-side towards the inside viewing window. To achieve a positive AOA on the model, the model was mounted 90° off the balance axis. The turntable value of AOA was the value entered into MULTI3.BAS. AOA for the model was determined by MULTI3.BAS by subtracting the desired AOA from 90° . Lift and drag equations (4) & (5) compensate for this mounting orientation.

The next step was to zero out the amplifiers. This step was the same as earlier described in the Pre-calibration Section. Adjusting the "out" screw was only required once every four hours and for the first run of the day. After the amplifiers were adjusted to zero, the signal

from the multiplexer was verified and adjusted as necessary. The span was set as close to 10.0 volts as possible and the zero as close to 0.0 μ volts as possible. The span, as a rule, only required adjusting once a day and when going to and from high angles of attack ($AOA > 50^\circ$). The cause for the high AOA drift in the zero reading was never determined. Visual inspection ruled out binding of the model or balance on the reflection plane. Data collected from high AOA runs were free of any biases if the multiplexer was adjusted.

The next step was to initialize MULTI3.BAS to test parameters. Since MULTI3.BAS was designed to operate with parallel data files, a different color screen was presented depending on the section of the program being executed. Color scheme is found in the program listing. The first step in the process was to record tare values. MULTI3.BAS recorded and applied tare values automatically. Tare values were then confirmed by taking "no-force" readings and verifying the axial and normal force read-outs to be less than 0.01 lbs. If the forces were less than 0.01 lbs, the program was restarted and new tare values recorded.

3. Tests Holding C_μ Constant Varying AOA

The first type of test conducted was comparing the blowing case to the non-blowing case over a range of AOA holding C_μ constant. This test was conducted over a series of wind tunnel runs with the data files being appended to

each other. The purpose in conducting each AOA sweep in multiple runs was three-fold. First, it allowed for a reduction in amplifier drift. Shorter runs resulted in smaller drift affecting data less. Second, shorter runs helped to keep tunnel temperature from reaching above 70°F. Third, it allowed for a measurement of a blowing tare at the beginning or end of each AOA recorded. The blowing tare is the momentum force exerted by the jet of air on the model. It was later determined that the blowing force induced was more than the momentum force of the jet. The recorded tare values contained significant aerodynamic forces from the jet blowing over the surface of the wing. For this reason, the blowing tare was never subtracted from the data, but was instead considered an actual effect of blowing.

There were some disadvantages of multiple runs as well. First, there was a significant increase in the amount of time required to collect the data. This was due to the time required to re-zero all the amplifiers. Second, it was hard to precisely set the fluid to the exact micromanometer reading as the prior run. Since blowing was only being compared to the non-blowing for the same AOA, this did not effect the results significantly.

After tares were taken the wind tunnel was started and the airspeed was set to 8.44 cm of water (125 ft/s). Data was collected for angles of attack from 0° to 70°.

Five sample groups were taken for each of the non-blowing and blowing cases. The model's AOA was then increased to the next position and a second set of data was recorded. Angle-of-attack increments were 5° for all relatively linear portions of the lift and drag curves and 2.5° for the non-linear portions.

Angle-of-attack sweeps were conducted for the following:

- Blowing Port #1, Jet $\angle=45^{\circ}$, Incl. $\angle=0^{\circ}$, $C_{\mu}=0.0035$
- Blowing Port #1, Jet $\angle=45^{\circ}$, Incl. $\angle=0^{\circ}$, $C_{\mu}=0.0022$
- Blowing Port #1, Jet $\angle=45^{\circ}$, Incl. $\angle=10^{\circ}$, $C_{\mu}=0.0022$
- Blowing Port #2, Jet $\angle=45^{\circ}$, Incl. $\angle=0^{\circ}$, $C_{\mu}=0.0022$
- Blowing Port #3, Jet $\angle=45^{\circ}$, Incl. $\angle=-25^{\circ}$, $C_{\mu}=0.0022$

Data for Blowing Port #2, Jet angle = 45° , Inclination angle = 0° , $C_{\mu}=0.0022$ was accidentally destroyed irretrievably during backup. The test was not conducted again due to lack of time.

After each test run was completed the wind tunnel was shut down. The vents and doors were opened to assist in the stopping of the airflow. Opening the doors also allowed for air to be exchanged as the airflow slowed down, thus allowing more runs to be conducted before the tunnel temperature reached 70°F . When the airflow came to rest, which was confirmed by a 0.00 reading on the digital

manometer and a stable digital multimeter reading on one of the amplifiers, two final readings were taken to measure hysteresis and drift. The averages of these two readings were subtracted from each sample during data reduction. Data output files were recorded on a disk and later processed on spreadsheets applying all error corrections (see Section III.E).

4. Tests Holding AOA Constant Varying C_{μ}

The second type of test conducted varied C_{μ} while holding angle of attack constant at 35° . This method was chosen to compare different blowing configurations while saving the time that was expended in the AOA sweep procedure. An AOA of 35° was chosen for two reasons. First, there were two regions in the previously recorded data that showed the maximum effect of blowing. The first region ($AOA \cong 20^{\circ}$) was where the wing initially started to stall. The second region ($AOA \cong 35^{\circ}$) was in the fully-stalled-wing region. The second region was chosen since it was primarily vortex flow.

Procedures for this experiment were similar to those in the previous section. However, each run was conducted all at once instead of in segments. This difference is primarily due to the need of a precise velocity maintained during each angle of attack. In the previous section only two sample groups were taken for each angle of attack. This

experiment required ten sample groups. Table 1 lists the sample groups taken during this procedure. Table 2 lists the different blowing configurations tested.

Table 1: Plenum Pressure Sample Groups

Plenum Pressure (psig)	Blowing Coefficient (C_u)
40.0	0.0035
35.0	0.0030
30.0	0.0026
25.0	0.0022
20.0	0.0017
15.0	0.0013
10.0	0.0009
5.0	0.0004
0.0	0.0000

Table 2: Blowing Configurations Tested

Blowing Port	Jet Angle	Incl. Angles
1	30	0, 10, 25, -10
1	45	0
1	60	0, 10, 25, -10
2	30	0, 10, 25
2	45	0, 10, 20, -10
2	60	0, 10, 25, -10
3	30	-90
3	45	-25
3	60	-20

After initializing all the equipment and recording tare values, the wind tunnel was started and set to 8.44 cm of water (125 ft/s). Blowing was turned on and the plenum pressure was set to 40.0 psig. This value was near the maximum plenum pressure achievable with shop air. At this pressure, a constant watch on the plenum pressure gage was required. It was found that as the shop-air storage tank

bled down, the plenum pressure could drop to 37.5 psig before the shop air compressor activated. Once the compressor started the pressure would maintain the desired pressure for three minutes. The best technique was to turn on blowing and set to 40 psig before starting the tunnel. Wait until the compressor kicked in and then shut the T-valve. Then start the wind tunnel and turn the blowing back on. Plenum pressures ≤ 35.0 psig were not effected by the compressor. After completing sample groups at 40 psig, pressure was decreased in 5 psig increments until 5.0 psig. After the 5.0 psig sample group, the T-valve was shut and one last sample group was taken with no blowing.

For reasons discussed in Section IV.D.1, a modification was made to the above procedures. Sample groups were enlarged from five samples to ten samples to obtain better results. Also, a non-blowing sample group was placed first before any blowing groups were taken. This group was later compared to a non-blowing group taken at the end of each run in order to compute a drift.

The average run time for this series of experiments was 11 minutes. During this time the wind-tunnel temperature would increase 1°F for tunnel starting temperatures $< 65^{\circ}\text{F}$ and would increase 2°F for tunnel starting temperatures $> 65^{\circ}\text{F}$. Opening all cooling doors

after each run was essential if it was desired to conduct more than six wind-tunnel runs in a session.

E. EXPERIMENTAL CORRECTIONS

For all wind tunnel testing it is required that certain corrections to the lift and drag information be made. These corrections were applied after the testing was completed as part of the spreadsheet data reduction. The corrections applied were wake blockage and solid blockage corrections and tunnel-velocity drift corrections. Wall interference corrections were not performed. Since this was a comparative study, the lack of wall interference corrections did not adversely effect the results except as mentioned in Section IV.B.

1. Wake and Solid Blockage Corrections

Corrections of particular importance were solid blockage and wake blockage corrections. The total solid- and wake-blockage corrections can be represented by: [Ref. 15]

$$\epsilon_t = \epsilon_{sb} + \epsilon_{wb} \quad (6)$$

Where:

ϵ_t	total blockage correction
ϵ_{sb}	solid blockage correction
ϵ_{wb}	wake blockage correction

This can also be estimated for models where corrections cannot easily be derived by: [Ref. 10, 15]

$$\epsilon_1 = \frac{1}{4} \cdot \frac{\text{Model Frontal Area}}{\text{Test Section Area}}$$

Equation (7) is the equation used for the blockage correction during this study. The blockage factor, ϵ_1 , was then applied to lift and drag coefficients by correcting dynamic pressure (q) and freestream velocity (V_∞) using equations (8) and (9). [Ref. 15]

$$q = q_m (1 + \epsilon_1) \quad (8)$$

$$V_\infty = V_{\infty m} (1 + 0.5\epsilon_1) \quad (9)$$

Where:

q	adjusted dynamic pressure
q_m	measured dynamic pressure
V_∞	freestream velocity
$V_{\infty m}$	measured freestream velocity

Model frontal area is a function of angle of attack. Effects of blockage were considered negligible at low AOA. Thus the model's axial cross-sectional area was not applied. The model's longitudinal cross-sectional area was determined to be 1.392 ft². Using the wind tunnel cross-sectional area of 8.75 ft², the total blockage correction became: [Ref. 10]

$$\epsilon_1 = .03977 \sin(\text{AOA}) \quad (10)$$

2. Tunnel Velocity Drift Corrections

As mentioned in Section III.D.4, procedures were modified to allow for the correction of test-section velocity changes during the tests where C_μ was varied. The test run for each C_μ sweep lasted approximately 11 minutes. During this time, the velocity slowly decreased the height of the meniscus in the micromanometer (≈ 0.15 cm). The result was a declining force on the model. The magnitude of this drift in forces was approximately the same magnitude as the effect of blowing. As seen later in the Section IV.D.2, this drift made high C_μ 's appear excessively effective in lift enhancement.

To correct for this drift, an additional sample group of baseline non-blowing data was taken at the beginning of each test run. The difference between this sample group and the non-blowing sample group obtained at the end of the test run was then divided by the total number of samples. This process yielded a drift-per-sample slope that was then linearly applied to the overall data. The effects of this drift correction are discussed in the Section IV.D.2.

3. Low Frequency Velocity Surge Correction

It was noted that a periodic surge in the micromanometer reading with an amplitude of approximately 0.05 cm of H_2O was present during wind tunnel operation.

The period of the surge was approximately 4 seconds. Source of this pressure surge was never discovered. Each group of 1000 samples was spaced apart by 2.25 seconds. This spacing acted as a low-pass filter of the data. It was decided to increase the number of samples from five to ten to reduce the standard deviation of the results. This was the only correction available at the time to correct for the surge.

IV. DISCUSSION AND RESULTS

A. OVERVIEW

This section discusses the results obtained from this study. The study consisted of two types of tests described in Sections III.D.3 and III.D.4. Data collected was imported into Microsoft Excel 4.0 for Windows™ where the individual samples of each sample group were collected and averaged. Once collected and averaged the amplifier drift and hysteresis were subtracted. Velocity drifts, for applicable tests, were also subtracted at this point. Excel™ user defined macros were used to calculate blockage errors, convert cm of H₂O to lbf/ft², and convert forces into coefficient form. Macros were saved under the filename THESIS.XLM. Resulting tabular data was exported to Axum™ graphical software in Lotus™ format. [Ref. 16, 17]

B. BASELINE MODEL PERFORMANCE

Since the configuration of the model was patterned after the NADC study by Kern, it is important to compare the baseline results of the two studies. Figure 15 is the model's lift curve. The curve shows the characteristic linear lift-curve slope from 0° to 22° AOA. Above 22° angle of attack the curve flattened out as the outer wing stalled. In this region most of the lift being generated was from the

strake vortex extending over the wing. The wing maintained at or above $C_L = 1.45$ until 47° AOA. Above 47° AOA the curve experienced a sharp drop-off as the vortex started to disintegrate. A wing reference area of 0.969 ft^2 (projected through the fuselage of the model) was used for all coefficient calculations. [Ref. 8]

A comparison of Figure 15 with Figure 16 [Ref. 8] shows that the wind-tunnel model had a higher maximum lift and steeper lift curve slope ($C_{L\alpha}$) than Kern's computer model. This was probably due to the effect of using a round leading edge on the wing, whereas the computer wing was a sharp flat plate. Also the wind-tunnel model had a fuselage section that also generated lift. The computer model started to exhibit a stall at 19° AOA. The wind-tunnel model's stall was delayed until 24° AOA. The wind-tunnel model's baseline $C_{L\alpha}$ was $0.066 / \text{deg}$, while the computer model's $C_{L\alpha}$ was $0.050 / \text{deg}$. Another factor influencing the wind-tunnel model's results was the lack of wall interference corrections. This this lack of correction tends to make the $C_{L\alpha}$ of the model's lift curve appear steeper. Both figures showed a relatively flat curve in the stall region indicating vortex flow. [Ref. 8]

Figure 17 shows the model's drag polar. Again the model out performed the predicted values by the computer study (Figure 18 [Ref. 8]). The model's drag polar showed a

higher lift per drag throughout the spectrum. C_{D0} for the model was < 0.02 . The computer study showed a C_{D0} approximately 0.02. [Ref. 8]

C. TESTS HOLDING C_μ CONSTANT VARYING AOA

Four tests were conducted using the procedures previously outlined in Section III.D.3. Three plots were generated for each of the tests: a lift curve, a drag curve, and a plot of the ΔC_L and ΔC_D versus AOA.

1. Blowing Port #1, Jet $\angle=45^\circ$, Incl. $\angle=0^\circ$, $C_\mu=0.0035$

Figures 19a & 19b show the lift and drag curves for the wind-tunnel model with and without blowing turned on. Figure 19c shows the ΔC_L and ΔC_D vs. AOA for the same blowing configuration. At 0° AOA, blowing seemed to slightly increase the lift. This effect was probably not due to any modification of the vortex since none should have been developed at this angle of attack. Drag was virtually unaffected.

Figure 19c shows almost an oscillatory nature to the ΔC_L curve. Peaks were found at 20° , 38° , 47° and 56° AOA. The maximum peak was found at 20° AOA. The figure shows a $\Delta C_L = 0.05$, which was a 3.75 percent increase over the non-blowing baseline. Standard deviation of this sample group was found to be equal to a ΔC_L of 0.0034. Figure 19a shows that the data point for the blowing-on case was in line with the linear portion of the lift-curve slope.

Therefore, it was believed that the majority of the increase observed was due to the reattachment of the flow over the wing. Thus blowing delayed the stall of the model's wing.

The peaks in Figure 19c at 38° and 47° AOA are in the pure vortex-flow region. The maximum and minimum values of these peaks and valleys are nearly identical with $\Delta C_{Lmax} \cong 0.026$ and $\Delta C_{Lmin} \cong 0.009$. This effect was probably due to constructive and destructive interference between two vortex sheets.

As two vortex sheets of the same direction of rotation move closer together, the momentum of the flow of one vortex upon the other creates a shearing effect. An oscillatory flowfield develops that is similar to waves upon the ocean [Ref. 18]. This effect would create an oscillatory pressure field as the two vortex sheets move closer together. A flow visualization study will be required to determine which vortex sheets are interfering.

Figures 19a and 19c show that the ΔC_L peaks are always 2.5° after the C_L peaks. This may give a clue as to which vortex sheets were interfering. Three probable candidates are the wing and strake vortex sheets, the strake and jet plume vortex sheets [Ref. 4] or the wing and forebody vortex sheets.

Figure 19b shows the drag curve for this blowing configuration. It can clearly be seen that the blowing and non-blowing curves are the same. The effects of blowing seemed to be limited to the lift direction. Figure 19c confirms this with seven of the sixteen sample groups lying within the standard error of zero. Below 30° AOA the trend indicates that blowing decreased drag slightly. Above 30° the profile tends to match that of the ΔC_L curve with blowing slightly increasing drag. The tendency of the ΔC_D profile to match that of ΔC_L increases with AOA. This makes sense since total drag is mostly induced drag at high AOA.

All of the drag curves (Figures 19b, 20b, 21b, & 22b) exhibited the same behavior. All curves show negligible effects of blowing with a slight tendency to decrease drag $< 30^\circ$ AOA and with induced drag effects $> 30^\circ$ AOA. For these reasons, the discussion of the effects of blowing will be limited to lift effects from here on.

2. Blowing Port #1, Jet $\angle=45^\circ$, Incl. $\angle=0^\circ$, $C_\mu=0.0022$

The second test run conducted was an attempt to determine the best blowing coefficient for the remainder of the tests (Figures 20a, 20b & 20c). The results of this test run are discussed in detail in Section IV.D.2. From this run a blowing coefficient of 0.0022 was determined to be the best and was used for the remainder of the study.

Following the optimum C_{μ} determination, an AOA sweep of the previous blowing configuration was conducted for AOA's from 20° to 65° . Figure 20a is an expanded plot of the lift curve of this region and Figure 20c shows the ΔC_L plot for this region. The vertical lines extending through the data points in Figure 20a show the maximum and minimum reading of each sample group. Essentially the same effects seen for the $C_{\mu}=0.0035$ plot were also seen in this plot. The ΔC_L curve was still found to be oscillatory. Peak ΔC_L points lagged the peak C_L points by 2.5° AOA.

There are two distinct differences to the plots. A new peak and a deep dip were formed. A new maximum ΔC_L was created at 30° AOA. This point was immediately followed by a destructive blowing point at 32.5° AOA (Figures 20a & 20c). This could be the result of coupling by two vortex sheets such as shown by LeMay [Ref. 3]. Again, flow visualization will be needed to confirm this possibility.

Other differences between the two tests were that the ΔC_L peak at 47° AOA disappeared and the first peak (20° AOA) was either shifted forward a few degrees or is at a lower magnitude. Figure 20c only shows a portion of the peak. The later peaks and valleys are assumed to still be caused by constructive and destructive interference between vortex sheets.

3. Blowing Port #1, Jet $\angle=45^\circ$, Incl. $\angle=10^\circ$, $C_\mu=0.0022$

The next test was conducted with the blowing tube angled up away from the strake by 10° (Figures 21a, 21b & 21c). The results from this test more closely resemble the previous test than the first test. Figure 21c has the double high magnitude peaks at 22.5° and 30° AOA. The first peak was believed to be the same as the first peak in Figure 19c and 20c. The extension of $C_{L\alpha}$ and the apparent delay in stall were the reasons for believing that it was a possible reattachment of the flow during the initial stall. The second peak appears to be a result of vortex interaction. There was still an area of destructive interference from 32.5° to 35° AOA.

The major difference in this test was that there was no oscillatory effect above 40° AOA. The ΔC_L curve slowly tapered off above this point. Above 60° AOA the effect of blowing becomes destructive. The lack of oscillatory behavior would be indicative of a lack of vortex interaction above 40° AOA. The tapering effect would thus result from the strake vortex moving farther away from the wing. This would also tend to indicate that the vortex sheets interacting in this study are not the forebody and strake vortex sheets. The forebody vortex would normally be above the strake vortex. Angling the blowing jet up would pull the strake vortex up through induction [Ref. 3]. Thus, if

the strake and forebody vortex sheets were the ones interacting, an inclination angle of 10° would cause greater oscillatory effect.

Figure 22 is a plot of all three of the previous tests superimposed upon each other. It is clear from this plot that the peaks at 20° AOA are common to all blowing configurations. The peaks at 30° AOA are common only to the $C_\mu=0.0022$ curves. The peak and rise at 37.5° AOA are common to all curves, except it is more pronounced at an inclination angle of 0° . The peak at 47.5° AOA is only present for $C_\mu=0.0035$. Finally, the peak at 55° AOA is only present for inclination angle = 0° .

4. Blowing Port #3, Jet $\angle=45^\circ$, Incl. $\angle=-25^\circ$, $C_\mu=0.0022$

The last test comparing the effects of blowing with angle of attack was conducted at blowing port #3. The same blowing tube used on the top side of the strake was mounted underneath. The tube was angled in towards the strake (incl. angle = -25°). It was hoped that this blowing configuration would provide positive results over the entire range of AOA. The concept behind this hope was that the strake vortex sheet intensity would be increased by increasing the mass flow of air circumnavigating around the edge of the strake. Results did not meet expectations.

Figures 23a, 23b, & 23c show a blowing effect of significantly lower magnitude. Some of the same

characteristics of the topside blowing were found on the bottom side. These were:

- A peak at 20° AOA
- A destructive interference point at 27.5° AOA
- Negligible effect on drag

Although a region similar to the last case (Figure 21c) was found at $AOA > 30^\circ$, there was a solitary peak found at 45° AOA. The only other peak that could correspond to that peak was the peak found at 47.5° AOA in the first case (Figure 19c). However, that peak was part of an oscillatory region and this peak was not. Again, flow visualization will be required to determine what happened at this point.

D. TESTS HOLDING AOA CONSTANT VARYING C_μ

1. Overview

Twenty-three test runs were conducted using the procedures previously outlined in Section III.D.4. Tables 3 and 4 list each run and their respective Figure numbers. One plot of C_L vs. C_μ was generated for each run. Every plot displayed one standard deviation for each of the sample groups in the form of error bars. Although recorded, C_D vs. C_μ curves were not plotted and are not discussed for reasons mentioned in Section IV.C.1.

The results of the previously mentioned test runs were for the most part inconclusive. Almost all the curves

were flat, showing virtually no change with respect to C_μ . For almost every blowing configuration, the difference between the C_μ 's sampled was within the standard error of the adjacent sample group. The initial runs listed in Table 3 were taken before the discovery of a drift in the wind tunnel velocity. These runs did not have drift corrections applied to them. The effects of the drift are discussed below. Scheduling limitations for the wind tunnel prevented performing these test runs again.

Table 3: Blowing Configurations Without Drift Checks

Blowing Port	Jet Angle	Incl. Angles	Figure #
1	45	0	24
2	45	0, 10, 20	25(a b c)
3	30	-90	26
3	45	-25	27

Table 4: Blowing Configurations with Drift Checks

Blowing Port	Jet Angle	Incl. Angles	Figure #
1	30	0, 10, 25, -10	28 (a b c d)
1	60	0, 10, 25, -10	29 (a b c d)
2	30	0, 10, 25	30 (a b c d)
2	45	-10	25d
2	60	0, 10, 25, -10	31 (a b c d)
3	60	-20	32

2. Blowing Configurations Without Drift Corrections

During the early runs the liquid micromanometer was adjusted, if necessary, after each adjustment in the plenum pressure. This procedure was performed in attempt to keep the results as accurate as possible. It was not until six

test runs were completed that it was noticed that the effect of blowing on the wing/strake was equivalent to adjusting the micromanometer column height $1/2$ of the meniscus of the fluid. Thus every increase in the micromanometer height resulted in a peak in the C_L vs. C_μ curve.

The time required to conduct a C_L vs. C_μ test run was 11 minutes. During that time the micromanometer column of fluid would decrease approximately 0.15 cm, or roughly the height of the meniscus. After the effects of adjusting the fluid column were noticed, the test procedure was changed to allow the fluid column to drop and adjust for the drift in the data reduction procedures. This adjustment was accomplished by taking an initial non-blowing sample group before any blowing sample groups were taken. Another non-blowing sample group was taken at the end. A slope of $\Delta(\text{force value})$ per sample was calculated and then linearly applied to the results. The effects of this adjustment are discussed in Section IV.D.4.

a) Early Test Runs

The first blowing configuration in Table 3 (Figure 24) was also the first test run attempting to find the optimum blowing rate. It is the test run mentioned in Section IV.C.2. This plot is the clearest example of a peak being introduced by the adjustment of the micromanometer-fluid column. Just before taking the reading at 25 psi

($C_\mu=0.0022$), it was noticed that the micromanometer fluid was a meniscus height too low. The adjustment was made and the sample group taken. According to notes on the back of the test run checklist, after this run it was noticed that the fluid was now half a meniscus high and was adjusted. At the time it was not realized that the effects of adjusting the column were so sensitive. The decision to conduct all the remaining angle-of-attack studies at $C_\mu=0.0022$ was based on this plot. Most of the figures mentioned in Table 3 exhibit to some degree these operator-induced peaks.

Figures 25 through 27 also exhibit the sloping effect as the micromanometer-fluid level falls. Adjustments to the micromanometer fluid were only made when the fluid column was clearly half a meniscus off. These plots had only minor adjustments and showed the slope effect of the curve caused by the gradual decrease in velocity. The right sample groups, taken at $C_\mu=0.0035$, were taken first and have higher force readings. The left sample groups, taken at $C_\mu=0.000$, were taken last and exhibit lower readings.

3. Blowing Configurations With Drift Checks

Table 4 is a list of all the test runs that were conducted after the drift check procedure was introduced. During each of these runs no adjustment was made to the micromanometer-fluid column. Almost every plot shows that there were only negligible effects with respect to blowing

rate. There were some rises and dips in the various plots. However, most of these were within the standard error as exhibited by the error bars. Any trends noted are described in the following Sections.

a) Blowing Port #1

Six test runs varying C_μ at blowing port #1 were conducted after drift corrections were applied. These were with tube #1 (jet angle 30°) and tube 3 (jet angle 60°). All the results for tube #1 were within the standard error of each other (Figure 28a, 28b, 28c, & 28d). All curves were flat and did not even show a difference between blowing and non-blowing.

Most of tube #3 results did show a significant increase in lift for the blowing compared to non-blowing (Figures 29a, 29b, & 29d). Above $C_\mu=0.0004$ the lines were flat and did not show an optimum point. Figure 29d does show a gradual trend favoring the highest blowing rate. These are still within the standard error of each other.

b) Blowing Port #2

Eight test runs varying C_μ at blowing port #2 were conducted after drift corrections were applied. Blowing tube #1 (Jet angle = 30°) had the same effect at port #2 as it had at port #1 (Figures 30a, 30b, & 30c). Only Figures 30a and 30b show any effect from blowing and

the effect was within the standard error. All curves are flat and without significant peaks or dips.

Tube #2 had only one test run (Figure 25d) that was conducted after the drift correction was applied. Its effect was the same as Figure 29d; showing a gradual increase in lift as C_{μ} increased. Most points are still within the standard error of each other.

Blowing tube #3 at inclination angles of 0° and 10° are the only two blowing configurations where the plot exhibits a possible optimum at a C_{μ} other than $C_{\mu}=0.0035$ (Figures 31a, & 31b). Although the curvatures of these plots are gradual and within the standard error, C_{μ} 's between 0.0013 and 0.0022 appear to be optimum. Above $C_{\mu}=0.0022$ there is a distinct drop in effectiveness, particularly in Figure 31a. All other inclination angles (Figure 31c, & 31d) showed that blowing was effective but did not show any optimum points.

c) Blowing Port #3

Only one test run varying C_{μ} at blowing port #3 was conducted after drift corrections were applied. It was for blowing tube #3 (Jet angle = 60°) and at an inclination angle of -20° (underneath the strake angling up toward it; Figure B4 of Appendix B). Its plot (Figure 32) resembled the mirror image of the blowing configuration (Figure 29d). Each showed an increase in lift from blowing when compared

to the non-blowing case. The trend is gradual favoring the maximum blowing ($C_{\mu}=0.0035$), but within the standard error of the other sample groups.

V. CONCLUSIONS AND RECOMMENDATIONS

A. CONCLUSIONS

The objective of this low-speed wind-tunnel study was to investigate the lift and drag effects of pneumatically controlling a leading edge vortex generated by a half-span, generic-fighter-wing model. Baseline results were compared to numerical predictions for a wing of the same geometry [Ref. 8]. Particular emphasis was on the acquisition of quantitative lift and drag data. Blowing ports of different positions and angles about the strake were examined. Effects of blowing upon the high pressure side of the strake were also investigated.

The baseline lift and drag curves out-performed the predictions of Kern for a generic fighter wing of the same shape. The model had a 32 percent increase in the lift curve slope and a 47.6 percent increase in maximum lift. Stall on the wind-tunnel model occurred 5° AOA later than the Kern prediction. C_{D0} was nearly identical. These comparative results to Kern's study must be tempered by the knowledge that different reference areas and Reynolds numbers were used. Also this study added a fuselage that also contributed to lift. [Ref. 8]

Blowing appeared to partially reattach the flow during the initial stages of wing stall. Blowing increased lift by a maximum of 3.75% in the vortex flow region. The effect of blowing appeared oscillatory with respect to angle of attack. Oscillations were believed to be the result of the interactions of two or more vortices. The peak ΔC_L values consistently occurred 2.5° AOA after the peak C_L values. Peak ΔC_L values for different blowing configurations were consistent in magnitude. Some correlation between blowing configurations and peak ΔC_L locations were noted. The effect of blowing upon drag was negligible. Blowing on the high pressure side of the strake did increase lift, but was not as effective as blowing on the low pressure side.

Blowing rates were varied from $C_{\mu} = 0.0$ to 0.0035 while holding angle of attack constant at 35° in an attempt to determine an optimum. The change in blowing rates in this range seemed to have little effect upon ΔC_L values. Most blowing configurations showed a definite increase in lift when compared to non-blowing values. The differences between ΔC_L values for $C_{\mu}=0.0005$ to $C_{\mu}=0.0035$ were within the standard error of the individual data-sample groups.

B. RECOMMENDATIONS

The following are recommendations for future experimental research and suggestions for reducing the error:

1. Flow Visualization

There is a need to understand the cause of the oscillatory nature in the ΔC_L values requiring flow visualization. Understanding this phenomenon can only be accomplished by understanding which vortices are interacting and how they are interacting. The process of understanding these interactions is only possible through flow visualization or flowfield mapping. There are three flow visualizations that have been performed by previous authors:

- Smoke and Laser Light Sheet
- Laser Doppler Anemometry
- Water-tunnel Testing

It is recommended that water-tunnel testing on an identical model of smaller scale be conducted in addition to any wind-tunnel flow visualization. Differences between the results of Roach and LeMay, on identical (but different scale) models, suggested that the blowing effect may not have been a function of C_{μ} . Since the Naval Postgraduate School has both types of facilities, the school is in the best position to examine any discrepancies. [Ref. 1,2,3, & 4]

2. Provide Velocity Sampling to Reduce Error

As mentioned in Section IV.D.2, the effect of blowing was found to be masked within the standard error cause primarily by velocity fluctuations. Providing

velocity sampling as part of the data sampling would reduce the errors when results are placed in coefficient form. By applying a more precise velocity to equation (11), the lift term will be more balanced out by the velocity term.

$$C_L = \frac{\text{Lift}}{\frac{1}{2} \rho V^2 S} \quad (11)$$

3. Conduct More Tests Varying C_μ at AOA's other than 35°

The test varying C_μ at constant angle of attack was conducted at 35° AOA. This was a region where the ΔC_L peak was not consistent during all blowing configurations tested (Figure 22). Most common peak angles of attack were at 20° , 30° , and 37.5° . This study could be conducted simultaneously with flow visualization with two thesis students working in conjunction with each other. One student could perform force measurement as the other records the positions of the vortices. This would be more efficient and reduce wind tunnel time required.

4. Conduct More Tests Varying AOA at Constant C_μ

There is a need to study more in-depth the angle of attack profiles of different blowing configurations. The accidental deletion of the angle of attack experiment conducted at Blowing Port #2 resulted in no data being

available for the position. Future runs need to concentrate on the region above 19° AOA.

LIST OF REFERENCES

1. Wright Laboratory Final Report WL-TR-91-3065, "Experimental Investigation of the Effects of Blowing on Bursting of Strake Vortices," by R. A. Roach, and J. M. Kuhlman, July 1991.
2. Roach, R. A. and Kuhlman, J. M., "Strake Vortex Control Using Pneumatic Blowing," AIAA Paper 91-3274-CP, 1991.
3. LeMay, S. P. and Rogers, L. W., "Pneumatic Vortex Flow Control on a 55 Degree Cropped Delta Wing with Chined Forebody," AIAA Paper 90-1430, June 1990.
4. Roth, K. R., Fearn, R. L. and Thakur, S. S., "Evaluation of a Navier-Stokes Prediction of a Jet in a Crossflow," *Journal of Aircraft*, Vol. 29, No. 2, pp 185-193, March-April 1992.
5. Celik, Z. Z. and Roberts, L., "Aircraft Control at High-Alpha by Tangential Blowing," AIAA Paper 92-0021, January 1992.
6. Cornelius, K. C., Pandit, N., Osborn, R. F., and Guyton, R. W., "An Experimental Study of Pneumatic Vortex Flow Control on High Angle of Attack Forebody Model," AIAA Paper 92-0018, January 1992.
7. Guyton, R. W., and Maerki, G., "X-29 Forebody Jet Blowing," AIAA Paper 92-0017, January 1992.
8. Kern, S. B., "Numerical Investigation of Vortex Flow Control through Small Geometry Modifications at the Strake/Wing Junction of a Cropped Double-Delta Wing," AIAA Paper 92-0411, January 1992.
9. Schmidt, D. C., "Lift Enhancement Using a Close-Coupled Oscillating Canard," Master's Thesis, Naval Postgraduate School, Monterey, California, September 1992.
10. Kersh, J. M., Jr., *Lift Enhancement Using Close-Coupled Canard/Wing Vortex Interaction*, Master's Thesis, Naval Postgraduate School, Monterey, California, December 1990.

11. *NPS Laboratory Manual for Low Speed Wind Tunnel Testing*, Rev. Department of Aeronautics and Astronautics, Naval Postgraduate School, Monterey, California, August 1989.
12. Telephone Conversation between Richard Chumita, Materials Engineering, Norton Plastics Corporation and the author, 12 August 1992.
13. Zucker, R. D., *Fundamentals of Gas Dynamics*, pp. 235-264, Matrix Publishers, Inc., 1977.
14. Hewlett Packard Company, *HP Solve Equation Library Application Card Owner's Manual*, p. 193, July 1990.
15. Pope, A., and Harper, J. J., *Low-Speed Wind Tunnel Testing*, John Wiley & Sons, Inc., 1966.
16. Microsoft Corp., *Microsoft Excel 4.0 for Windows User's Guide*, 1992.
17. TriMetrix, Inc., *Axum User's Manual*, 1989.
18. Kuethe, A. M., and Chow, C. Y., *Foundations of Aerodynamics: Bases of Aerodynamic Design*, 3rd ed., John Wiley & Sons, Inc., 1976.

APPENDIX A. FIGURES

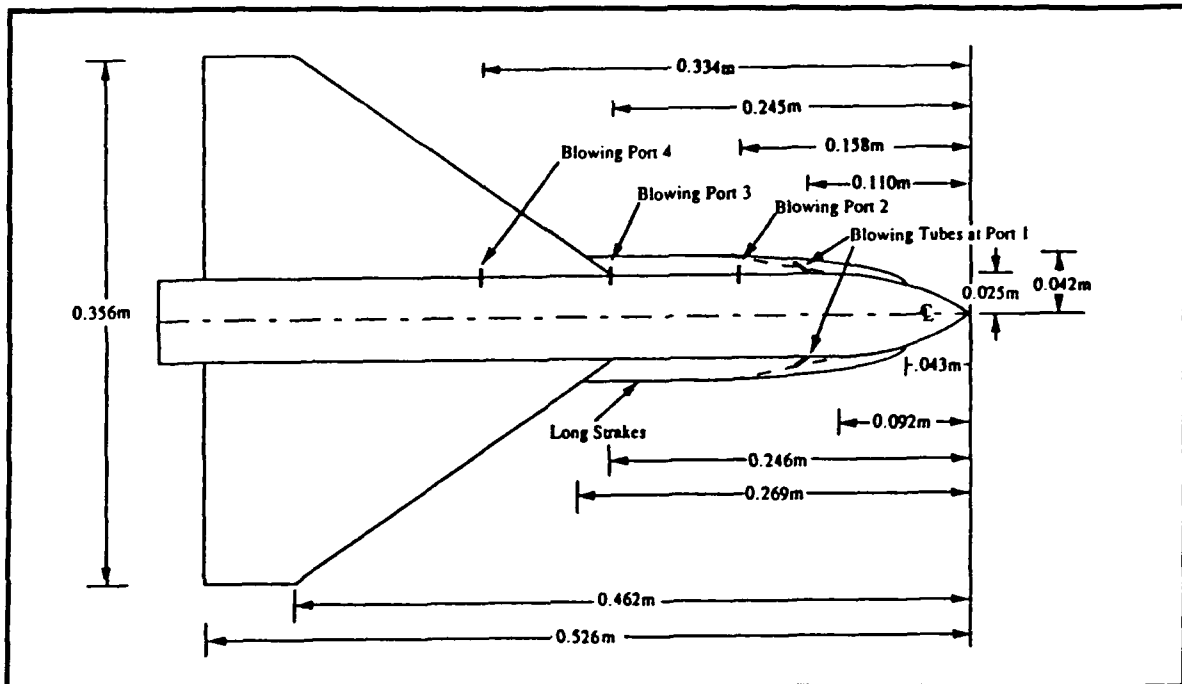


Figure 1. Roach and Kuhlman's Generic Fighter Model [Ref. 4]

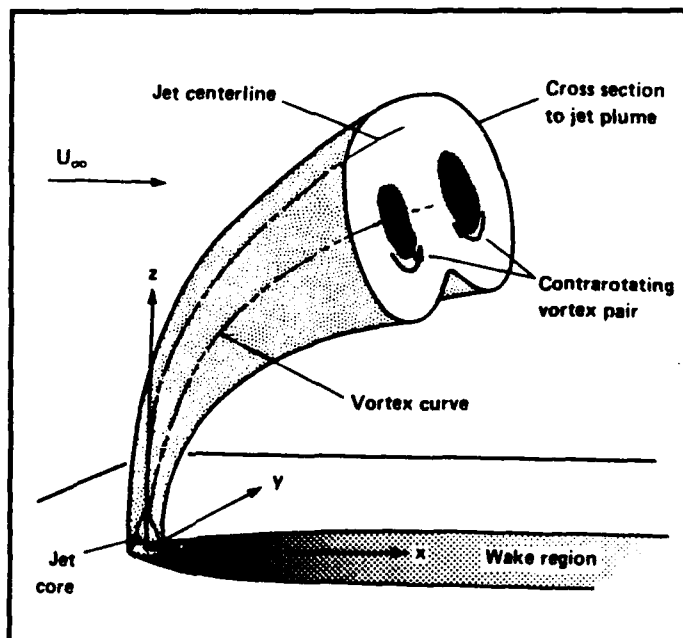


Figure 2. Schematic of an Air Jet in Crossflow [Ref. 4]

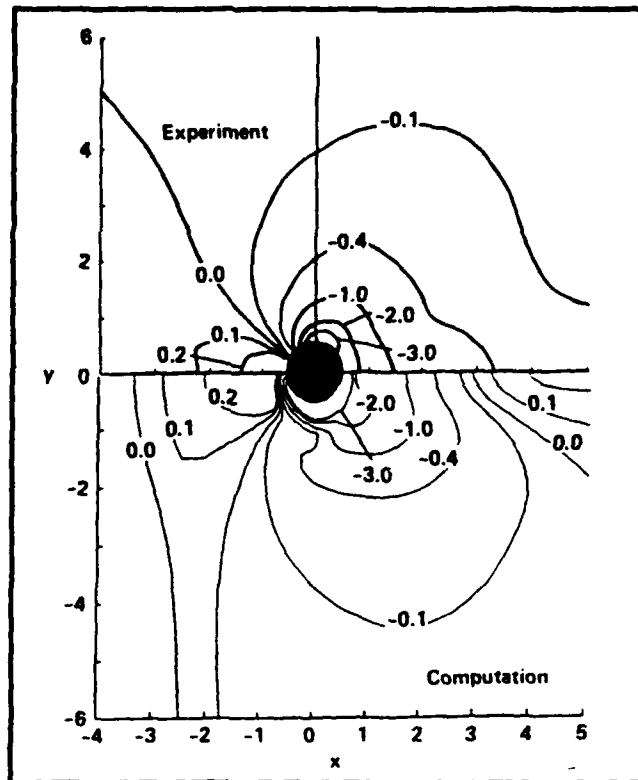


Figure 3. Constant Pressure Contours [Ref. 4]

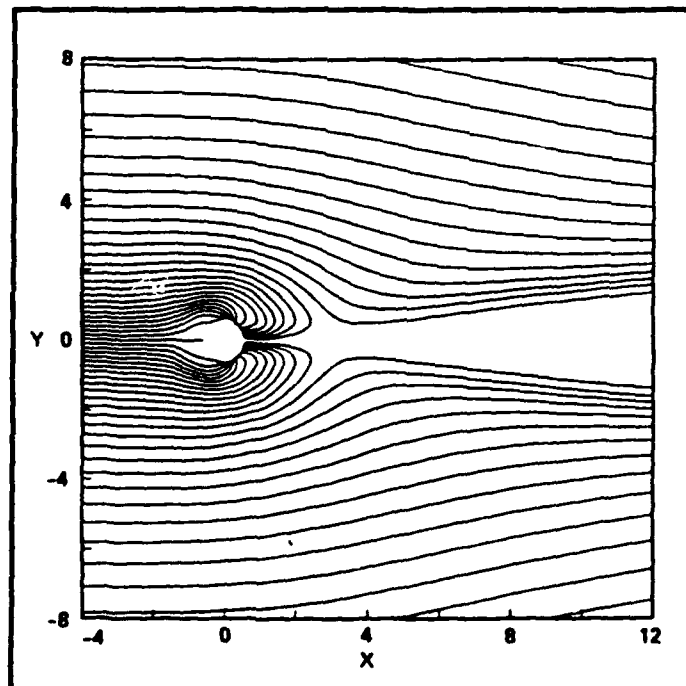


Figure 4. Streamlines Showing Entrainment [Ref. 4]

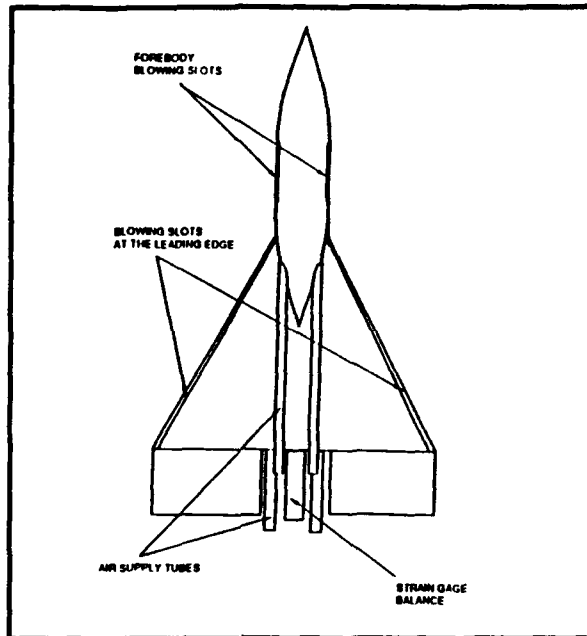


Figure 5. Celik and Robert's Model
[Ref. 5]

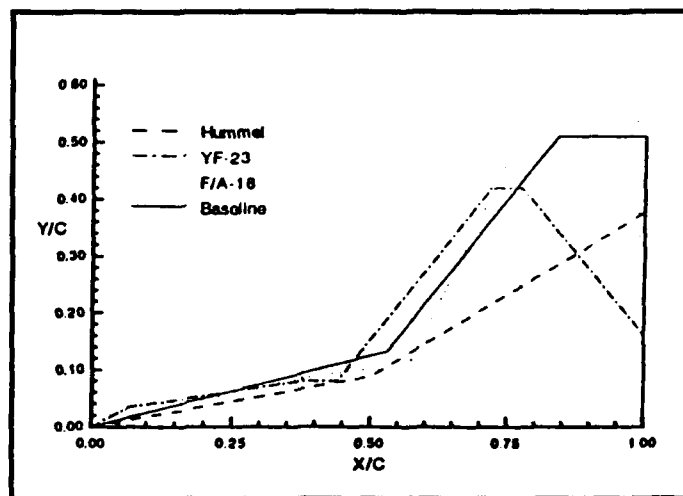


Figure 6. Kern's Wing/Strake Model and
other Fighter Wings [Ref. 8]

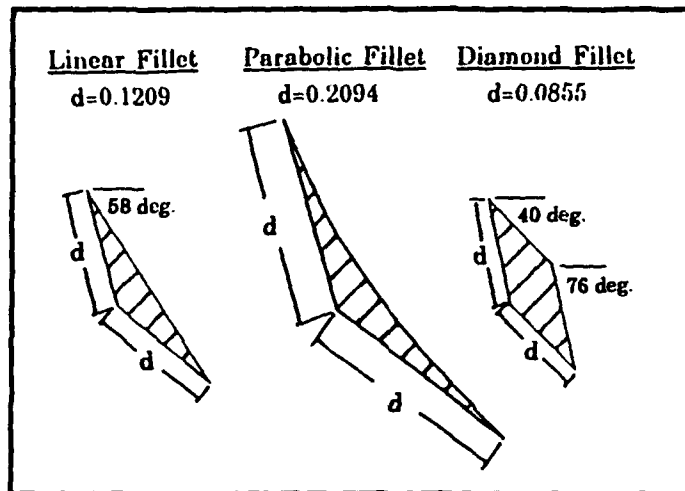


Figure 7. Kern's Fillet Dimensions [Ref. 8]

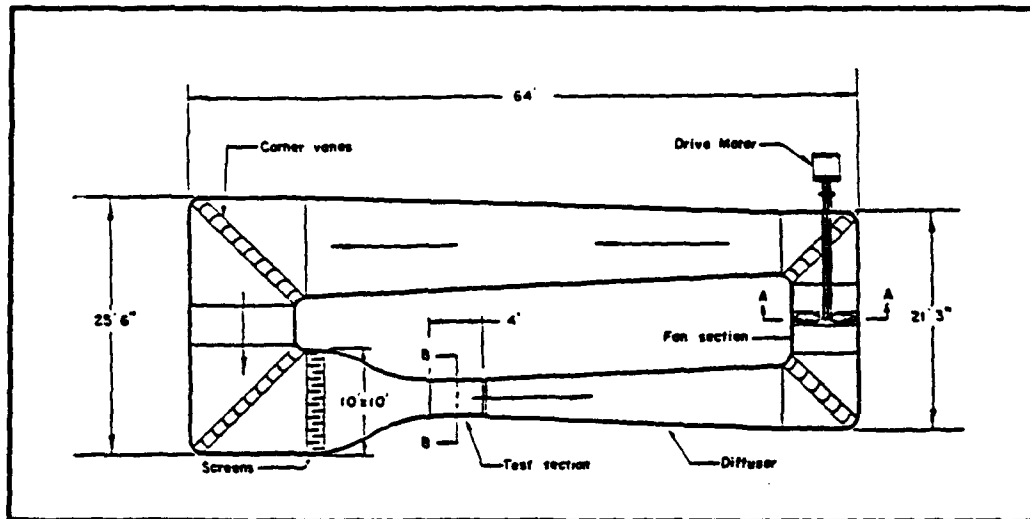


Figure 8. NPS Aerolab Low Speed Wind Tunnel

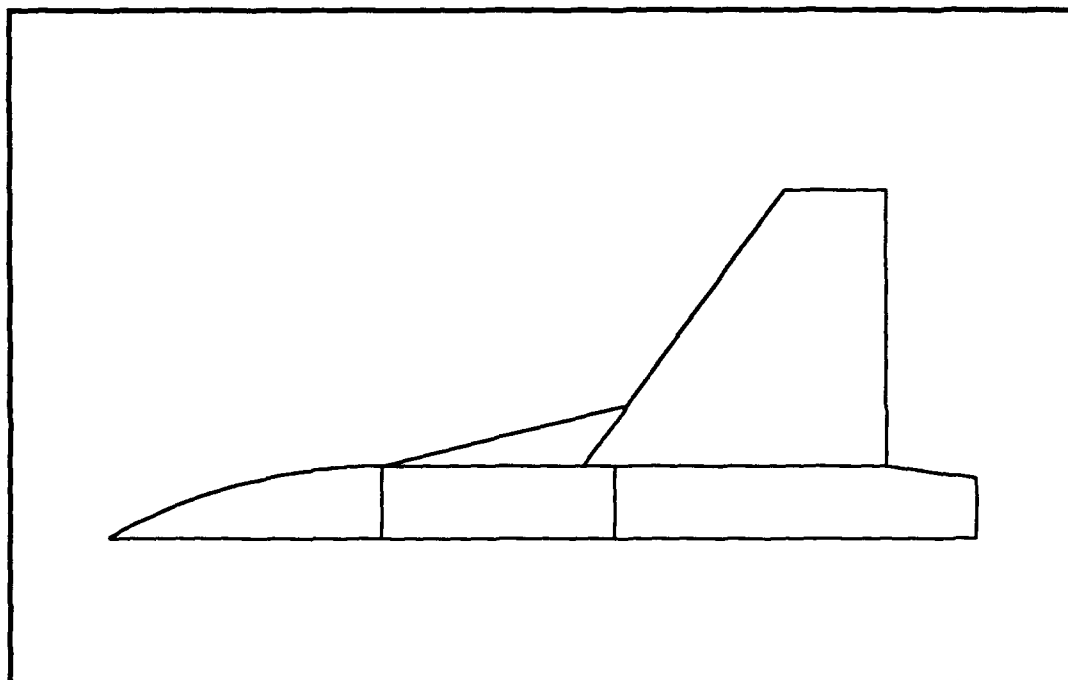


Figure 9. Sketch of Wing/Strake Model

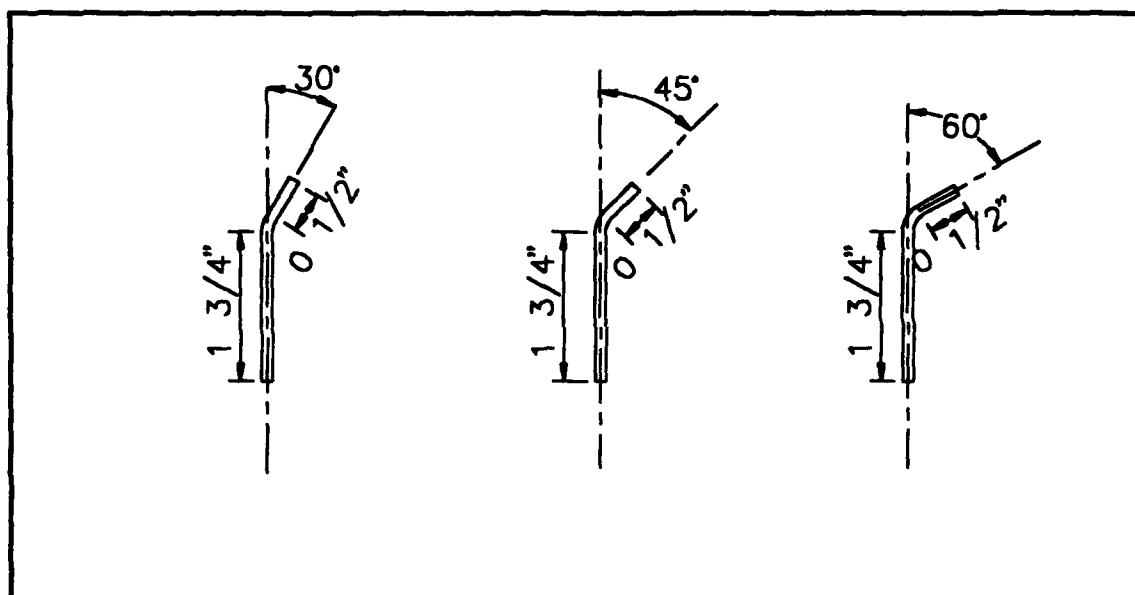


Figure 10. Brass Blowing Tubes

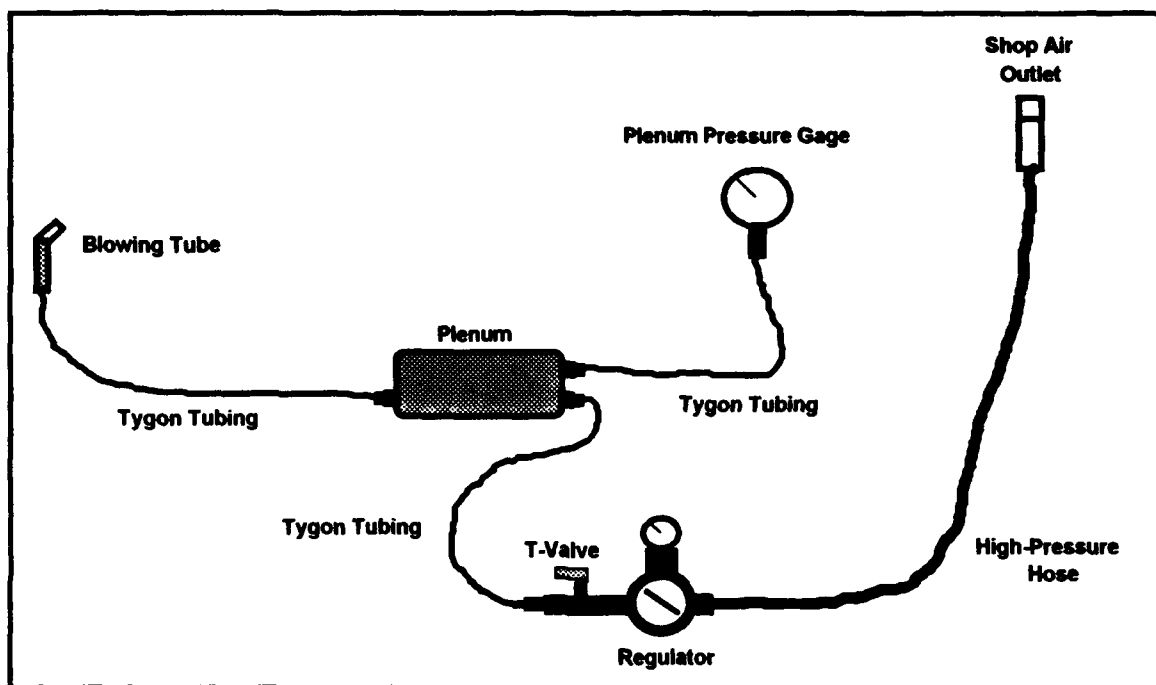


Figure 11. Blowing-Air Supply System

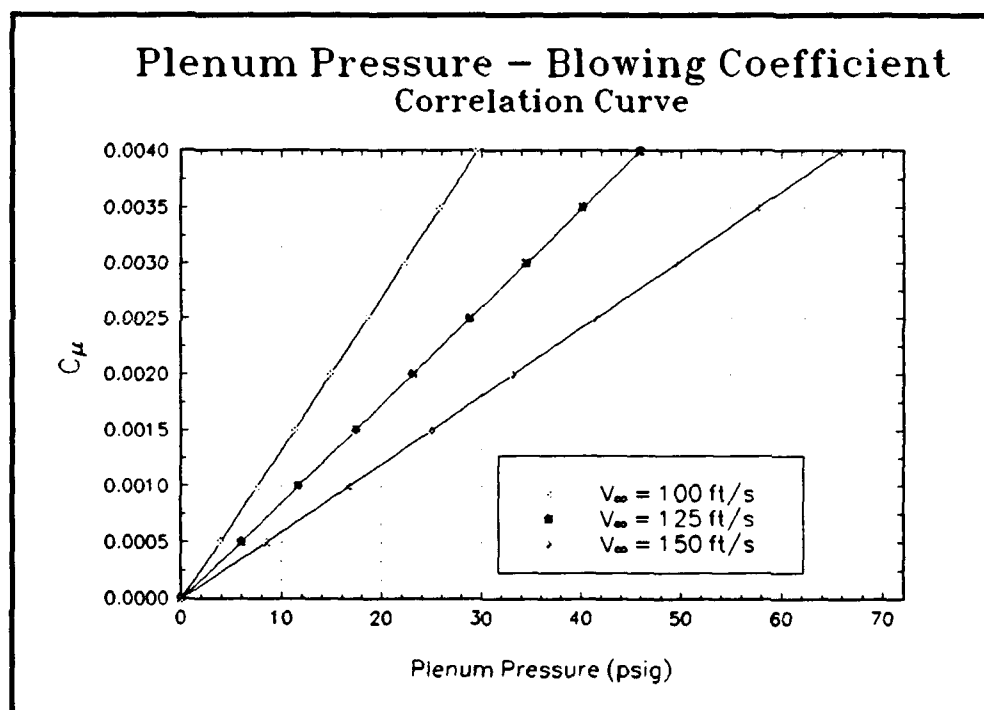


Figure 12

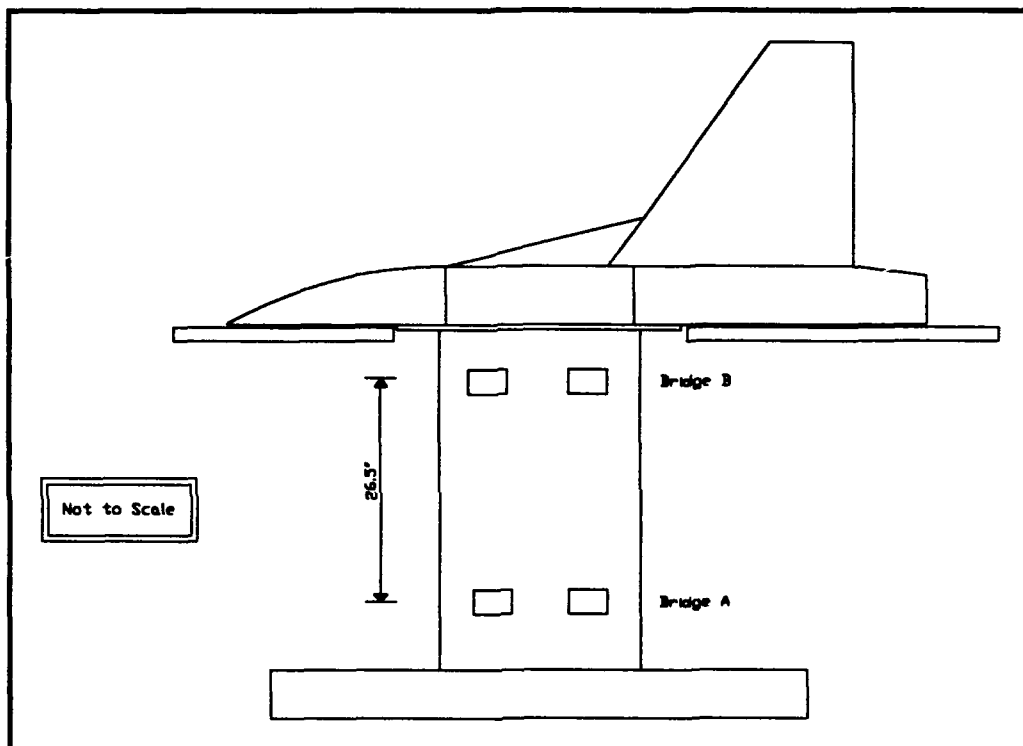


Figure 13. Wing/Strake Model on Balance

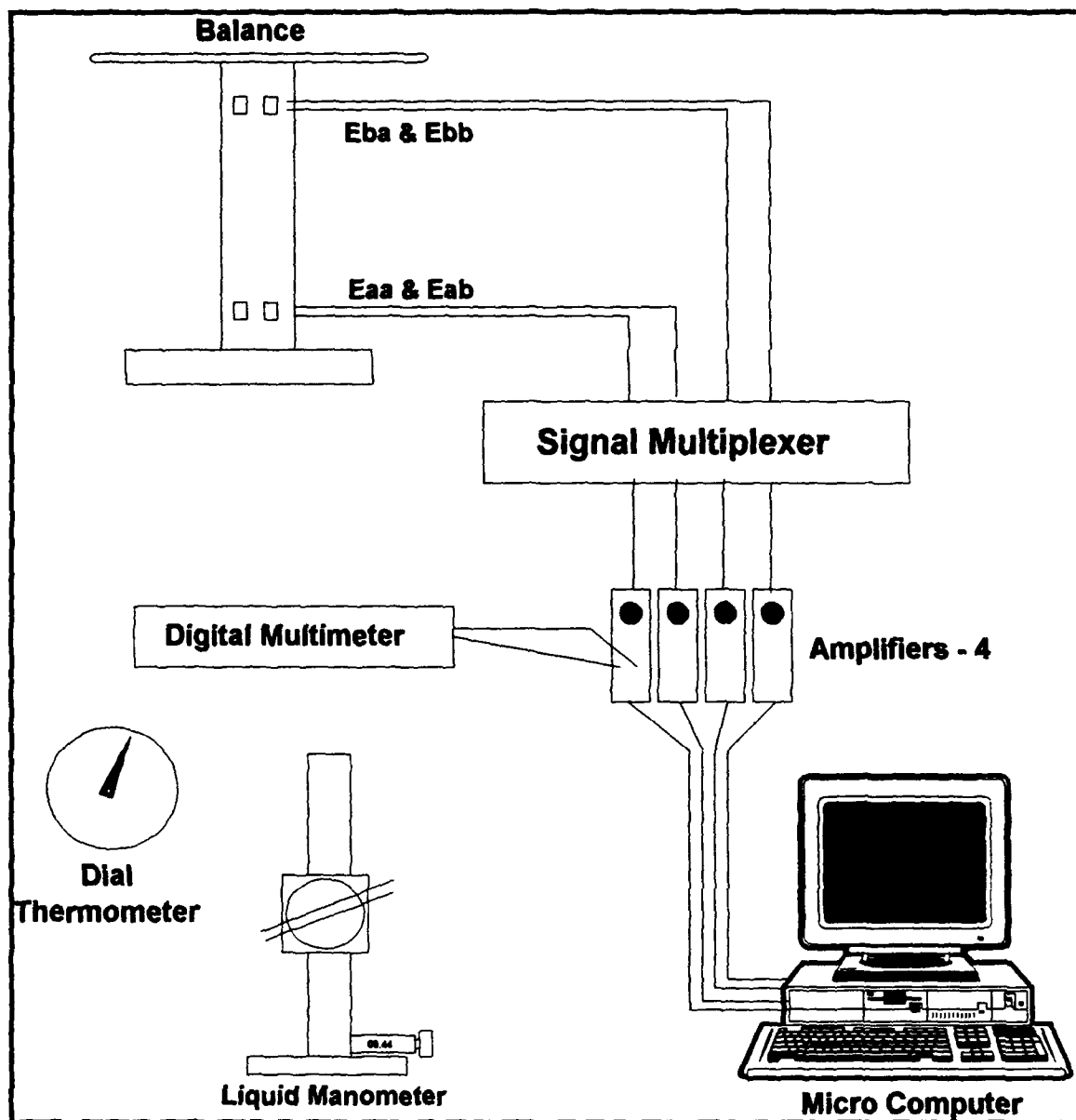


Figure 14. Wind-Tunnel Data Aquisition System

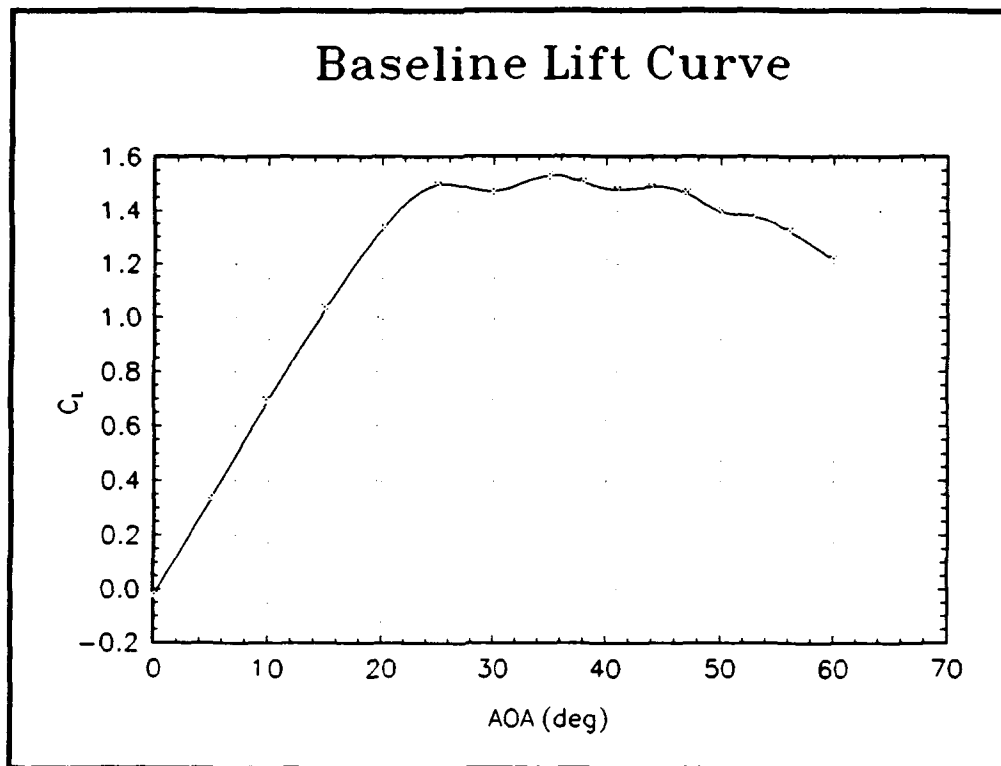


Figure 15.

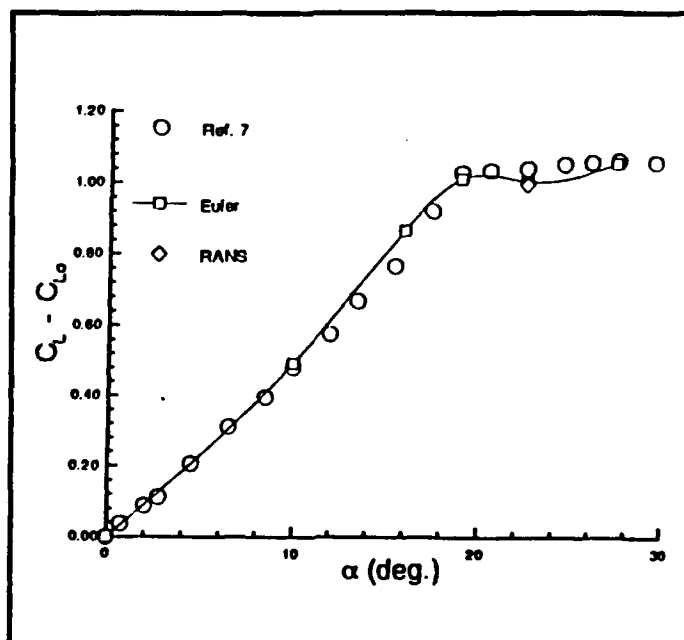


Figure 16. Kern's Predicted Lift Curve [Ref. 8]

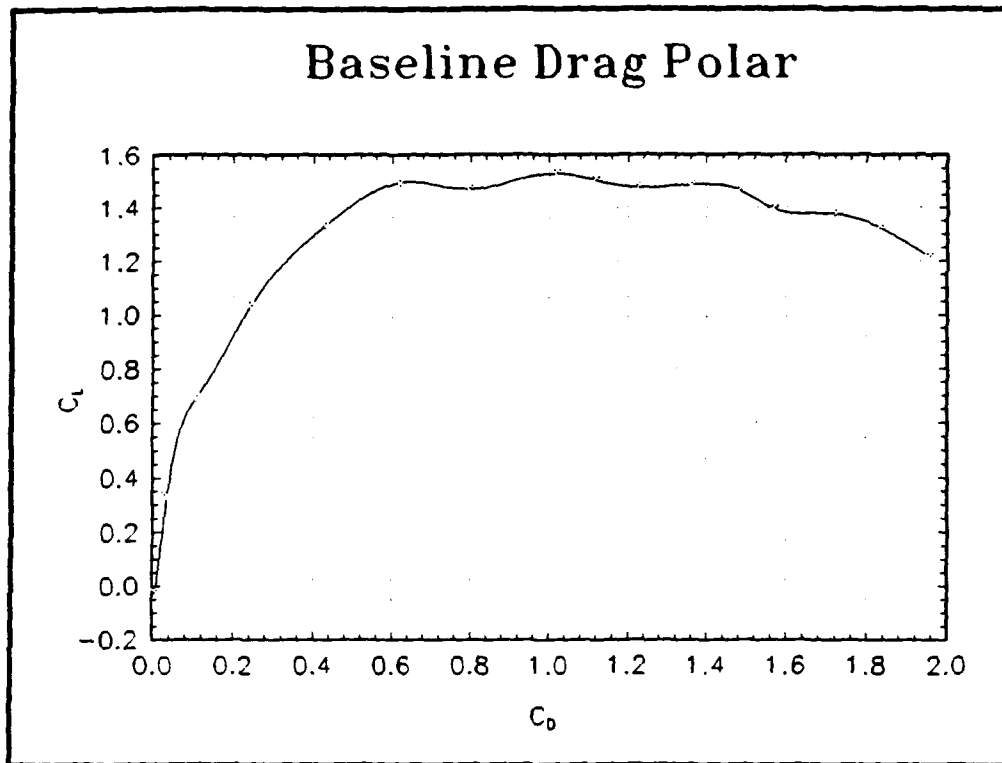


Figure 17.

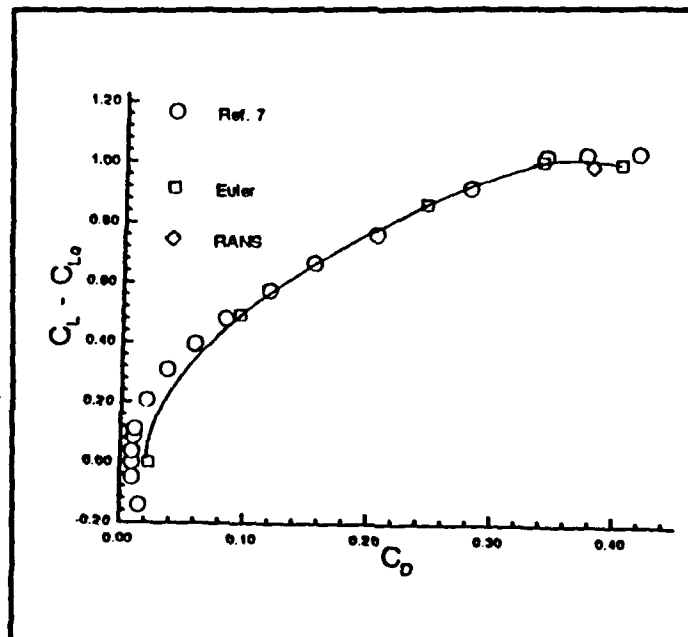


Figure 18. Kern's Predicted Drag Polar [Ref. 8]

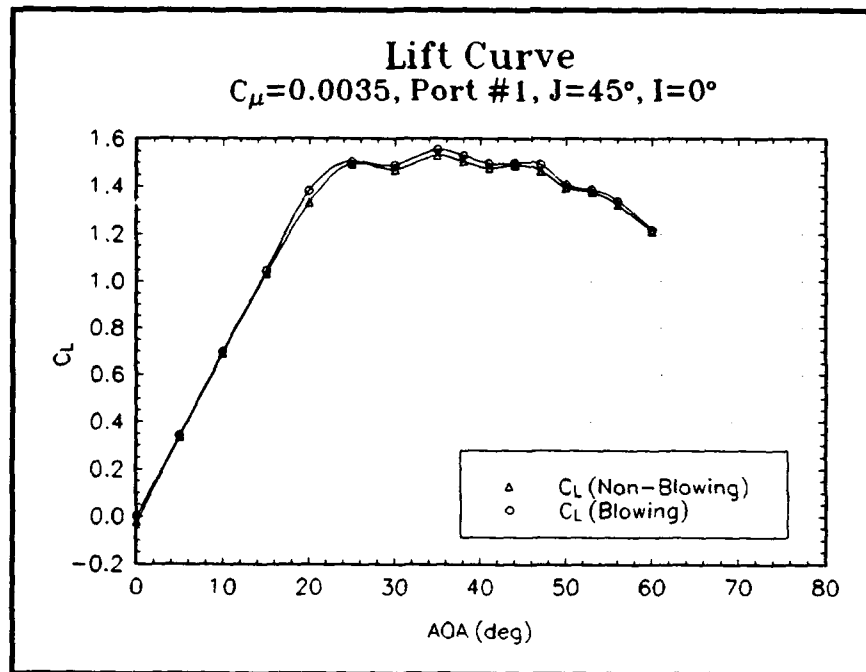


Figure 19a.

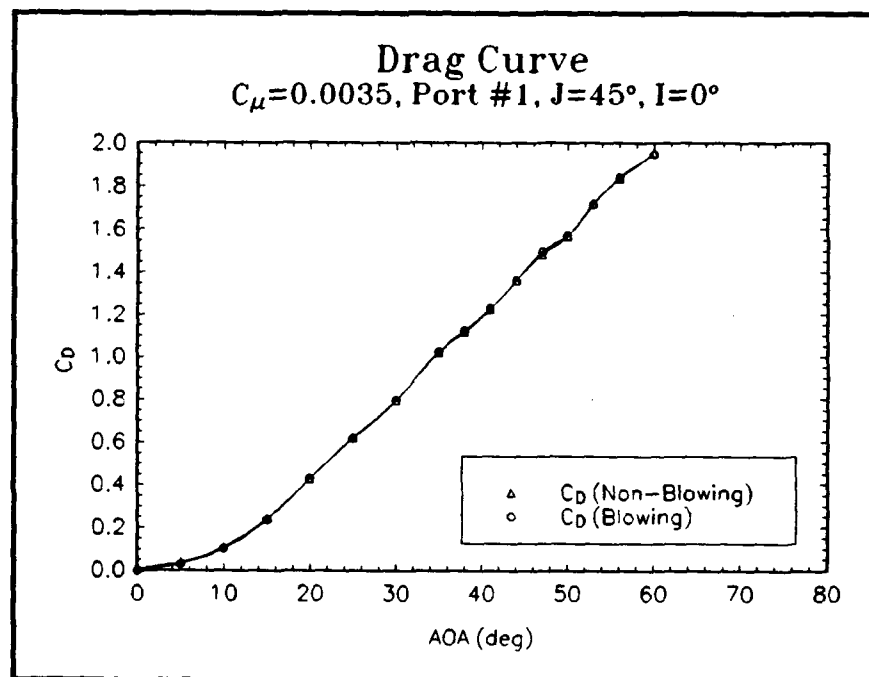


Figure 19b.

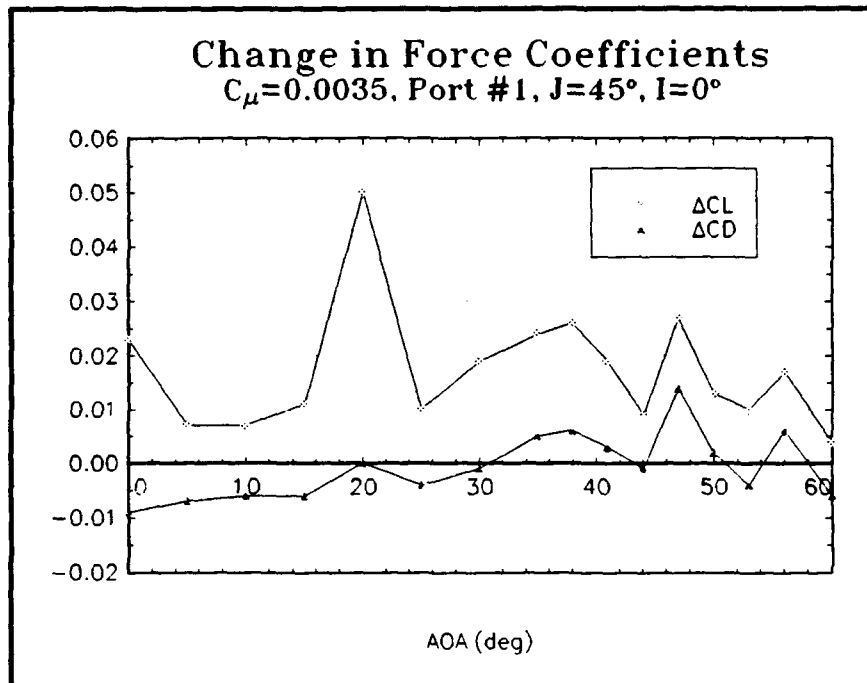


Figure 19c.

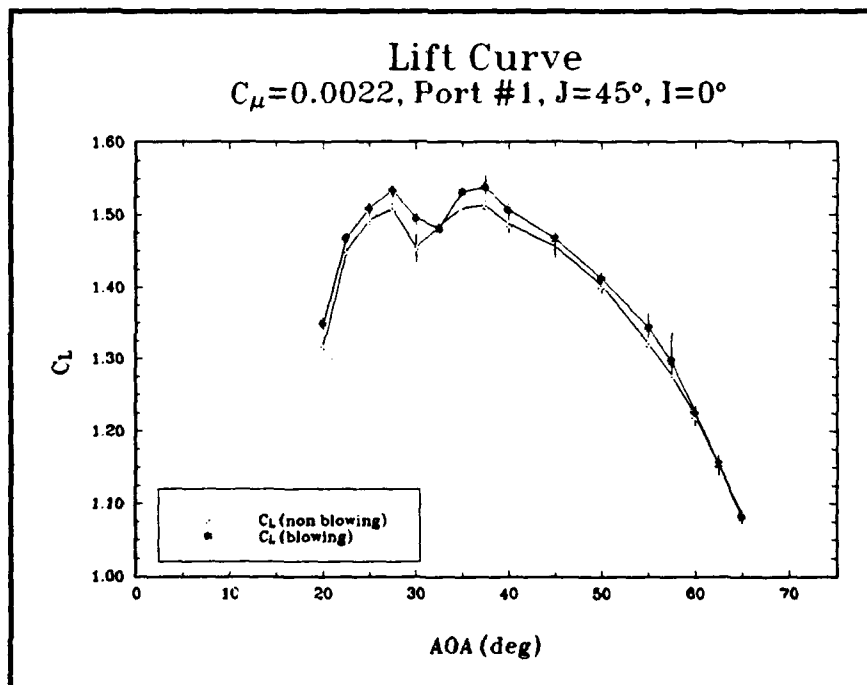


Figure 20a.

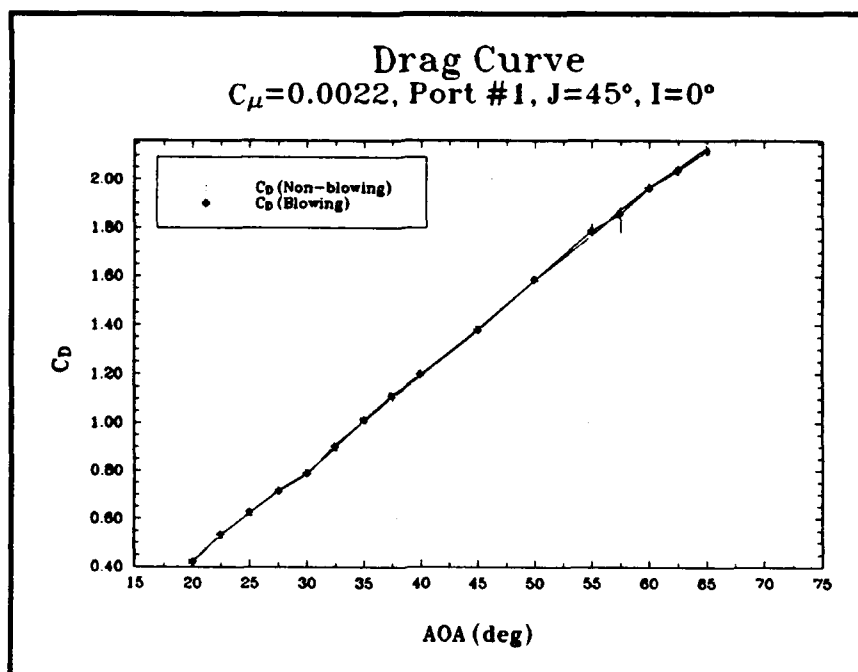


Figure 20b.

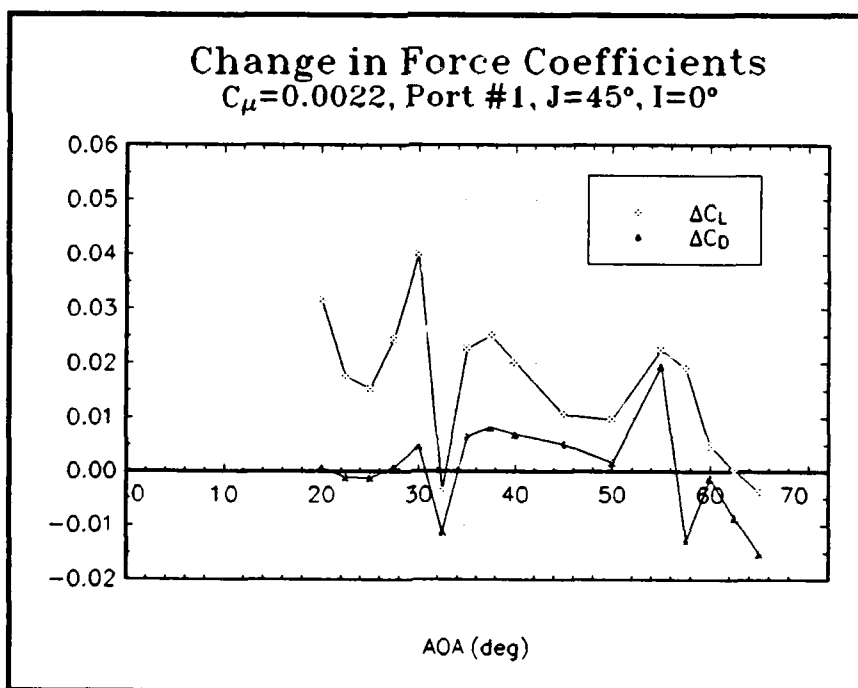


Figure 20c.

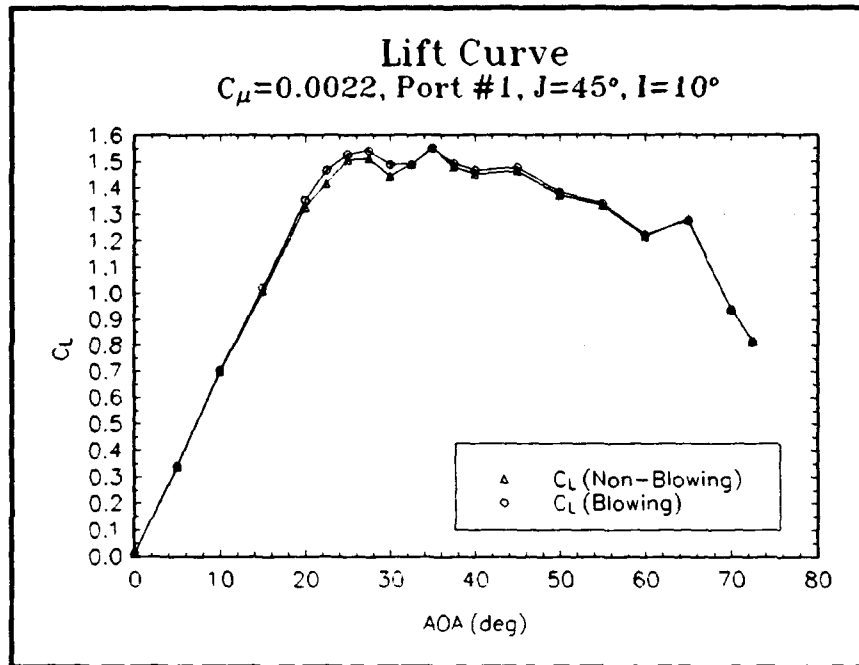


Figure 21a.

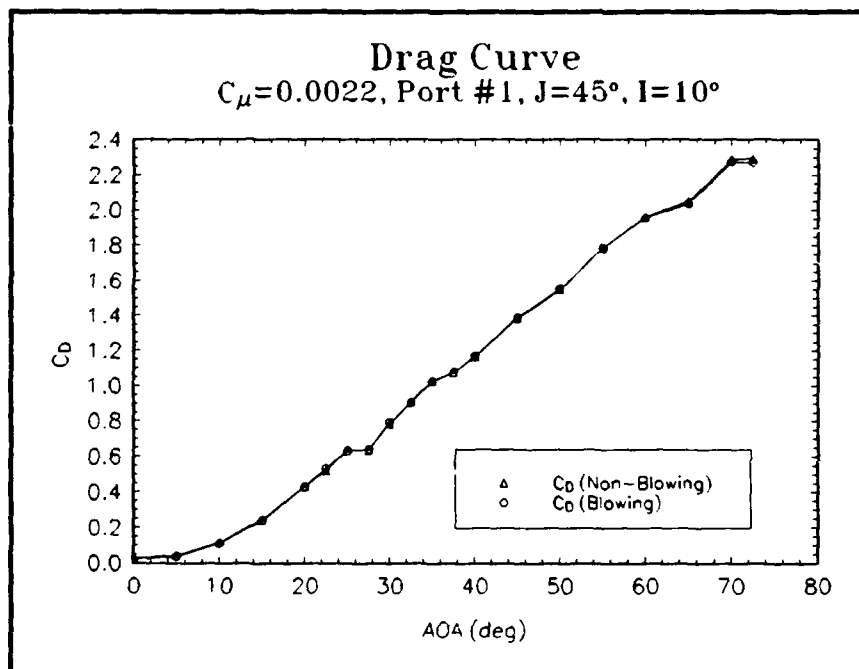


Figure 21b.

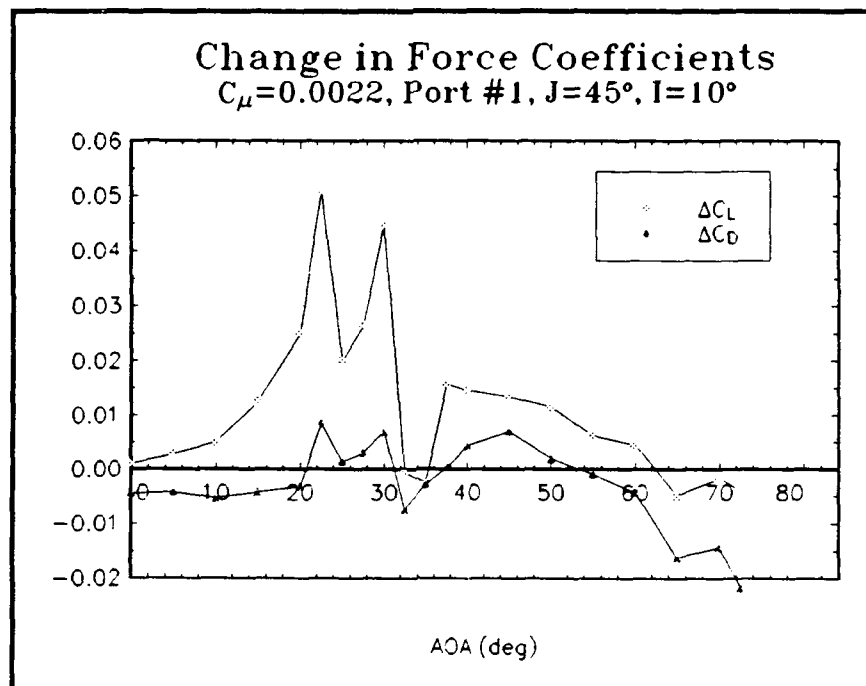


Figure 21c.

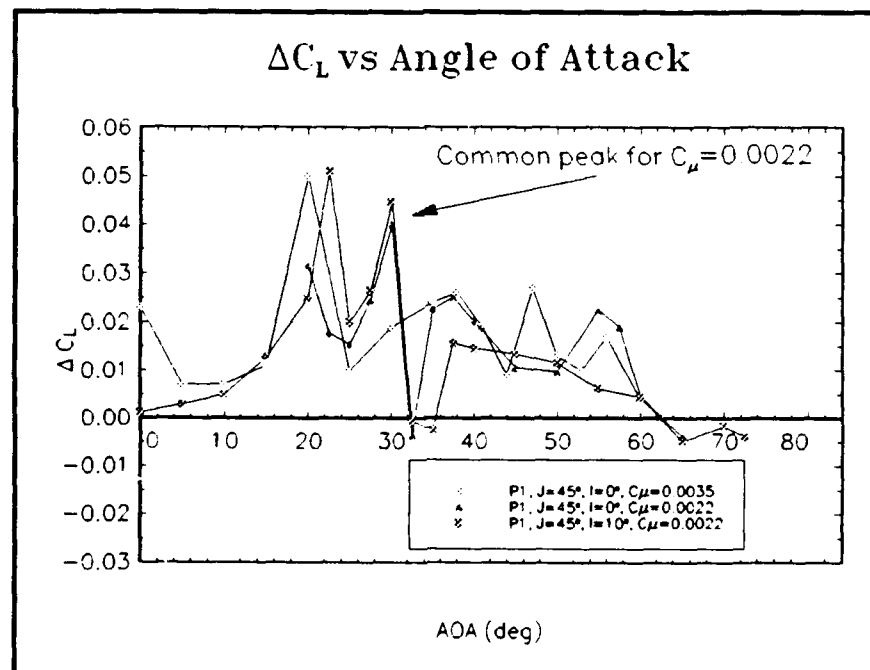


Figure 22.

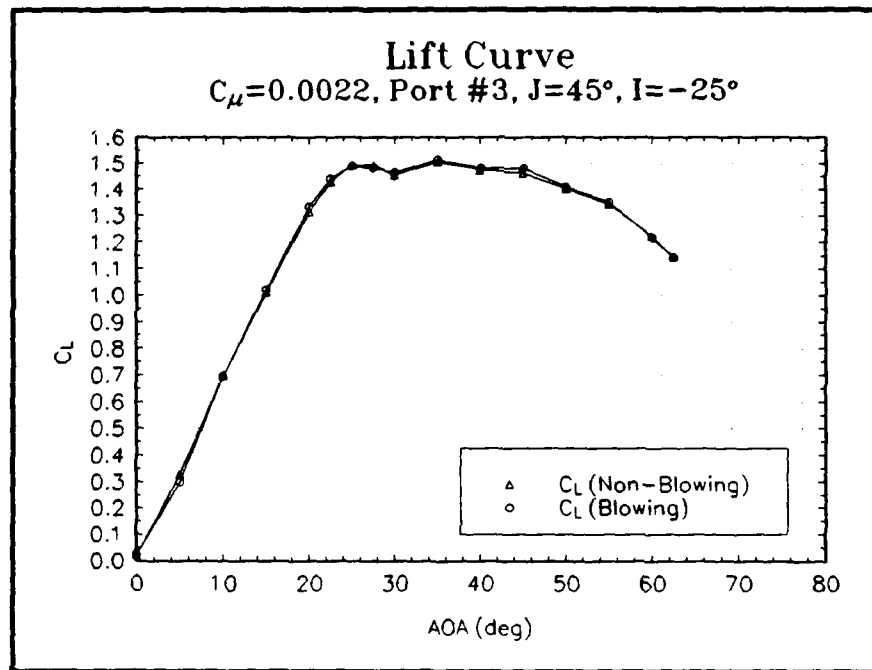


Figure 23a.

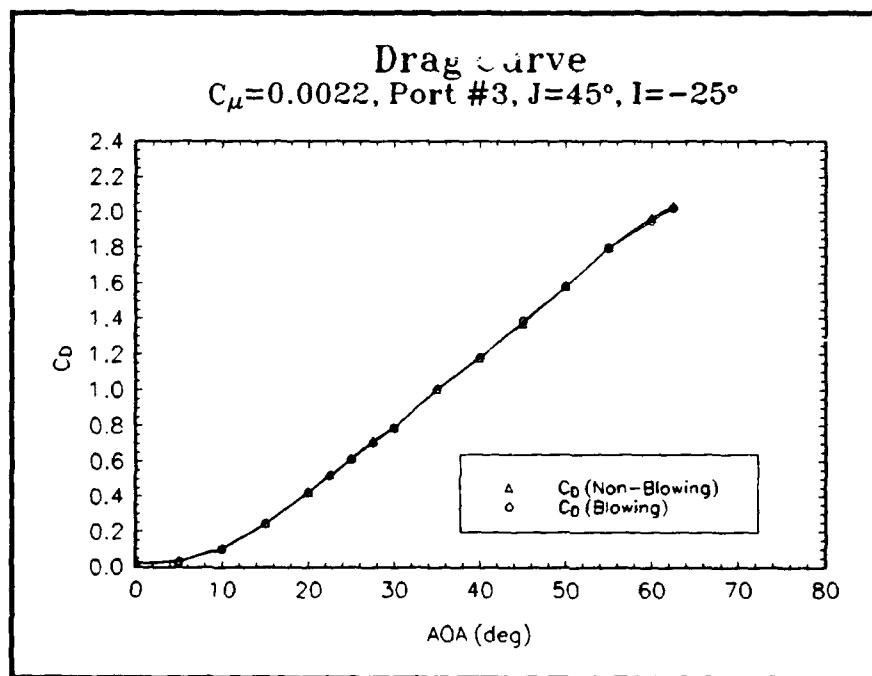


Figure 23b.

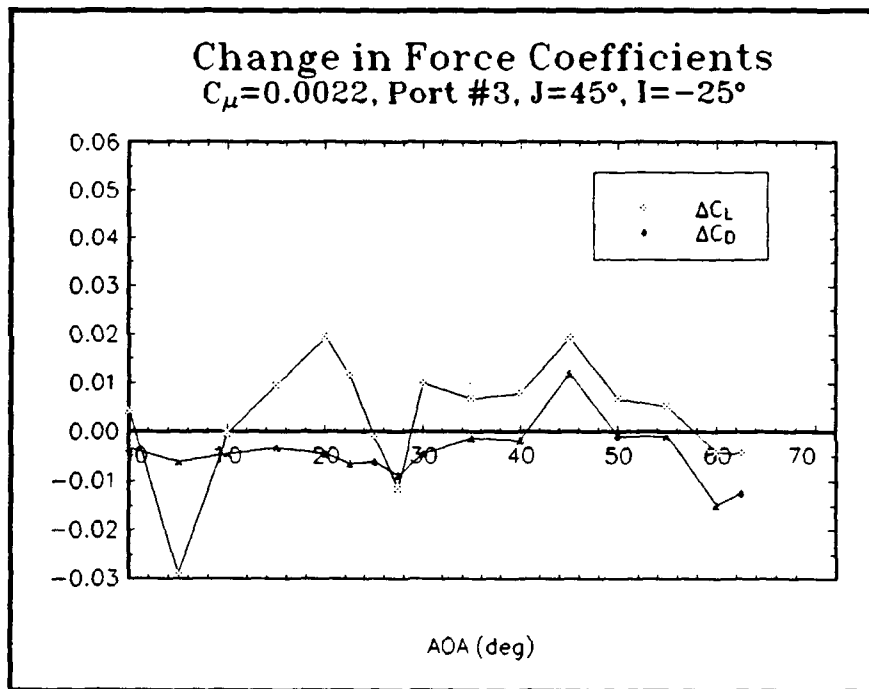


Figure 23c.

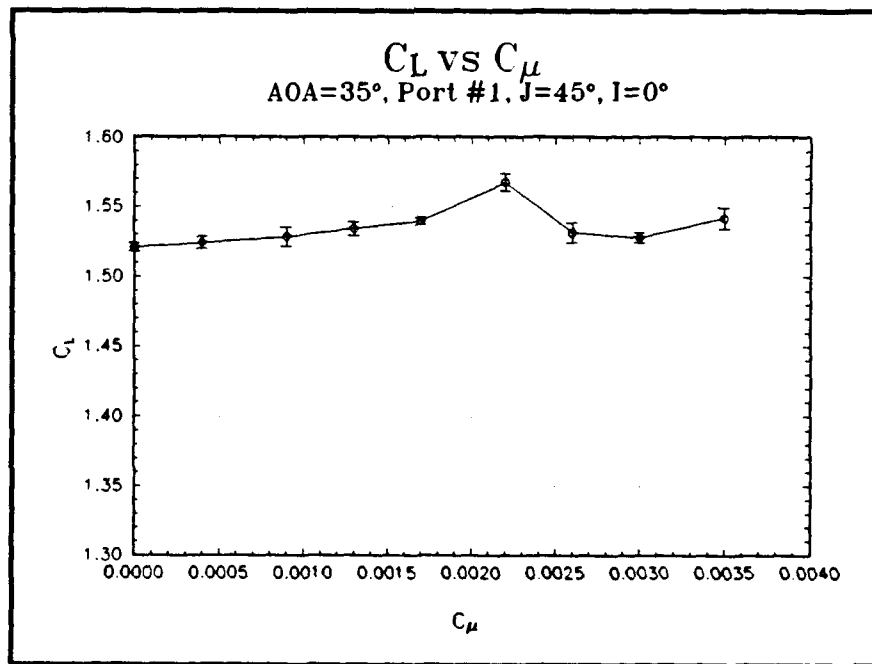


Figure 24.

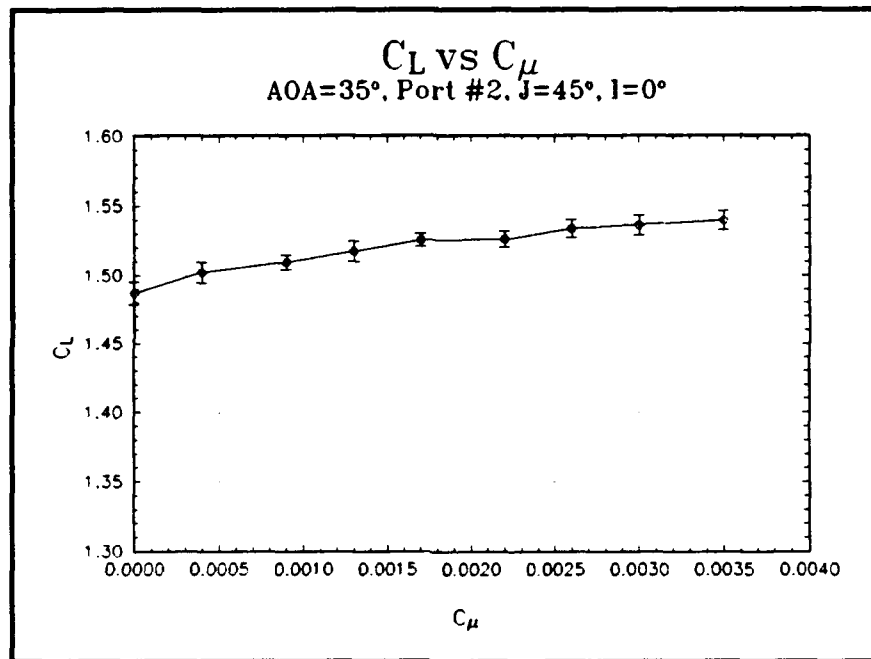


Figure 25a.

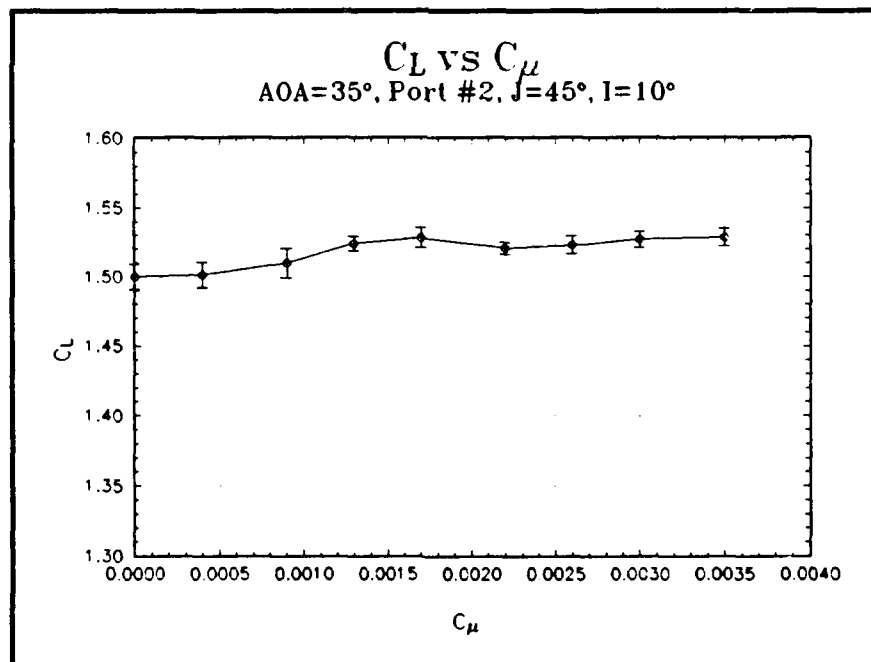


Figure 25b.

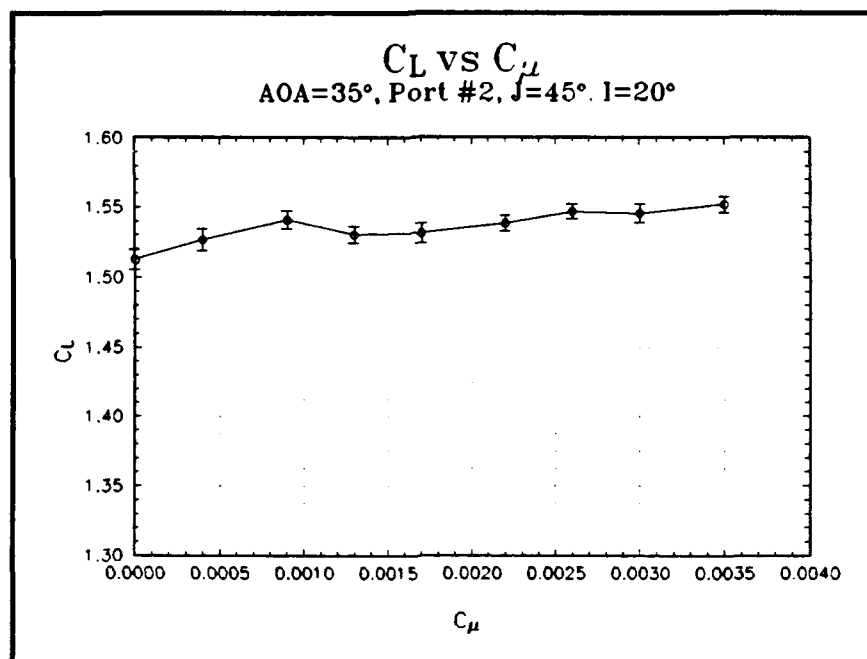


Figure 25c.

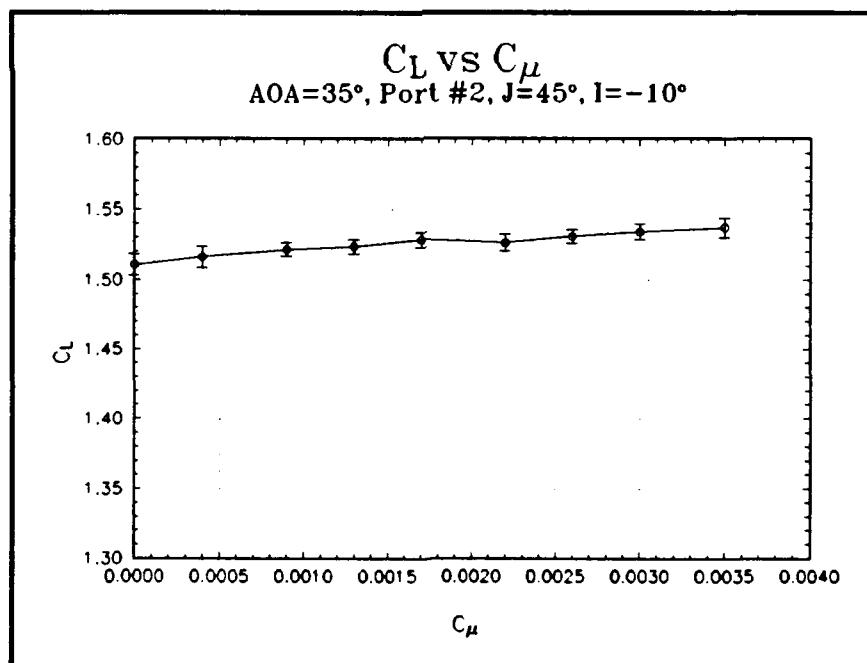


Figure 25d.

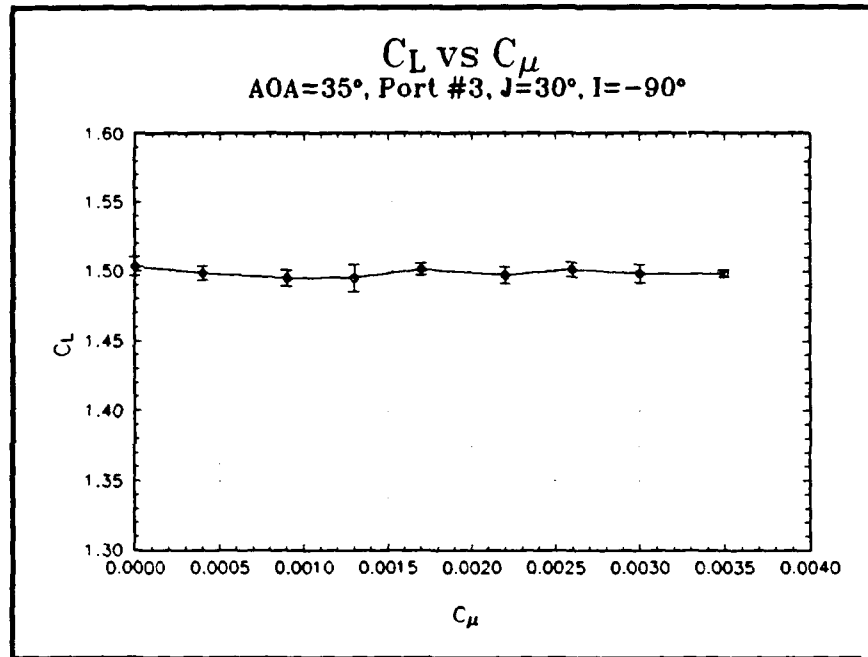


Figure 26.

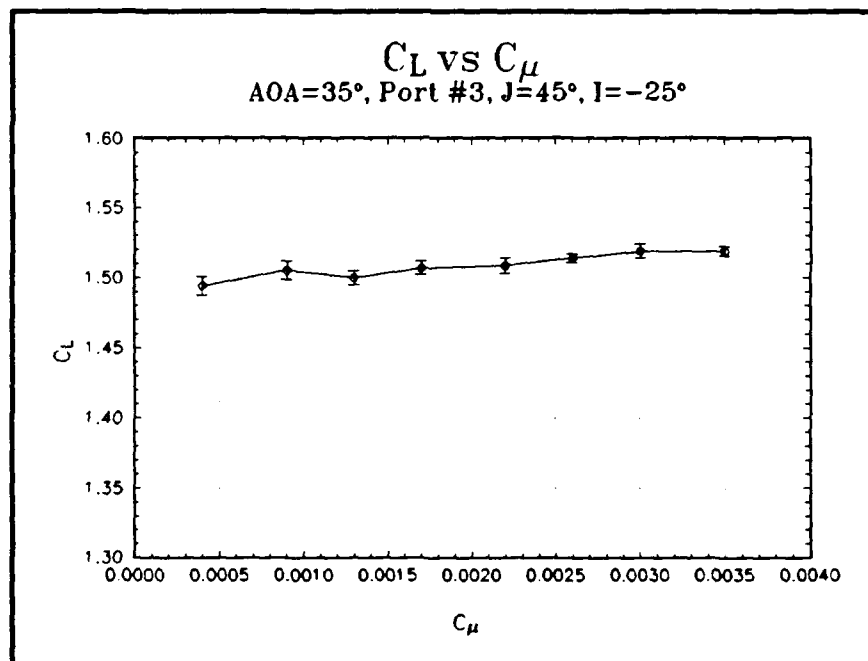


Figure 27.

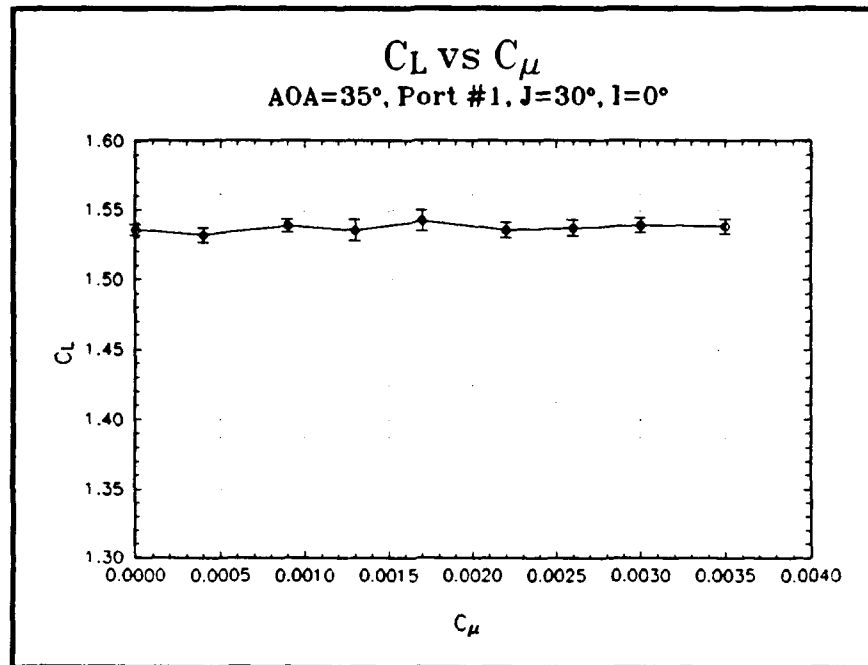


Figure 28a.

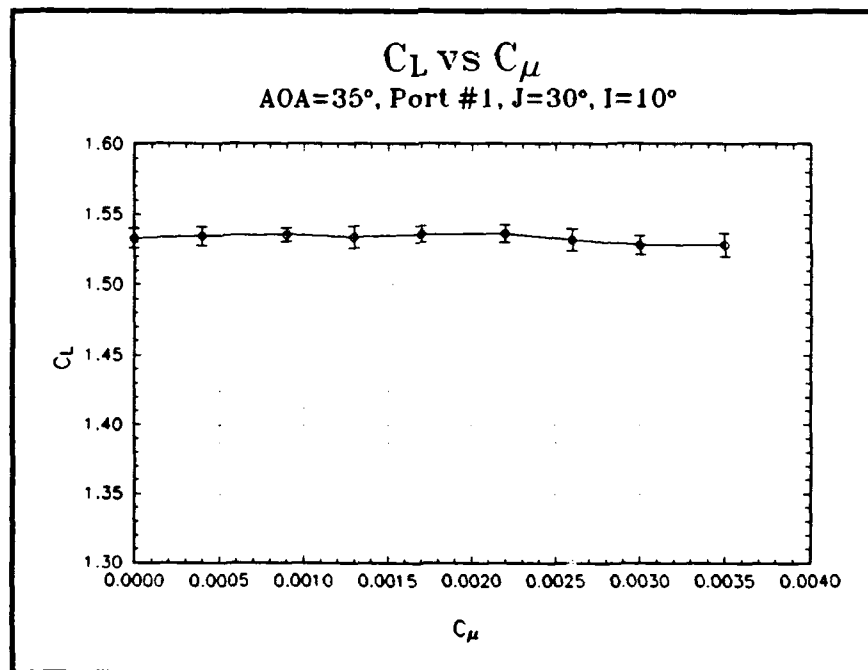


Figure 28b.

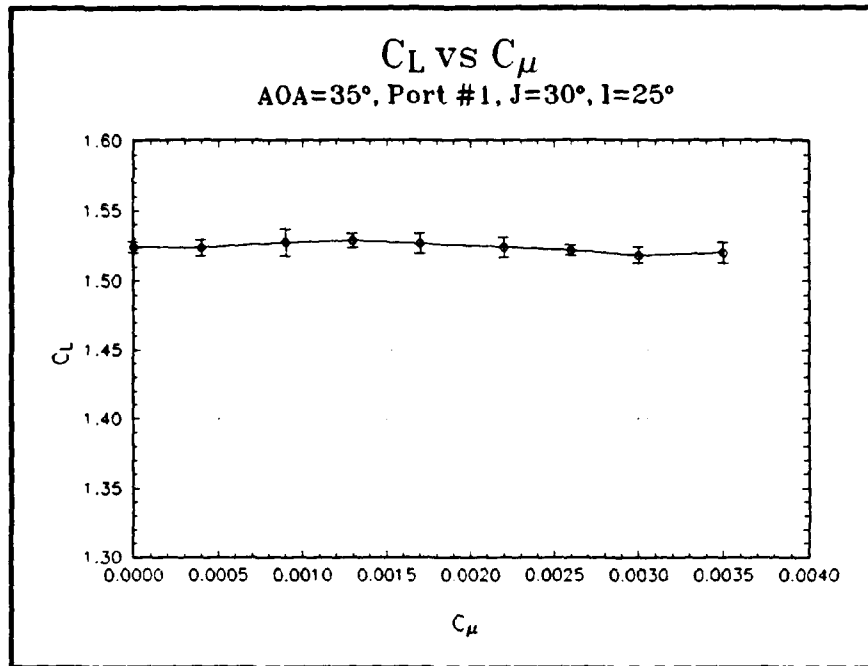


Figure 28c.

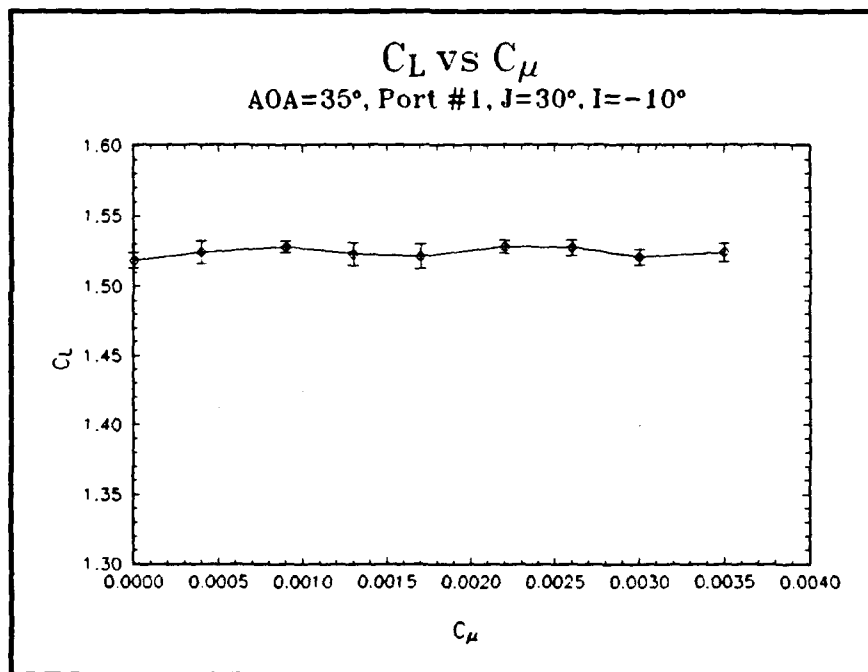


Figure 28d.

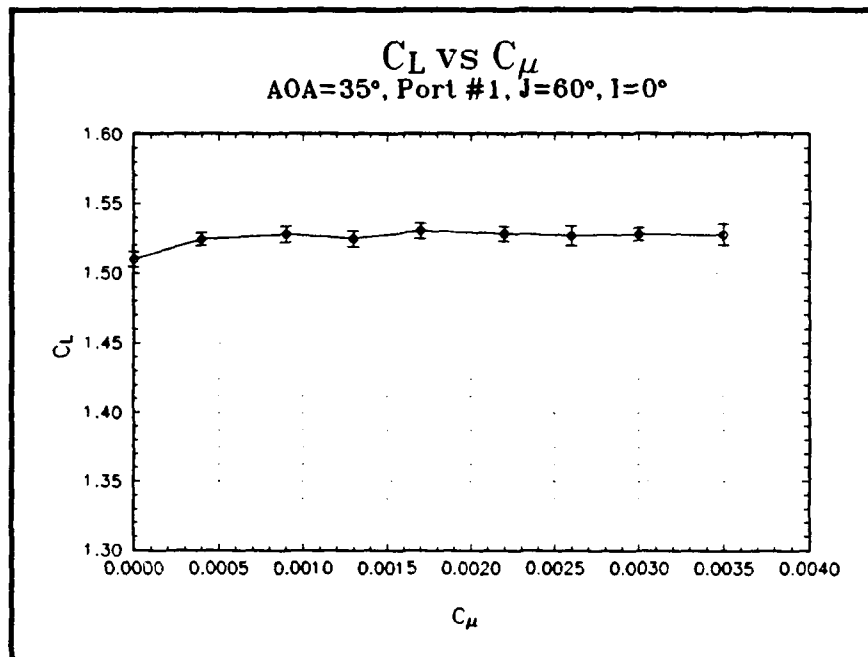


Figure 29a.

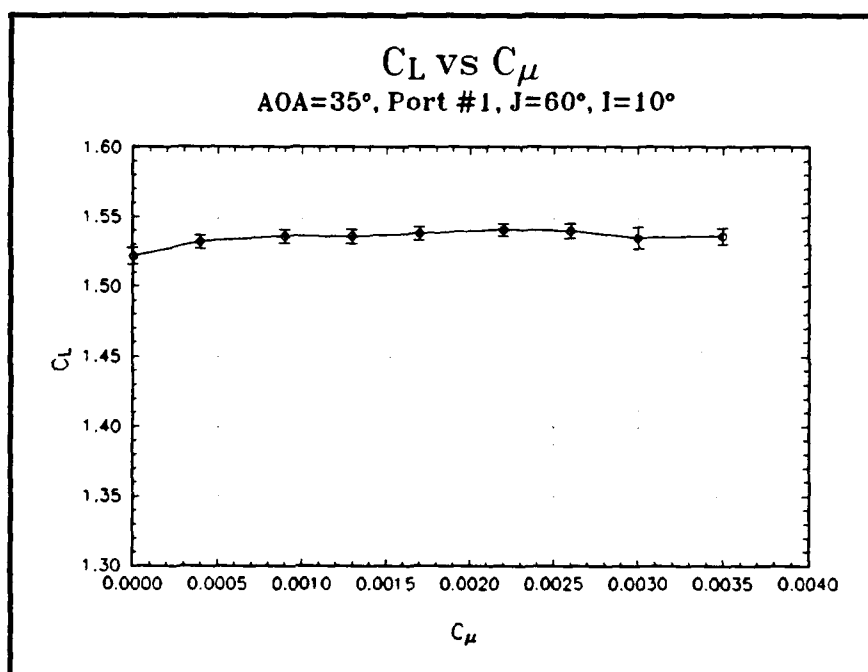


Figure 29b.

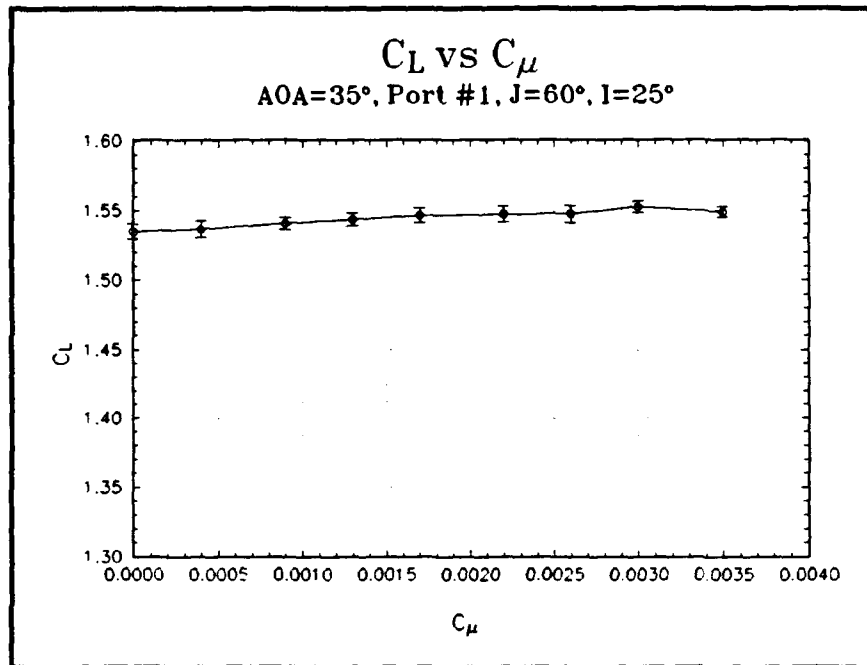


Figure 29c.

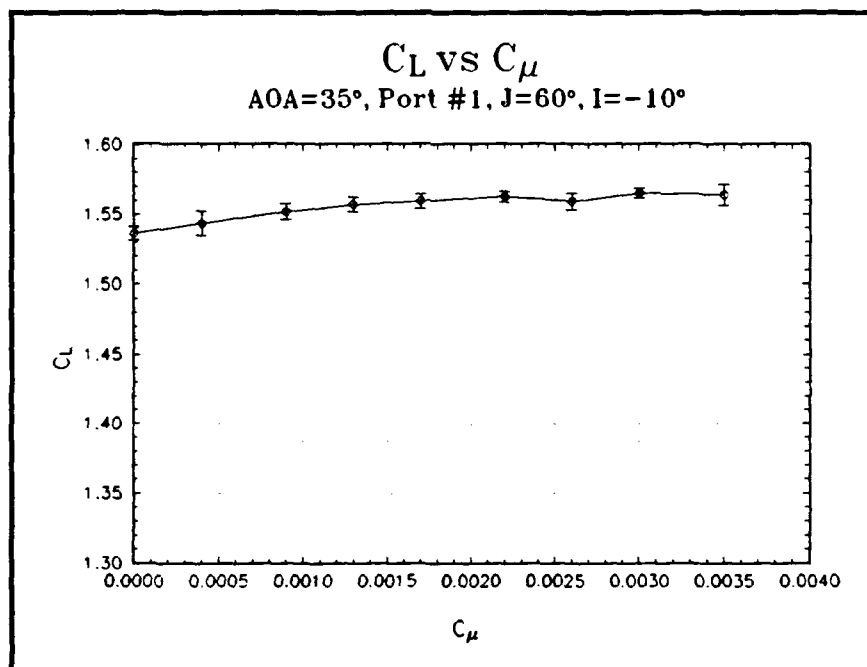


Figure 29d.

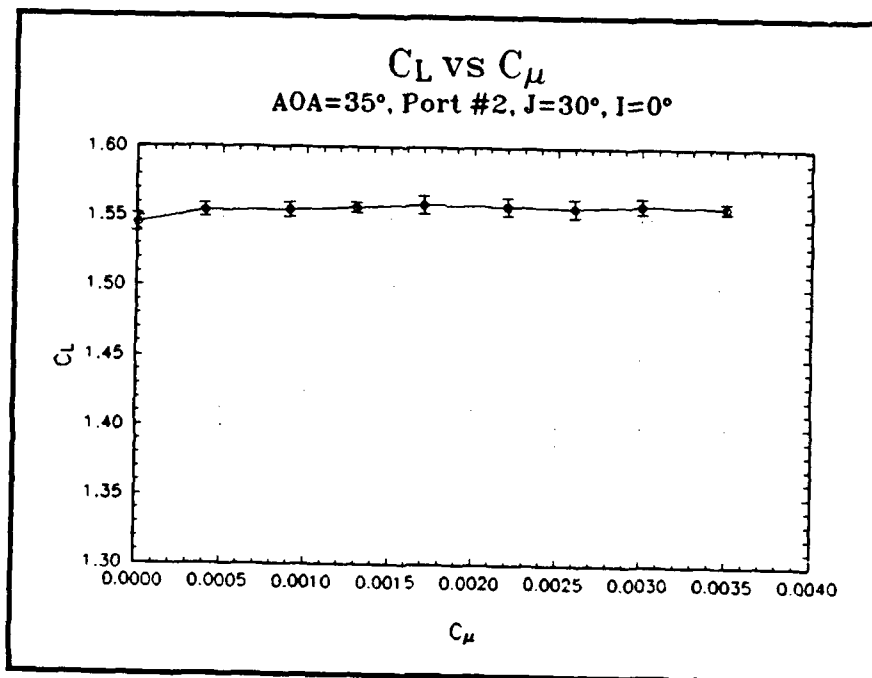


Figure 30a.

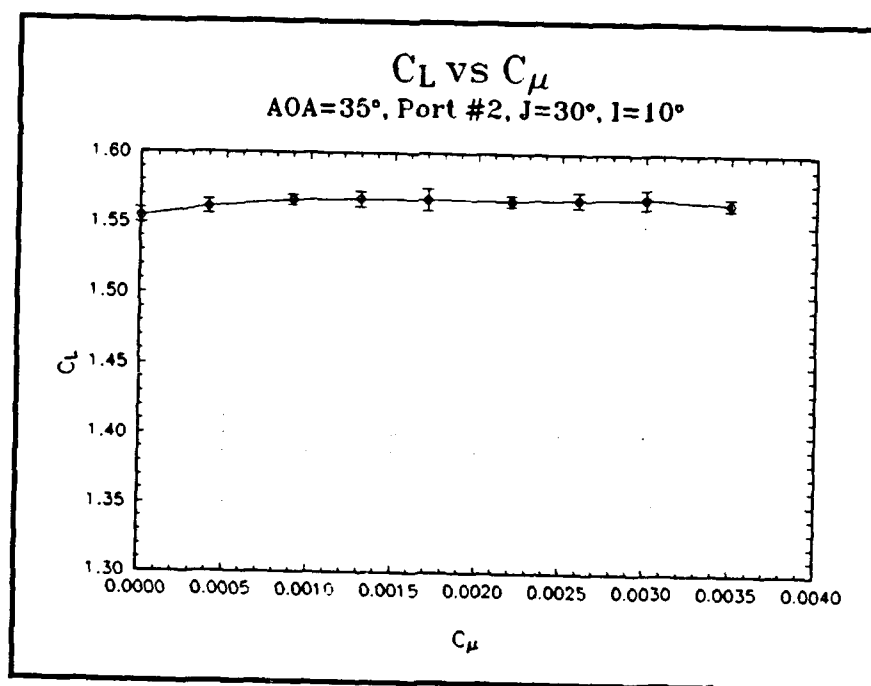


Figure 30b.

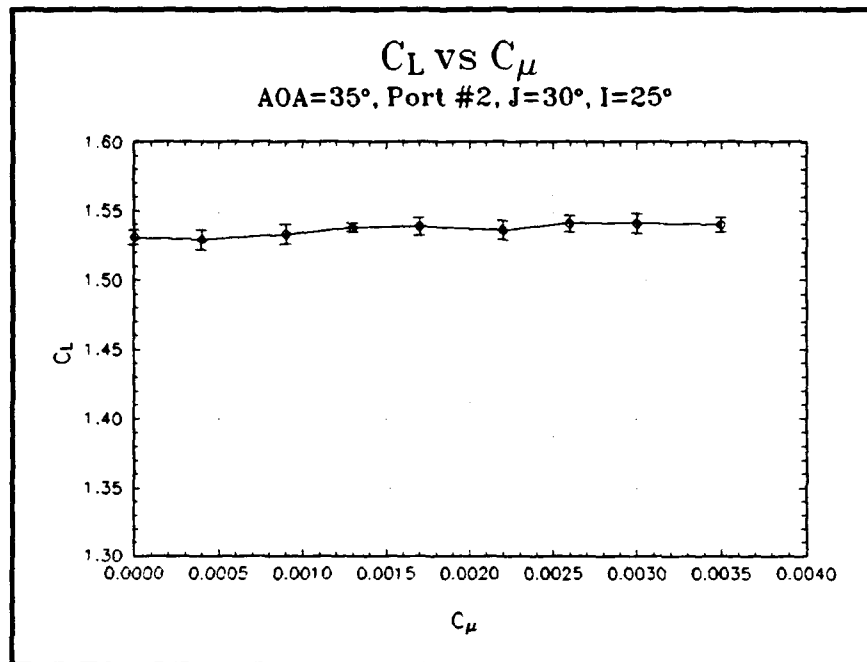


Figure 30c.

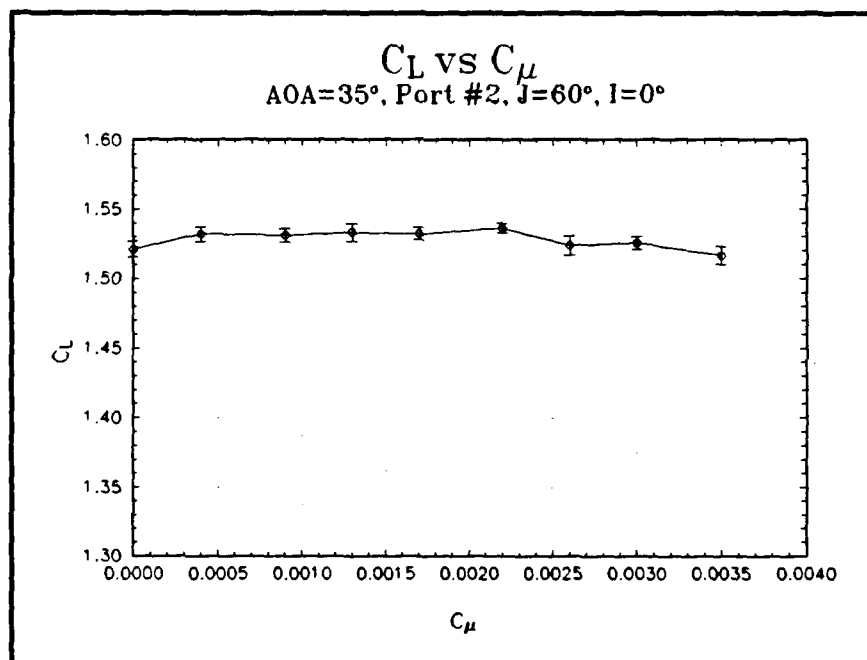


Figure 31a.

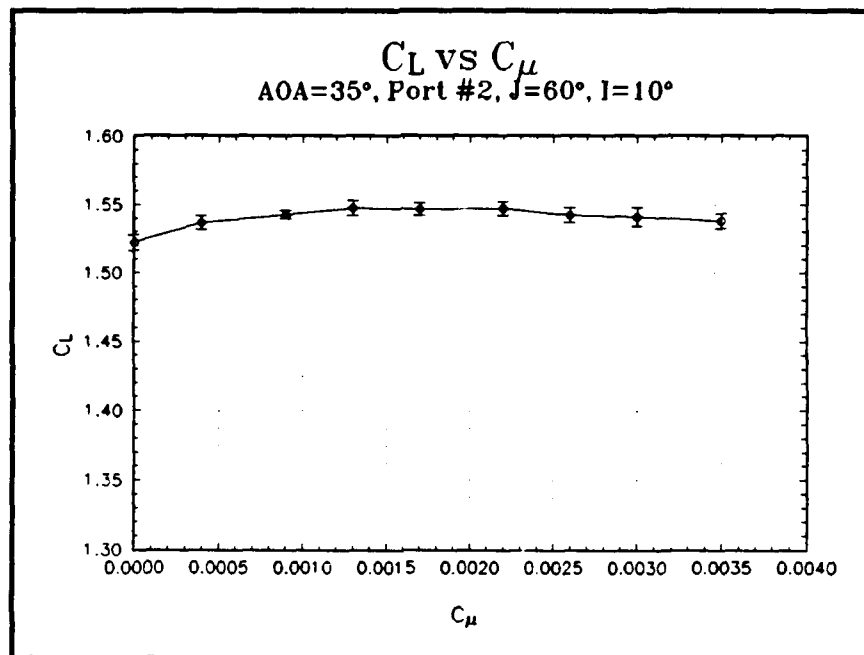


Figure 31b.

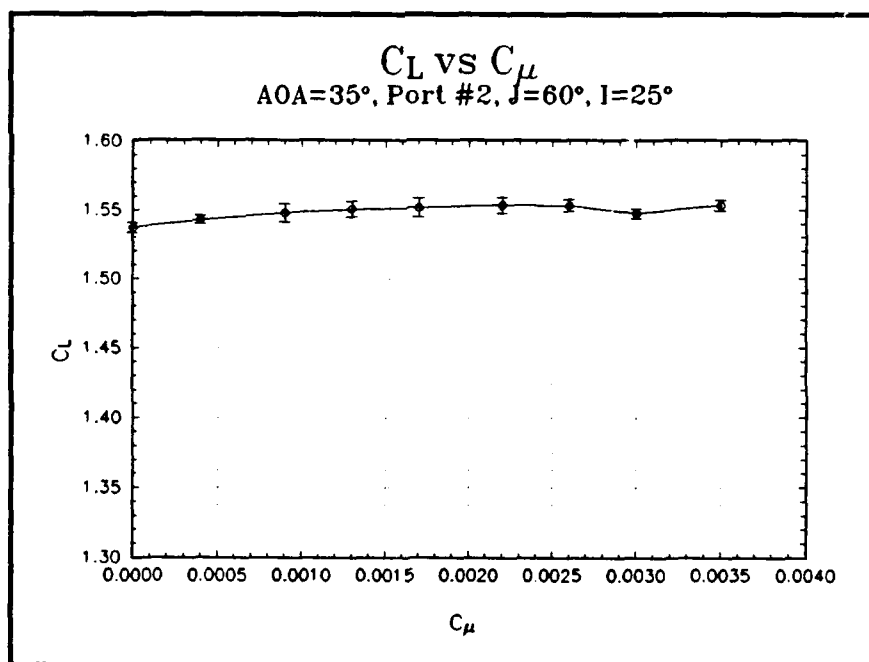


Figure 31c.

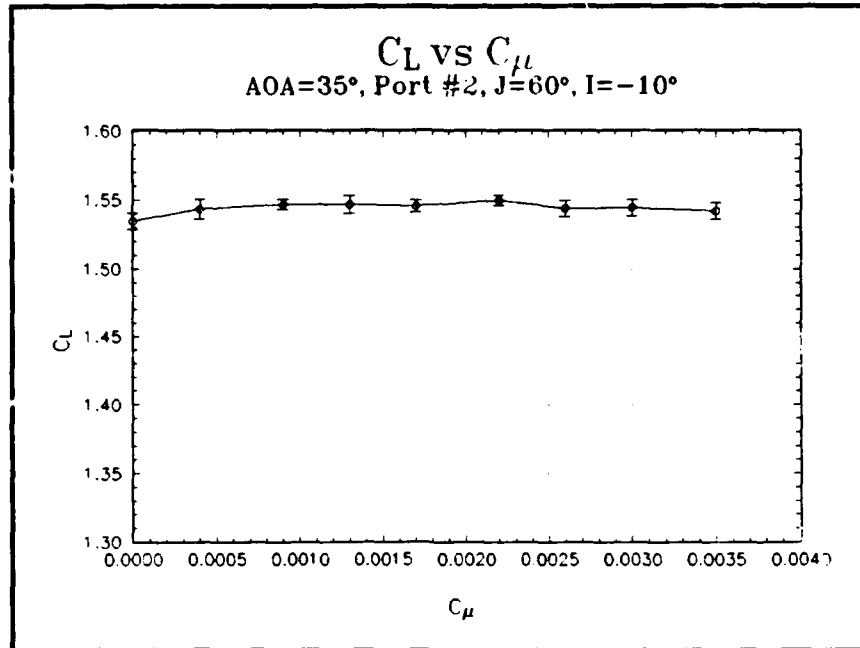


Figure 31d.

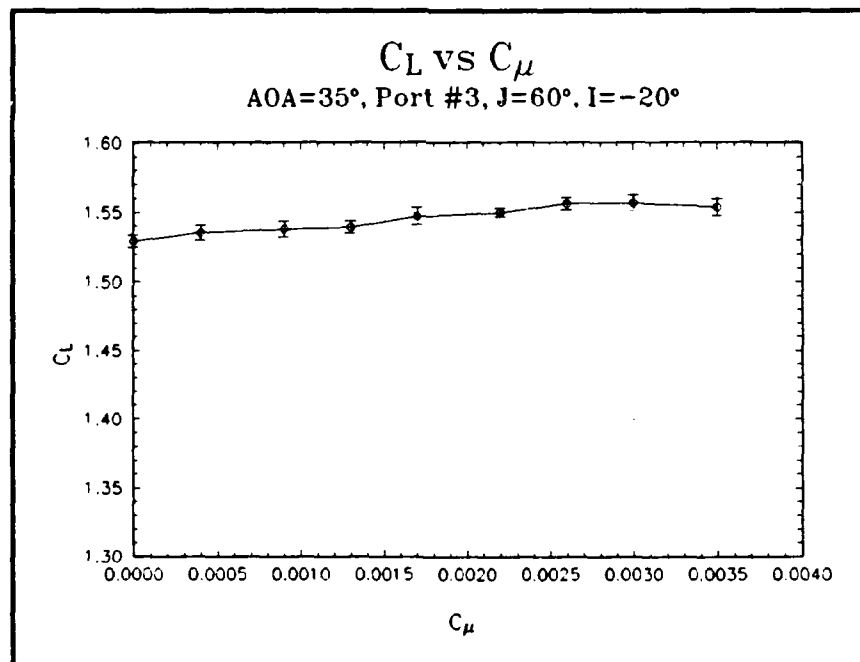


Figure 32.

APPENDIX B. MODEL DESIGN

The design of the wing/strake for the model was based on the design used in a numerical study by Steven Kern (Sections II.E & III.B.2). Using Kern's design provided some predicted lift and drag performance and vortex flow patterns. The vortex flow patterns will be particularly useful in the follow-on research to be conducted. There are some distinct differences between Kern's design and the design used in this study. [Ref. 8]

Kern's study uses a flat plate with beveled edges. Whereas, this approach may be optimum for vortex generation and numerical grid generation, modern fighters of today do not fly around with flat plates for wings. The strakes, chines, and leading edge extensions of today's fighters do at times have relatively sharp leading edges. In an attempt to pattern this study after aircraft being designed today, a NACA 64A008 airfoil section was chosen for the wing. A symmetric airfoil was chosen so that C_{L0} would pass through the origin of the lift curve. Eight percent thickness was chosen to represent thicknesses found on modern day fighter aircraft. The strake for this study was designed with a sharp leading edge to facilitate vortex development. The strake is wedged shaped and has a wedge angle of 18° .

Wing/strake geometric characteristics are shown in Figure B1 and are listed in Table B1. [Ref. 8]

Table B1: Wing/Strake Geometric Characteristics

Airfoil Section	NACA 64A008
Wing Area (semi-span)	
Projected ¹	0.969 ft ²
Exposed	0.679 ft ²
With Strake (exposed)	0.750 ft ²
Cord	
Root (exposed)	12.75 in
Root (centerline)	15.00 in
With Strake (exposed)	21.00 in
Aspect Ratio (w/o strake)	1.51
Taper Ratio	.283
Sweepback Angle	35.8°
Mean Aerodynamic Cord	10.63 in
Incidence Angle	0°
Dihedral Angle	0°
Twist Angle	0°

¹ Wing Reference Area

Kern's study did not have a fuselage section. The lack of a fuselage prevents the examination of interaction between wing/strake vortices and vortices originating from the forebody of the aircraft. The forebody vortex would be present in the actual flight-dynamics of today's aircraft. The model for this study includes a fuselage with a ogive forebody so that these effects could be observed (Figure B1). The fuselage used for this study is the identical fuselage used by Kersh and Schmidt. The wing was design to be removable so that it could be interchanged with Dean Schmidt's wing during overlapping periods of research (Figure B2). [Ref. 8, 9, 10]

The wing was positioned along the top of the fuselage section as shown in Figure B3 (oriented with the normal vector towards the bottom of the Figure). Figure B4 shows the position of the blowing ports. Inclination angles were measured with the zero reference axis parallel to the surface of the strake facing aft. Inclination angles were defined as increasing in angle as the blowing tube was turn away from the strake. Thus, a positive inclination angle at ports #1 and #2 would be turned toward the bottom of Figure B4. Inclination angle at port #3 would be turned toward the top of Figure B4. Blowing tubes were mounted in an aluminum bracket and secured with set screws as shown in Figure B5.

Figures B6 through B10 are photos of the combined wing model installed in the wind tunnel.

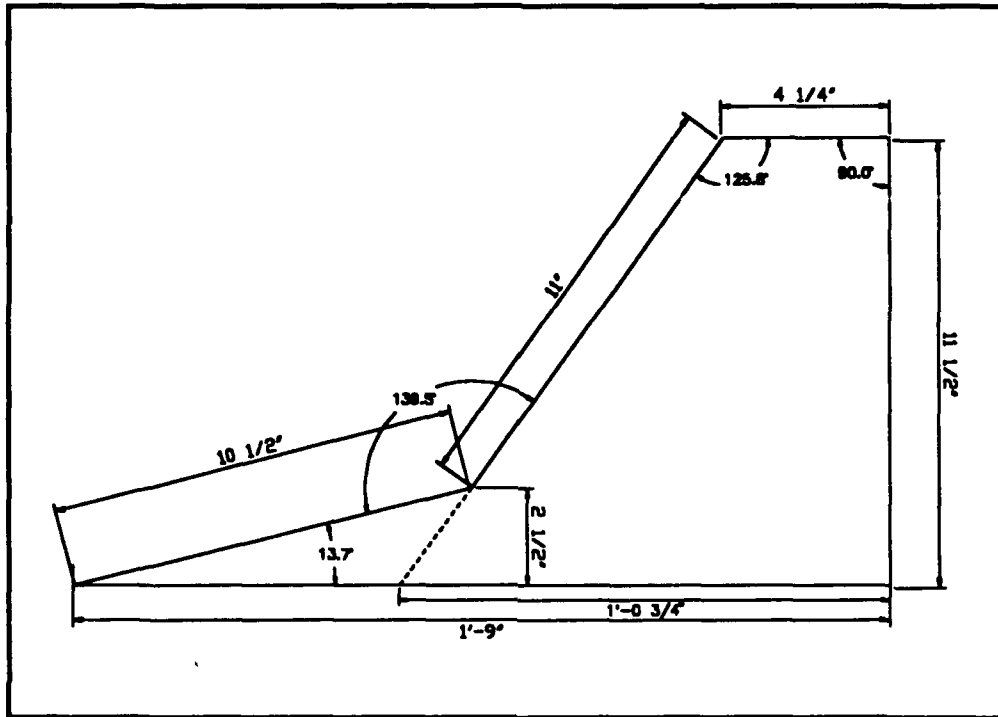


Figure B1. Wing/Strake Geometric Characteristics

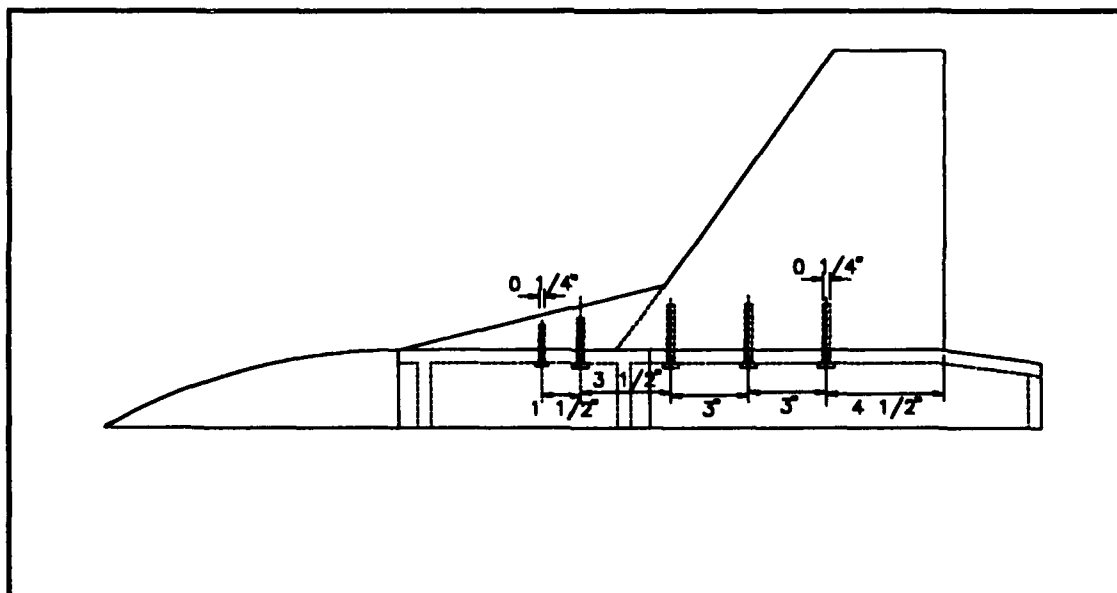


Figure B2. Wing/Strake Attached to Model

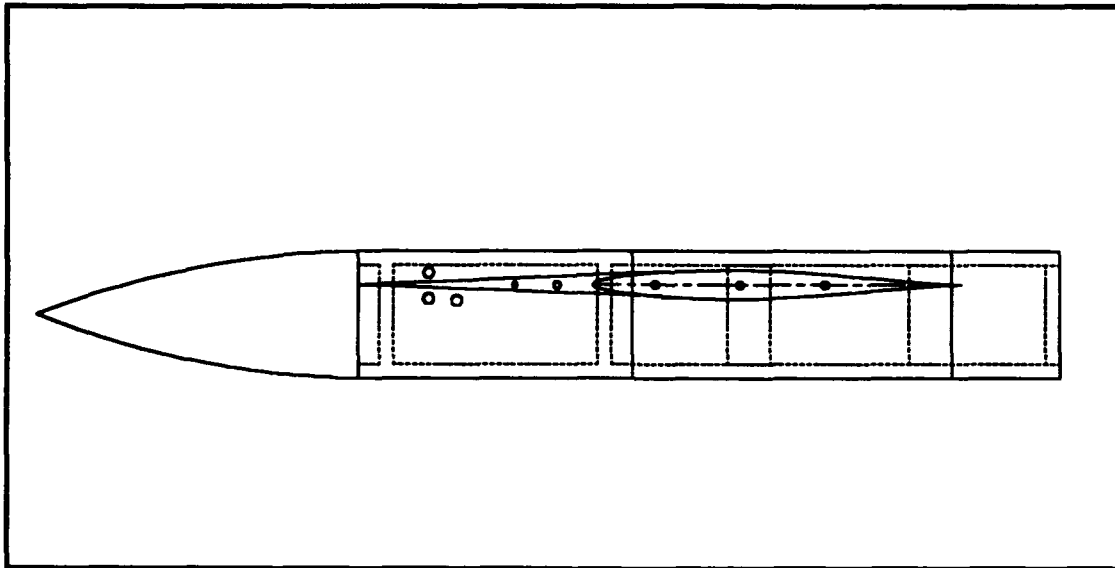


Figure B3. Top View of Wing/Strake Model

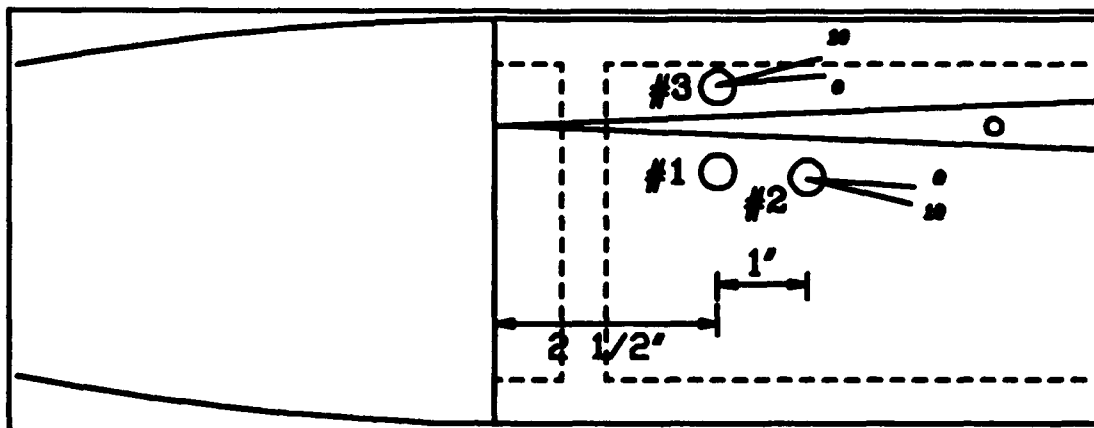


Figure B4. Blowing Port Locations

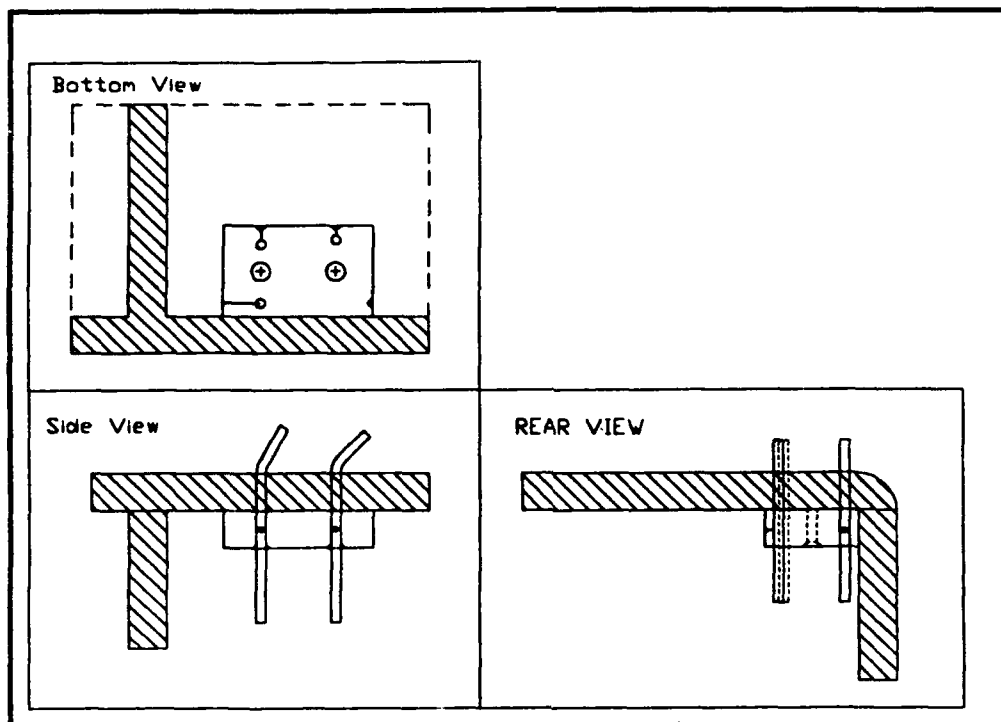


Figure B5. Blowing Tube Mounting Brace

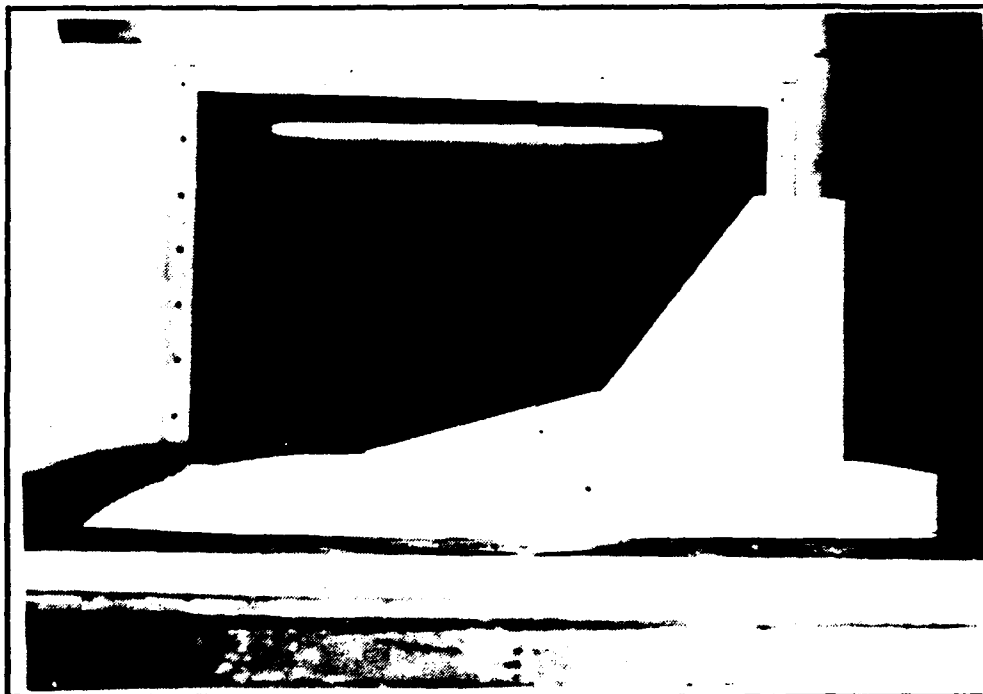


Figure B6. Wing/Strake Model in Wind Tunnel

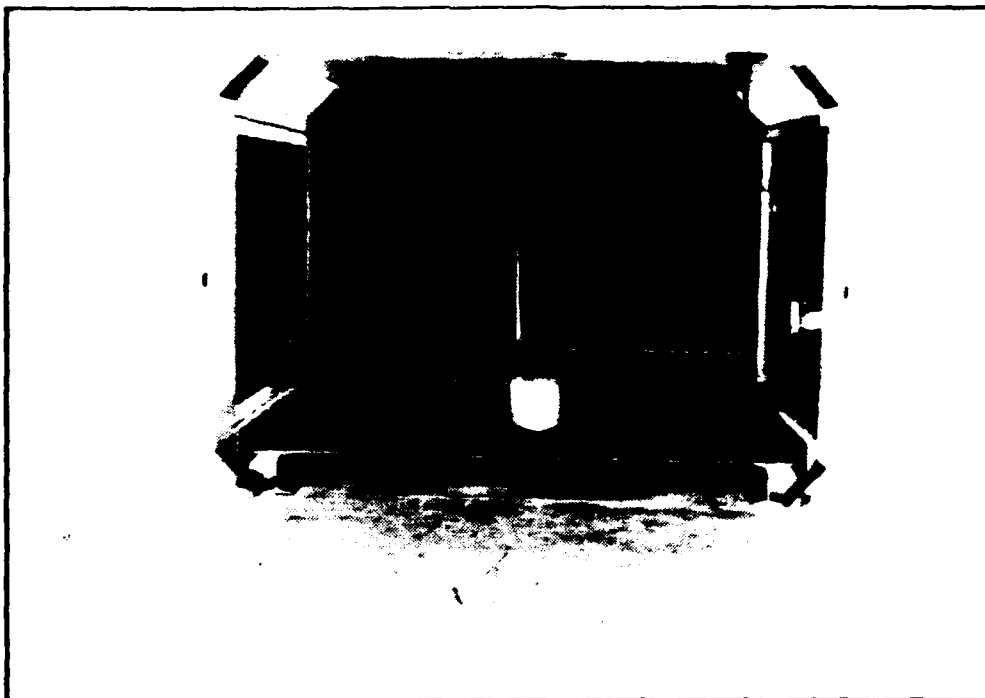


Figure B7. Model on Reflection Plane

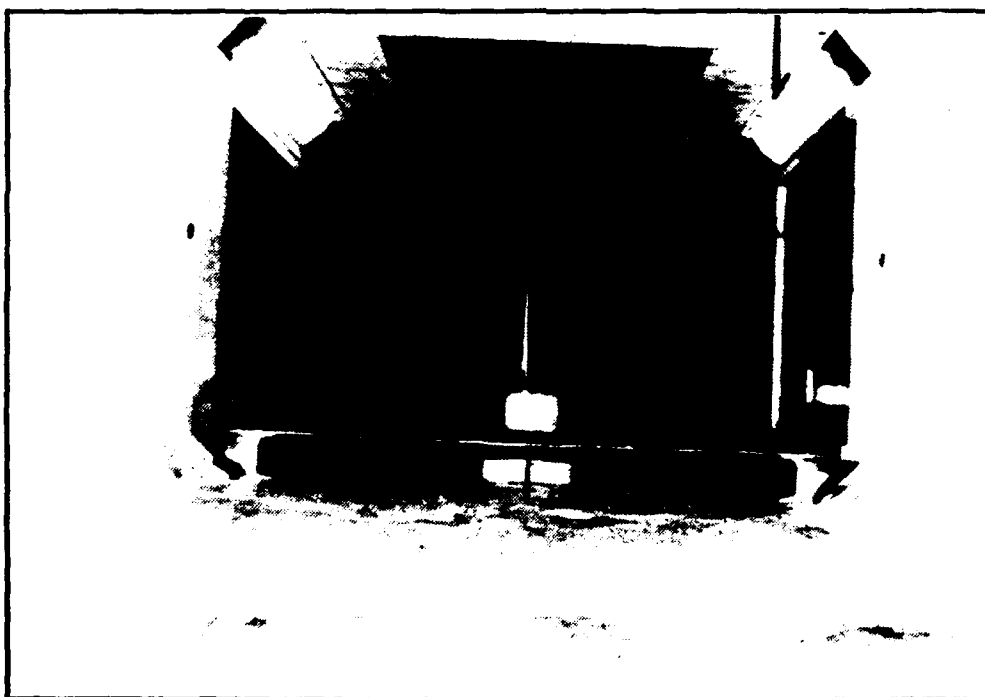


Figure B8. Model on Reflection Plane



Figure B9. Blowing Tube #2 in Port #3

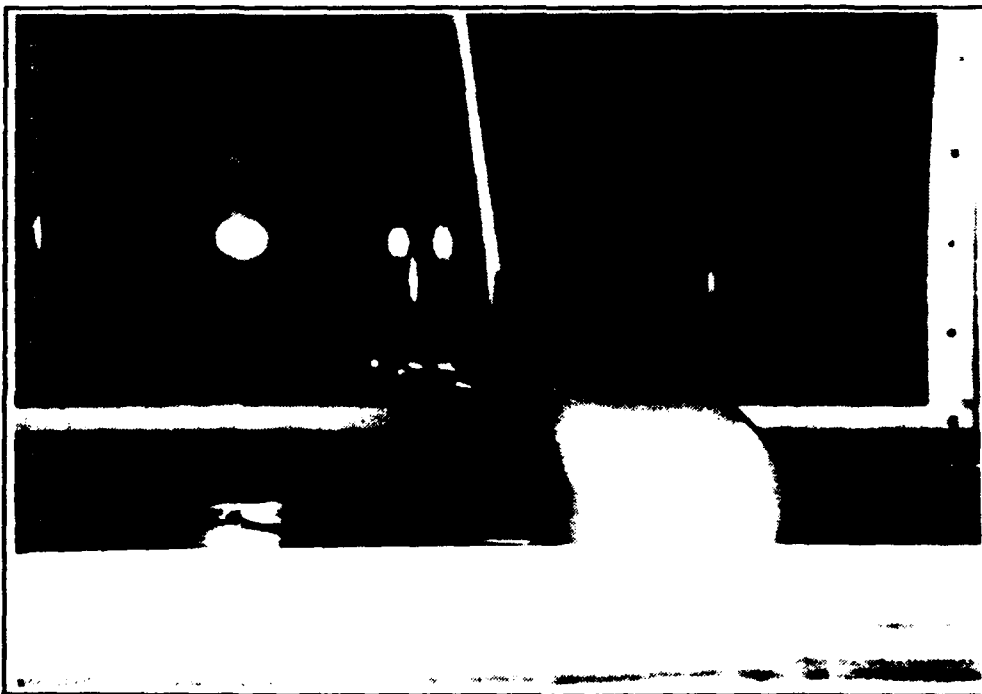


Figure B10. Forward View of Blowing Tube #2 in Port #3

APPENDIX C. HP48SX PLENUM PRESSURE PROGRAM

PLENUM:

```
%HP: T(3)A(D)F(.);
<< "PLENUM TEMP?" ":TEMP F:" INPUT OBJ→ '1_F' * '1_R'
CONVERT UVAL 1.2 / DUP 'T3' STO R * γ * √ 'Vj' STO 3 FIX "Cμ
=" Cμ →STR + "?" + ":Cμ:" INPUT OBJ→ DUP 'Cμ' STO .5 *
.002377 * 1 FIX "V∞=" V∞ →STR + "?" + ":V∞:" INPUT OBJ→
DUP 'V∞' STO SQ * S * Vj / "CALCULATIONS IN PROGRESS" CLLCD
1 DISP 'mdot' STO PTHRT EVAL 'P3' STO 3 ENG EVAL DUP 'Re'
STO εD3 SWAP DARCY ΔXp * D3 / 12 / 'FLD' STO 'FRICT' EVAL
'M' .1 ROOT 'M2' STO 'AAREA' EVAL 'AA' 1.1 ROOT A2 A3 / *
'AA' STO 'AAREA' EVAL 'M' .5 ROOT 'M21' STO 'FRICT' EVAL
'FLD' DUP →NUM ROOT 'FLD21' STO 1 'Pt' STO 'TPRESS' EVAL
'P' .9 ROOT M2 'M' STO 'TPRESS' EVAL 'P' .9 ROOT / 'PRAT'
EVAL 'PP' 1.8 ROOT * P3 * 'P21' STO εD2 Re DARCY ΔXp2 * D2
/ 12 / FLD21 + 'FLD' STO 'FRICT' EVAL 'M' .1 ROOT 'M1'
STO CLEAR P21 'PRAT' EVAL 'PP' 4 ROOT * M21 'M' STO 'PRAT'
EVAL 'PP' 1.9 ROOT / DUP 'P1' STO 144 / 'P' STO M1 'M' STO
'TPRESS' EVAL 'Pt' 300 ROOT 1 FIX "ANSWER IN psi" CLLCD 1
DISP 1 FREEZE "PLENUM Pt" →TAG -56 CF 840 1 BEEP -56 SF >>
```

VARIABLES:

A2:	Area of brass tube	gc:	gravitation constant
A2:	Area of nylon tube	M:	Mach number
AA:	Fanno Star reference area	M1:	Mach Number @(1)
Cμ:	Blowing Coefficient	M2:	Mach Number @(2)
D2:	Diam of nylon tube	M21:	Mach Number @(2')
D3:	Diam brass tube	mdot:	Mass flow rate
ΔXp:	Blow Tube Length	P1:	Static Press @(1)
ΔXp2:	Nylon tube length @(2)	P21:	Static Press @(2')
εD2:	Relative Roughness of nylon (ε/D)	P3:	Static Press @(3)
εD3:	Relative Roughness of brass tube (ε/D)	PP:	Fanno Star reference pressure
FLD:	Frictional Length	Pt:	Total Pressure
FLD21:	Frictional Length (2')	Re:	Reynolds number
		S:	Wing Reference area
		T3:	Static temp. @(3)
		V∞:	Freestream Velocity
		Vj:	Jet velocity

EQUATIONS:

PTHRT: $\sqrt{\gamma g_c / (R T_3)} / A_3$

REYNEQ: $P_3 / (R T_3) * V_j * D_3 / (\mu g_c)$

FRICT: $FL/D = (\gamma + 1) / (2 \gamma) * \ln((\gamma + 1) / 2 * M^2 / (1 + \gamma - 1) / 2 * M^2)) + 1 \gamma * (1 / M^2 - 1)$

AAREA: $AA = 1 / M * ((1 + \gamma - 1) / 2 * M^2 / ((\gamma + 1) / 2))^{(\gamma + 1) / (2 * \gamma - 1)}$

TPRESS: $P_t = P * (1 + \gamma - 1) / 2 * M^2)^{1 / (\gamma - 1)}$

PRAT: $PP = 1 / M * ((\gamma + 1) / 2 / (1 + \gamma - 1) / 2 * M^2))^{(1 / 2)}$

FUNCTIONS:

DARCY($\epsilon/D, Re$): Calculates Darcy friction factor (Moody Diagram). No listing available.²

APPENDIX D. MULTI3.BAS PROGRAM LISTING

```
'      This program was written and compiled using LabWindows and
'      QuickBasic 4.5. (used "bc /o multi" to compile) It's purpose
'      is to read and convert voltages from four channels connected to
'      the strain gauges on the Acedemic wind tunnel. The voltages are
'      converted to normal and axial forces and moments with respect to
'      the balance. It was written and modified by LT Tom D. Stuart and
'      LT Dean C. Schmidt, 20 June 92.
'      Modified, 14 AUG 92, by LT James G. Willson to conform to data
'      parameters for pneumatic blowing tests. Since runs are conducted in
'      parallel during blowing tests, different color screens are used to
'      verify to the operator what phase of the program he/she is in. The
'      following is the color scheme:
'          Green: Test Parameters
'          Blue:  Blowing OFF
'          Red:   Blowing ON

'      Variables explained

'          eaa = Strain gauge voltage at point A in Axial direction.
'          eba = Strain gauge voltage at point B in Axial direction.
'          ean = Strain gauge voltage at point A in Normal direction.
'          ebn = Strain gauge voltage at point B in Normal direction.

'          AX  = Axial force
'          Max = Axial moment
'          NORM = Normal force
'          Mnorm = Normal moment

'          alpha = Angle of Attack of the model
'          tube = Blowing tube position
'          blow = Blowing Coefficient (Cmhu)
'          Jangle = Jet angle of the tube
'          Iangle = Angle of incidence of the tube
'          LIFT = Lift force
'          DRAG = Drag force

'*****
**

REM      $INCLUDE: 'C:\LW\INCLUDE\LWSYSTEM.INC'
REM      $INCLUDE: 'C:\LW\INCLUDE\GPB.INC'
REM      $INCLUDE: 'C:\LW\INCLUDE\FORMATIO.INC'
REM      $INCLUDE: 'C:\LW\INCLUDE\GRAPHICS.INC'
REM      $INCLUDE: 'C:\LW\INCLUDE\ANALYSIS.INC'
REM      $INCLUDE: 'C:\LW\INCLUDE\DATAACQ.INC'
```

```

REM      $INCLUDE: 'C:\LW\INCLUDE\RS232.INC'

DIM K$(4,4)
DIM ean.array$(1000), eaa.array$(1000), ebn.array$(1000), eba.array$(1000)
COMMON SHARED ean.array(), eaa.array(), ebn.array(), eba.array()

DECLARE SUB volt (ean#, eaa#, ebn#, eba#, alpha!)
DECLARE SUB aero (AX#, NORM#, LIFT#, DRAG#, alpha!)
DECLARE SUB forces
(K#(), eaa#, eba#, ean#, ebn#, AX#, Max#, NORM#, Mnorm#, alpha!)

SCREEN 9, 0
COLOR 15, 1

ANS2$ = "N"
C$="N"

' Set non-blowing tares to zero
eaa0# = 0
eba0# = 0
ean0# = 0
ebn0# = 0

' Set blowing tares to zero
eaa0b# = 0
eba0b# = 0
ean0b# = 0
ebn0b# = 0

*****
**

' CALIBRATION MATRIX INPUT (See Dean Schmidt's thesis for explanation)

DATA 0.009292, -0.007686, -0.000053, -0.000209
DATA -0.033079, 0.246045, 0.007737, 0.003644
DATA 0.000063, -0.000417, 0.009682, -0.004241
DATA 0.002432, -0.006519, -0.033848, 0.126897

FOR L% = 1 TO 4: FOR M% = 1 TO 4
READ K$(L%,M%) : NEXT M%
NEXT L%

*****
**

CLS: LOCATE 05, 20: PRINT "Type the last six characters of"
LOCATE 06, 20: INPUT "your output files:"; DFILE$
VOL$ = "C:\LW\INSTR\JIM\NV" + DFILE$ + ".DAT"
OPEN VOL$ FOR APPEND AS #1
BVOL$ = "C:\LW\INSTR\JIM\BV" + DFILE$ + ".DAT"

```

```

OPEN BVOL$ FOR APPEND AS #2
FM$ = "C:\LW\INSTR\JIM\NF" + DFILE$ + ".DAT"
OPEN FM$ FOR APPEND AS #3
BM$ = "C:\LW\INSTR\JIM\BF" + DFILE$ + ".DAT"
OPEN BM$ FOR APPEND AS #4
COLOR 15, 2
LOCATE 10, 10
PRINT "DATA FILES ARE:"
PRINT "          "; VOL$
PRINT "          "; BVOL$
PRINT "          "; FM$
PRINT "          "; BM$
INPUT "COPY THEM ONTO CHECKLIST."; ZZ$

' See Lt. Willson's thesis for tube position numbering.
CLS: LOCATE 10, 20: INPUT "Blowing tube position? (1,2,3)"; Tube%
LOCATE 15, 20: INPUT "Input tube jet angle (deg)"; Jangle!
LOCATE 20, 20: INPUT "Input tube incidence angle (deg)"; Iangle!

500
COLOR 15, 2
CLS: LOCATE 10, 20: PRINT "Input the Test AOA"
LOCATE 11, 20: INPUT "from turntable markings (deg.)"; alpha!
alpha! = 90 - alpha!

LOCATE 20, 20: INPUT "Input blowing coefficient (Cu)"; blow!

' Prevent asking for tare calculation a second time. ANS$ is defined
' as "N" at the begining of the program and must be <> "N" in order
' to loop back to 500.

IF ANS2$ <> "N" THEN
    COLOR 15, 1
    GOTO 600
END IF

COLOR 15, 1
CLS: LOCATE 5, 20: INPUT "Is this a tare (zero load) reading? (Y/N)"; A$

IF A$ = "Y" THEN
    CALL tare (ean0#, eaa0#, ebn0#, eba0#, alpha!, tube%, 0.0, Jangle!, Iangle!)
700
    LOCATE 15, 20: INPUT "Are blowing tares to be taken? (Y/N)"; C$

    IF C$ = "Y" THEN
        COLOR 15, 4
        CALL tare
(ean0b#, eaa0b#, ebn0b#, eba0b#, alpha!, tube%, blow!, Jangle!, Iangle!)
        COLOR 15, 1
    ELSEIF C$ = "N" THEN

```

```

        LOCATE 17, 10: PRINT "Setting blowing tare in program equal to
non-blowing tare."
        eaa0b# = eaa0#
        eba0b# = eba0#
        ean0b# = ean0#
        ebn0b# = ebn0#
    ELSE
        GOTO 700
    END IF
    C$ = "N"

ELSE LOCATE 15, 20: PRINT "Data will not be accurate!!!"
END IF

600
LOCATE 22,20: INPUT "Ready to take readings? (Y/N)"; B$

LOCATE 23,20: INPUT "HOW MANY SAMPLES?"; NSAMP%

IF B$ = "y" THEN
    CLS: LOCATE 15,20: PRINT "TURN ON CAPS LOCK"
    GOTO 600
END IF

IF B$ <> "Y" THEN GOTO 5000

LOCATE 24, 20: INPUT "Is this with blowing or not? (B/N)"; BN$

FOR NN% = 1 TO NSAMP%

IF B$ = "Y" THEN CALL volt (ean#,eaa#,ebn#,eba#,alpha!)

' Correcting for zero load values.

IF BN$ = "N" THEN
    COLOR 15, 1
    eaa# = eaa# - eaa0#
    eba# = eba# - eba0#
    ean# = ean# - ean0#
    ebn# = ebn# - ebn0#
ELSEIF BN$ = "B" THEN
    COLOR 15, 4
    eaa# = eaa# - eaa0b#
    eba# = eba# - eba0b#
    ean# = ean# - ean0b#
    ebn# = ebn# - ebn0b#
ELSE
    CLS: COLOR 12, 0
    LOCATE 15, 10: PRINT "BAD ANSWER TO BLOWING QUESTION.  CHECK CAPLOCK.
NODATA RECOERDED!!"
    GOTO 600

```

```

END IF

CALL forces (K#(), eaa#, eba#, ean#, ebn#, AX#, Max#, NORM#, Mnorm#, alpha!)

CALL aero (AX#, NORM#, LIFT#, DRAG#, alpha!)

PRINT " "
PRINT "          AOA          EAA (mV)          EBA (mV)          EAN (mV)
EBN (mV) "
PRINT "          *****          *****          *****          *****
*****"

PRINT USING "          ####.#####"; alpha!; eaa!; eba!; ean!; ebn!

PRINT " "
PRINT "          AXIAL (lb)          MOMax (ft-lb)          NORMAL (lb)          MOMnorm(ft-lb) "
PRINT "          *****          *****          *****          *****"

PRINT USING "          ####.#####"; AX!; Max!; NORM!; Mnorm!

PRINT " "
PRINT "                                     Blowing          Jet
Inclination"
PRINT "          Lift (lb)          Drag (lb)          Coeff          Angle (deg)
Angle (deg) "
PRINT "          *****          *****          *****          *****
*****"

PRINT USING "          ####.#####"; LIFT!; DRAG!; blow!; Jangle!; Iangle

IF BN$ = "B" THEN
    PRINT #2, USING "#####.#####";
alpha!; blow!; Jangle!; Iangle!; eaa!; eba!; ean!; ebn!
    PRINT #4, USING
"#####.#####"; alpha!; blow!; Jangle!; Iangle!; AX!; NORM!; LIFT!; DRAG#
ELSE
    PRINT #1, USING "#####.#####";
alpha!; blow!; Jangle!; Iangle!; eaa!; eba!; ean!; ebn!
    PRINT #3, USING
"#####.#####"; alpha!; blow!; Jangle!; Iangle!; AX!; NORM!; LIFT!; DRAG#
END IF

NEXT NN%

LOCATE 21, 20: INPUT "Do you want another reading? (Y/N)"; ANS$
IF ANS$ = "Y" THEN
    LOCATE 22, 20: INPUT "New parameters? (Y/N)"; ANS2$
    IF ANS2$ = "N" THEN GOTO 600
    IF ANS2$ <> "N" THEN GOTO 500
END IF

```

```

5000 CLOSE #1
CLOSE #2
CLOSE #3
CLOSE #4

```

```

END

```

```

'*****
**
'*****
**
SUB volt (ean#,eaa#,ebn#,eba#,alpha!)
'*****
**
'
' S/R to read Channel 0,2,4,6 on MIO-15L-9 for Analog Voltage
'
'*****
**

' Setting Board code for MIO-16L-9

board.code%=0

'*****
**

err1.num% = Init.DA.Brds(1, board.code%)

err2.num% = AI.Setup(1, 0, 1)
err3.num% = AI.Setup(1, 2, 1)
err4.num% = AI.Setup(1, 4, 1)
err5.num% = AI.Setup(1, 6, 1)

' Configure and set clock to 1MHZ

err6.num% = CTR.Clock (1, 1, 1, 1)
err7.num% = CTR.Config (1, 1, 0, 0, 0, 0)

LWtotal! = 0

FOR i% = 1 TO 1000

err8.num% = CTR.EvCount (1, 1, 1, 0)

' CH 0 = Eaa
    err9.num% = AI.Read(1, 0, 1, value0%)
    err10.num% = AI.Scale(1, 1, value0%, eaa.array#(i%))

' CH 2 = Eba

```



```

er11.num% = AI.Read(1, 2, 1, value2%)
er12.num% = AI.Scale(1, 1, value2%, eba.array%(i%))

' CH 4 = Ean
er13.num% = AI.Read(1, 4, 1, value4%)
er14.num% = AI.Scale(1, 1, value4%, ean.array%(i%))

' CH 6 = Ebn
er15.num% = AI.Read(1, 6, 1, value6%)
er16.num% = AI.Scale(1, 1, value6%, ebn.array%(i%))

er17.num% = CTR.EvRead (1, 1, overflo%, tcount%)

LWtotal! = LWtotal! + tcount%

NEXT i%

CLS:LOCATE 5,15:PRINT "Total Time is " LWtotal!*1E-6" seconds."

CALL Mean (eaa.array#(), 1000, eaa#)
CALL Mean (eba.array#(), 1000, eba#)
CALL Mean (ean.array#(), 1000, ean#)
CALL Mean (ebn.array#(), 1000, ebn#)

'*****
**

' This multiplication (*1000) will make the voltages in mV

eaa#=eaa#*1000
eba#=eba#*1000
ean#=ean#*1000
ebn#=ebn#*1000

END SUB

'*****
**
'*****
**

SUB forces (K#(),eaa#,eba#,ean#,ebn#,AX#,Max#,NORM#,Mnorm#,alpha!)

' FORCES AND MOMENTS CALCULATIONS (See thesis for explanation)

AX# = K#(1,1)*eaa# + K#(1,2)*eba# + K#(1,3)*ean# + K#(1,4)*ebn#
Max# = K#(2,1)*eaa# + K#(2,2)*eba# + K#(2,3)*ean# + K#(2,4)*ebn#
NORM# = K#(3,1)*eaa# + K#(3,2)*eba# + K#(3,3)*ean# + K#(3,4)*ebn#

```

```
Mnorm# = K#(4,1)*eaa# + K#(4,2)*eba# + K#(4,3)*ean# + K#(4,4)*ebn#
```

```
END SUB
```

```
*****
**
*****
**
```

```
SUB aero (AX#,NORM#,LIFT#,DRAG#,alpha!)
```

```
*****
**
```

```
PI# = 3.14159265359
```

```
' Transformed due to balance offset of 90 degrees.
```

```
LIFT# = AX# * COS(PI#/180*alpha!) + NORM# * SIN(PI#/180*alpha!)
```

```
DRAG# = AX# * SIN(PI#/180*alpha!) - NORM# * COS(PI#/180*alpha!)
```

```
END SUB
```

```
*****
**
*****
**
```

```
SUB tare (ean#,eaa#,ebn#,eba#,alpha!,tube%,blow!,Jangle!,Iangle!)
```

```
*****
**
```

```
' S/R to read Channel 0,2,4,6 on MIO-16L-9 for Analog Voltage
```

```
*****
**
```

```
' Setting Board code for MIO-16L-9
```

```
board.code%=0
```

```
*****
**
```

```
CLS: LOCATE 5, 20: INPUT "Ready to take tare readings? (Y/N)"; T$
```

```
IF T$ <> "Y" THEN RETURN
```

```
err1.num% = Init.DA.Brds(1, board.code%)
```

```
err2.num% = AI.Setup(1, 0, 1)
```

```

err3.num% = AI.Setup(1, 2, 1)
err4.num% = AI.Setup(1, 4, 1)
err5.num% = AI.Setup(1, 6, 1)

' Configure and set clock to 1MHZ

err6.num% = CTR.Clock (1, 1, 1, 1)
err7.num% = CTR.Config (1, 1, 0, 0, 0, 0)

LWtotal! = 0

FOR i% = 1 TO 1000

err8.num% = CTR.EvCount (1, 1, 1, 0)

' CH 0 = Eaa
    err9.num% = AI.Read(1, 0, 1, value0%)
    erl0.num% = AI.Scale(1, 1, value0%, eaa.array#(i%))

' CH 2 = Eba
    erl1.num% = AI.Read(1, 2, 1, value2%)
    erl2.num% = AI.Scale(1, 1, value2%, eba.array#(i%))

' CH 4 = Ean
    erl3.num% = AI.Read(1, 4, 1, value4%)
    erl4.num% = AI.Scale(1, 1, value4%, ean.array#(i%))

' CH 6 = Ebn
    erl5.num% = AI.Read(1, 6, 1, value6%)
    erl6.num% = AI.Scale(1, 1, value6%, ebn.array#(i%))

erl7.num% = CTR.EvRead (1, 1, overflo%, tcount%)

LWtotal! = LWtotal! + tcount%

NEXT i%

CLS:LOCATE 5,15:PRINT "Total Time is " LWtotal!*1E-6" seconds."

CALL Mean (eaa.array#(), 1000, eaa#)
CALL Mean (eba.array#(), 1000, eba#)
CALL Mean (ean.array#(), 1000, ean#)
CALL Mean (ebn.array#(), 1000, ebn#)

'*****
**

' This multiplication (*1000) will make the voltages in mV

eaa#=eaa#*1000
eba#=eba#*1000

```

```
ean#=ean#*1000
ebn#=ebn#*1000
```

```
PRINT " "
PRINT "          AOA          EAA (mV)          EBA (mV)          EAN (mV)
EBN (mV)"
PRINT "          *****          *****          *****          *****
*****"
```

```
PRINT USING "    ####.#####" alpha!; eaa#; eba#; ean#; ebn#
```

```
IF blow! = 0.0 THEN
```

```
    PRINT #1, USING "####.#####"
alpha!;blow!;Jangle!;Iangle!;eaa#;eba#;ean#;ebn#
ELSE
```

```
    PRINT #2, USING "####.#####"
alpha!;blow!;Jangle!;Iangle!;eaa#;eba#;ean#;ebn#
END IF
```

```
END SUB
```

APPENDIX E. WIND-TUNNEL CHECKLIST

(This page purposely left blank.)

Wind Tunnel Checklist for Pneumatic Vortex Control

Date: _____ Blowing Port #: _____ Jet Angle: _____

Tunnel Temp: _____ F C_{μ} : _____ Incl. Angle: _____

File Names: _____

Voltage: NV _____

BV _____

Force: NF _____

BF _____

(\$\$####)	
Y	Inclination Angle (N='-')
	Blowing Tube Number
	Blowing Tube Position
	Volt/Force (V/F)
	Blow/Non-blow (B/N)

AT THE BEGINNING OF EACH TUNNEL SESSION:

- ☐ Manometer Zeroed
- ☐ Manometer set to _____ cm. _____ ft/sec.
- ☐ Log Hobbs Meter
- ☐ Model config. checked, Air connected, Holes taped.
- ☐ FOD Sweep

FOR EACH AOA:

- ☐ Model AOA set
- ☐ Amps IN/OUT zeroed
- ☐ Signal Conditioners SPAN/ZEROS set
- ☐ Tare Readings taken (normal & axial < .01 lbs.)

START THE RUN:

Time Started: _____

☐ Tunnel ON, Set cm

☐ ☐ ☐ ☐ ☐ Five runs Non-Blowing

☐ Set Plenum Press. (Watch for fluxes) _____ . psig

☐ Turn on Valve

☐ ☐ ☐ ☐ ☐ Five runs Blowing

☐ Tunnel OFF

☐ Drift Check

Tunnel Temp. _____ F

Time Stopped: _____

End of Day:

Turn off Equipment (Leave Amps ON)

INITIAL DISTRIBUTION LIST

	<u>No. Copies</u>
1. Defense Technical Information Center Cameron Station Alexandria, VA 22304-6145	2
2. Library, Code 52 Naval Postgraduate School Monterey, CA 93940-5002	2
3. Chairman Department of Aeronautics and Astronautics, Code AA Naval Postgraduate School Monterey, CA 93940-5000	1
4. Steven B. Kern Naval Air Warfare Center, Aircraft Division, Code 6051 Warminster, PA 18974-5000	1
5. NASA Ames Research Center Technical Library Moffett Field, CA 94035	1
6. Prof. R.M. Howard Department of Aeronautics and Astronautics, Code AA/Ho Naval Postgraduate School Monterey, CA 93943-5000	3
7. LT. James G. Willson, USN 3544 Indiana St., #10 San Diego, CA 92103	2